

Physico-Chemical Properties of Polymers at Interfaces

Silvia Díez Orrite

Escola Tècnica Superior d'Enginyeria
Universitat Rovira i Virgili
Tarragona

Noviembre de 2002

Universitat Rovira i Virgili
Escola Tècnica Superior d'Enginyeria Química

Physico-Chemical Properties of Polymers at Interfaces

Memoria presentada por

Silvia Díez Orrite

para optar al Grado de
Doctor en Ingeniería Química

Tesis dirigida por el Dr. Josep Bonet i Avalos

Miembros tribunal de tesis

Presidente Dr. Raúl Toral

Secretario Dr. Allan Mackie

Vocales

Dra. Elvira Martín del Río

Dr. Albert Johner

Dr. Ignacio Pagonabarraga

Suplentes

Dr. Azael Fabregat

Dr. Joachim Wittmer

Evaluadores externos (Label Europeo)

Dr. Edgar Blokhuis

Dr. Carlos Marques

El Dr. Josep Bonet i Avalos, Professor Titular del Departament d'Enginyeria Química de l'Escola Tècnica Superior d'Enginyeria Química, de la Universitat Rovira i Virgili de Tarragona,

Faig constar que el present treball, amb el títol

PHYSICO-CHEMICAL PROPERTIES OF POLYMERS AT INTERFACES,

que presenta la doctorand na SILVIA DIEZ ORRITE per optar al grau de Doctor en Enginyeria Química, ha estat dut a terme sota la meva immediata direcció, i que tots els resultats obtinguts són fruit del treball i l'anàlisi realitzat per l'esmentada doctorand.

I per a què es faci saber i tingui els efectes que correspongui, signo aquesta certificació.

Tarragona, 7 d'octubre de 2002

Dr. Josep Bonet i Avalos
Professor Titular d'Enginyeria Química

Quiero expresar mi agradecimiento a todas aquellas personas que de una manera u otra han intervenido en el desarrollo de este trabajo.

En primer lugar quisiera agradecer a mi director de tesis, Dr. Josep Bonet i Avalos, el darme la oportunidad de introducirme en el mundo de los polímeros y querer transmitirme su ilusión por este trabajo.

También, al Dr. Raúl Toral, Dra. Elvira Martín, Dr. Ignacio Pagonabarraga, Dr. Albert Johner y al Dr. Allan Mackie, por formar parte del tribunal de defensa de esta tesis.

A los Drs. Edgar Blokhuis y Carlos Marques por aceptar ser los evaluadores externos de este trabajo y cuyos informes han permitido que pueda optar a obtener la calificación de Doctorado Europeo.

A los Drs. A. Johner y J. F. Joanny por su amabilidad y paciencia ya que parte de este trabajo ha salido adelante gracias a su experiencia. Además debo de agradecerles la financiación de parte de mi estancia realizada en Estrasburgo.

Al Dr. Igal Szleifer y su grupo de investigación por su hospitalidad, financiación y ayuda durante mi estancia en Purdue. A ellos les debo el haberme facilitado sus códigos del SCMF y el haberme enseñado su uso. Estos códigos fueron usados para comprobar los primeros resultados del tratamiento desarrollado en esta tesis.

A los Drs. Ioannis Bitsanis y Jason de Joannis por facilitarme sus resultados obtenidos por el método de Monte Carlo. Asimismo, agradezco a J. Van Male el haberme permitido calcular los perfiles mediante el método SCF de Scheutjens y Fleer así como al Dr. E. Blokhuis por haber ayudado en el cálculo de estos perfiles. Todos estos resultados han sido comparados con los obtenidos por medio del método SCMF.

También, dentro del Departamento de Ingeniería Química, quisiera agradecer a la Dra. Lourdes Vega por su apoyo y consejos ofrecidos durante este largo, y a veces difícil, periodo y también al Dr. Allan Mackie por sus constructivos comentarios que han sido de gran ayuda en el desarrollo de los códigos del SCMF.

A la Universidad Rovira i Virgili por otorgarme la beca con la que he vivido durante estos 5 años, además del proyecto 2000PIR-21. Al programa Beques fora de Catalunya, ofrecido por la Generalitat de Catalunya, que financió parte de la estancia realizada en el Institute Charles Sadron (CNRS), Estrasburgo (Francia); al Ministerio de Ciencia y Tecnología español por los proyectos: PB96-1025, PPQ2000-2888-E y PPQ2001-0671 y a la Generalitat de Catalunya por la financiación recibida dentro del programa ACES-1999 (Programa d'Accions Especials per a la Recerca).

Por supuesto, no quiero olvidarme de mis compañeros de fatigas: Oliver, Zaid, Josep Pàmies, Carlos, Felipe y Antonio por aguantarme cuando las cosas se ponían del revés. A mi amigo Sam por ayudarme en los temas burocráticos. A los del café: Alvarito, Mónica, Angel, Gabriela, Montse, Albert, Magda, Josep María, Roger, Mikaela, Dosi, al matrimonio Sonnemann (Guido y Marisa) que hicieron mi vida en Tarragona más divertida.

A mi familia que me dejen estar lejos de mi casa, cuyos consejos y apoyo han sido y son muy importantes para mí.

Y por último, a Θανάσης por no estar harto de la harta. Gracias por apoyarme.

Resumen

Palabras clave: *Adsorción de polímeros, paredes planas, partículas coloidales, teoría Single Chain Mean Field, Simulaciones de Monte Carlo, teorías de escala*

El estudio de las propiedades Físico Químicas de superficies con capas poliméricas, es un área de gran interés tanto a nivel científico como tecnológico. El trabajo que se presenta es orientado al desarrollo de técnicas de modelización, tanto analíticas como computacionales, y su aplicación a la descripción de la estructura de la capa de polímeros adsorbida en superficies heterogéneas. Con este propósito, la metodología conocida como Single Chain Mean Field (SCMF), utilizada anteriormente para el estudio de agregados micelares, ha sido modificada para describir la adsorción de polímeros. Así se han podido calcular numéricamente propiedades medibles experimentalmente como los perfiles de la fracción en volumen de monómeros, adsorbancia o el espesor de la capa adsorbida, para geometrías de la superficie absorbente tanto plana como esférica. En su comparación con otras metodologías, ya establecidas para la simulación numérica dentro de la física de polímeros, la aplicación de esta nueva versión del Single Chain Mean Field (SCMF) ha resultado ser más eficiente debido a un mejor muestreo del espacio de configuraciones de las cadenas poliméricas. De este modo, comparando los resultados obtenidos a partir del SCMF, con aquellos obtenidos mediante técnicas de simulación Monte Carlo o la teoría desarrollada en los años 80 por Scheutjens y Fleer (SCF), se ha podido encontrar un buen acuerdo en las propiedades calculadas para el caso de la adsorción en superficies planas. Debido a la dificultad intrínseca del estudio de la adsorción en superficies curvadas, nuestros resultados son los primeros que presentan predicciones cuantitativas sobre la estructura de la capa que se forma sobre una partícula coloidal. Finalmente, en este trabajo se ha desarrollado, también, una teoría analítica para la descripción de la mezcla polímero-coloide. De este modo, los resultados numéricos obtenidos con el SCMF han podido ser comparados con dicha teoría, obteniendo, de nuevo, un buen acuerdo, además de predecir comportamientos colectivos como la formación de geles.

Abstract

Keywords: *Polymer adsorption, flat surfaces, colloidal particles, Single Chain Mean Field theory, Monte Carlo simulations, scaling theory*

The study of the Physico-Chemical properties of surfaces with adsorbed polymeric layers is of interest both from a scientific as well as from technological point of view. The present work aims to develop appropriate numerical and analytical modelling techniques, which can describe the structure of a polymeric layer adsorbed on a heterogeneous surface. In the first place, the methodology known as Single Chain Mean Field (SCMF), originally used to study micellar aggregates, was modified to apply on polymer adsorption problems. In this way, it was possible to calculate numerically properties that can be experimentally measured, such as monomer volume fraction profiles, adsorbance or the thickness of the adsorbed layer. The structure of the polymeric layer was examined both for flat and spherical (colloidal particles) surface geometries. When compared with other well established methodologies for the numerical simulation of polymeric systems, this new version of SCMF was found to be more efficient due to the improved sampling of the polymer chain configuration space. Thus, SCMF method results for flat surfaces compare well with those obtained either with Monte Carlo simulations or with the method developed in the 80s by Scheutjens and Fleer. Due to the lack of studies focusing to polymer adsorption on colloidal particles, our results have been the first to present quantitative predictions of the structure of the polymeric layer adsorbed on a spherical surface. Finally, in this work an analytical approach for the description of polymer-colloidal mixtures, has been developed which compares well with the numerical results obtained from the SCMF methodology. Furthermore, the analytical approach is able to predict system behaviours, as for example the formation of gels.

Contents

1	Introduction	1
1.1	Polymers in solution	7
1.1.1	General aspects	7
1.1.2	Semidilute polymer solutions	13
1.1.3	Other theories	20
1.2	Polymer adsorption	21
1.2.1	Scaling Theory of polymer adsorption	21
1.2.2	Markovian self-consistent field description of polymer adsorption . .	23
1.2.3	Other theories	33
1.3	Experimental characterization of polymer interfaces	33
1.3.1	Layer thickness	34
1.3.2	Adsorbed amount	36
1.3.3	Volume fraction profile	36
	Bibliography	39
2	Theoretical approach	43
2.1	The Single Chain Mean Field theory	45
2.1.1	Calculation at a fixed chemical potential	50

2.1.2	Importance sampling of the phase space of one single self-avoiding chain	52
2.2	Appendix A	55
2.2.1	Monte Carlo simulation	55
	Bibliography	57
3	Adsorption on flat surfaces	59
3.1	Numerical calculation details	61
3.2	Structure of the adsorbed layer as predicted by SCMF.	64
3.3	Comparison with Monte Carlo simulations	72
3.4	Comparison with SCF methods based on Markovian chains	82
3.5	Conclusions	86
3.6	Appendix A	88
3.6.1	Periodic boundary conditions	88
	Bibliography	90
4	Adsorption onto colloidal particles	93
4.1	Numerical calculation details	94
4.2	Structure of the layer adsorbed onto a colloidal particle.	96
4.3	SCMF results for adsorption onto spheres	102
4.4	Conclusions	117
	Bibliography	119
5	Scaling analysis of polymer-colloid systems	121
5.1	Formation of colloid/polymer complexes	121
5.1.1	Adsorption on a flat wall	121
5.1.2	Adsorption onto colloidal particles: Adsorption Regimes	123

<i>CONTENTS</i>	xiii
5.1.3 Polymer/colloid star-shaped complexes	124
5.1.4 Star-shaped complexes at equilibrium in dilute solution	127
5.1.5 Gelation in semidilute solution	128
5.2 Conclusions	128
Bibliography	130
6 Perspectives	133
Bibliography	136
Curriculum Vitae	139

List of Figures

1.1	Representation of different types of polymers depending on their degrees of flexibility. a. Flexible chain; b. Stiff chain; c. Rigid chain.	7
1.2	Crossover between dilute and semidilute solutions: a. corresponds to the dilute conditions, b. overlap treshold and c. semidilute concentration.	14
1.3	The <i>blob</i> picture of a chain in a semidilute solution; some of the interacting chains are shown as dashed lines.	15
1.4	Presentation of the adsorbed polymer layer as a <i>self-similar mesh</i> in the semidilute regime. At a distance z from the adsorbing surface, the size of the correlation length, ξ , is itself of order z	22
1.5	Loops-tails-trains conformations of a homopolymer adsorbed on a plane surface	25
1.6	Division of the adsorbed polymeric layer on loops and tails regions. z^* is the crossover distance and λ is the thickness of the adsorbed layer being of the order of the radius of gyration of the polymer, $Rg \sim lN^\nu$, in a dilute solution.	26
1.7	Representation of the loops (ϕ_l), tails (ϕ_t) and free chains (ϕ_f) of the adsorbed layer, as a function of their corresponding partition functions. In this picture the variable z is the distance to the wall.	29
1.8	An adsorption isotherm for a monodisperse polymer solution.	37
3.1	Variation of the energy of the configurational file, $E = -\sum_{\gamma} H_{mf}(\gamma)$, with Monte Carlo (MC) steps for a system with $N = 100$, $\phi^0 = 0.058$ and $\varepsilon = -0.35 kT$	63
3.2	Variation of the average number of adsorbed monomers of the configurational file with respect to Monte Carlo (MC) steps for a system with $N = 100$, $\phi^0 = 0.058$ and $\varepsilon = -0.35 kT$	63

3.3	End-to-end distance corresponding to self-avoiding and markovian chains, obtained from SCMF method, as a function of chain length. Solid lines show the fitted power law, $N \geq 100$: $R_{end}/l = 1.27N^{0.587}$, for the case of self-avoiding walk chains (triangles), and $R_{end}/l = 1.02N^{0.495}$ for markovian chains (circles).	66
3.4	Representation of loop, tail and adsorbed monomer volume fraction profiles, obtained from Single Chain Mean Field method (SCMF), corresponding to chains of $N = 100$ (circles) and $N = 200$ (triangles) at bulk monomer volume fractions $\phi^0 \simeq 0.058$ and $\phi^0 \simeq 0.033$, respectively. In both cases $\varepsilon = -0.35 kT$	68
3.5	Representation of the adsorbed monomer volume fraction profiles corresponding to chains of $N = 100$ (circles) and $N = 200$ (triangles), obtained from Single Chain Mean Field approach (SCMF), at bulk monomer volume fractions $\phi^0 \simeq 0.058$ and $\phi^0 \simeq 0.033$, respectively. In both cases, $\varepsilon = -0.35 kT$	69
3.6	End-monomer distribution profile, corresponding to the adsorbed chains obtained from Single Chain Mean Field method (SCMF), for $N = 100$ (circles) and $N = 200$ (triangles) at bulk monomer volume fractions $\phi^0 \simeq 0.058$ and $\phi^0 \simeq 0.033$, respectively. Dashed line corresponds to a power law of -0.532 . In both cases $\varepsilon = -0.35 kT$	71
3.7	End-monomer distribution profile, corresponding to the adsorbed chains obtained from Single Chain Mean Field method (SCMF), for different bulk monomer volume fractions ($\phi^0 = 0.001, 0.03, 0.13$) considering $N = 200$ and $\varepsilon = -0.35 kT$. Dashed line corresponds to a power law of -0.532	71
3.8	Comparison of the total monomer volume fraction profiles obtained from Single Chain Mean Field (SCMF) and Monte Carlo (MC) simulations. Conditions of the system are: $N = 200$, $\phi^0 = 0.0026$ and $\varepsilon = -1 kT$. The dashed line corresponds to a power law $-4/3$. SCMF: triangles and MC: squares	73
3.9	Comparison of the loop volume fraction profiles obtained from Single Chain Mean Field (SCMF) and Monte Carlo (MC) simulations. Conditions of the system are: $N = 200$, $\phi^0 = 0.0026$ and $\varepsilon = -1 kT$. SCMF: triangles and MC: squares	73
3.10	Comparison of the tail volume fraction profiles obtained from Single Chain Mean Field (SCMF) and Monte Carlo (MC) simulations. Conditions of the system are: $N = 200$, $\phi^0 = 0.0026$ and $\varepsilon = -1 kT$. SCMF: triangles and MC: squares	74
3.11	Monomer volume fraction profiles obtained from Single Chain Mean Field (SCMF) and Monte Carlo (MC) simulations. Conditions of the system are: $N = 200$, $\phi^0 = 0.11$ and $\varepsilon = -1 kT$. The dashed line corresponds to a power law $-4/3$. SCMF: triangles and MC: squares	78

- 3.12 Loop volume fraction profiles obtained from Single Chain Mean Field (SCMF) and Monte Carlo (MC) simulations. Conditions of the system are: $N = 200$, $\phi^0 = 0.11$ and $\varepsilon = -1 kT$. SCMF: triangles and MC: squares 78
- 3.13 Tail volume fraction profiles obtained from Single Chain Mean Field (SCMF) and Monte Carlo (MC) simulations. Conditions of the system are: $N = 200$, $\phi^0 = 0.11$ and $\varepsilon = -1 kT$. SCMF: triangles and MC: squares 79
- 3.14 Variation of *rms* thickness as a function of bulk volume fraction. Conditions of the system: $N = 200$ and $\varepsilon = -1 kT$. Single Chain Mean Field results (SCMF) are represented by triangles and Monte Carlo results (MC) by squares. 80
- 3.15 Variation of loop *rms* thickness as a function of bulk volume fraction. Conditions of the system: $N = 200$ and $\varepsilon = -1 kT$. Single Chain Mean Field results (SCMF) are represented by triangles and Monte Carlo results (MC) by squares. 80
- 3.16 Variation of tail *rms* thickness as a function of bulk volume fraction. Conditions of the system: $N = 200$ and $\varepsilon = -1 kT$. Single Chain Mean Field results (SCMF) are represented by triangles and Monte Carlo results (MC) by squares. The value of ϕ^* , obtained from SCMF method, is equal to 0.061. 81
- 3.17 Variation of the adsorbance (number of monomers per l^2) in function of bulk volume fraction. Conditions of the system: $N = 200$ and $\varepsilon = -1 kT$. Single Chain Mean Field results (SCMF) are represented by triangles and Monte Carlo results (MC) by squares 82
- 3.18 Loop (a) and tail (b) monomer volume fraction profiles corresponding to markovian and self-avoiding walk (SAW) chains. Conditions of the system: $N = 200$, $\phi^0 = 0.0026$, $\varepsilon = -1 kT$. Markovian results are obtained from Scheutjens-Fleer method (SCF) (circles) and Single Chain Mean Field (SCMF) method (triangles). In the case of self-avoiding walk results (SAW), they are obtained from Monte Carlo method (MC), dashed line, simulations and Single Chain Mean Field method (SCMF), full line. 84
- 3.19 Loop (a) and tail (b) monomer volume fraction profiles corresponding to markovian and self-avoiding walk(SAW) chains. Conditions of the system: $N = 200$, $\phi^0 = 0.11$, $\varepsilon = -1 kT$. Markovian results are obtained from Scheutjens-Fleer method (SCF) (circles) and Single Chain Mean Field (SCMF) method (triangles). In the case of self-avoiding walk results (SAW), they are obtained from Monte Carlo (MC), dashed line, simulations and Single Chain Mean Field method (SCMF), full line. 85
- 3.20 Illustration of periodic boundary conditions in the case of adsorption of polymers. The part of the conformation (dotted line) that passes the boundary plane is re-inserted in the opposite plane as a continuation of the original chain 89

4.1	Variation of the energy of the configurational file, $E = -\sum_{\gamma} H_{mf}(\gamma)$, with Monte Carlo (MC) steps in the case of adsorption of polymers on a sphere of radius $R/l = 1.36$ with $N = 100$ and $\varepsilon = -0.35$	97
4.2	Variation of the energy of the configurational file, $E = -\sum_{\gamma} H_{mf}(\gamma)$, with Monte Carlo (MC) steps in the case of adsorption of polymers on a sphere of radius $R/l = 55.3$ with $N = 100$ and $\varepsilon = -0.35$	97
4.3	Variation of the average number of adsorbed monomers of the configurational file with Monte Carlo (MC) steps in the case of adsorption of polymers on a sphere of radius $R/l = 1.36$ with $N = 100$ and $\varepsilon = -0.35$	98
4.4	Variation of the average number of adsorbed monomers of the configurational file with Monte Carlo (MC) steps in the case of adsorption of polymers on a sphere of radius $R/l = 55.3$ with $N = 100$ and $\varepsilon = -0.35$	98
4.5	Representation of the adsorbed polymer layer on a particle whose radius R is $z_w^* < R < \lambda$, where z^* and z_w^* is the crossover distance corresponding to the adsorption on spherical and planar surfaces, respectively, and λ is the thickness of the layer of order the size of the polymer R_g	100
4.6	Total monomer volume fraction profiles for different sizes of sphere ($R/l = 1.36$ (circles), 5.08 (squares), 8.8 (diamonds), 18.1 (triangles), 36.7 (triangles left) and 55.3 (triangles down)) as a function to the center of the sphere. The total monomer volume fraction profile corresponding to the adsorption on flat surfaces (crosses) is also plotted.	104
4.7	Total monomer volume fraction profiles for different sizes of sphere ($R/l = 1.36$ (circles), 8.8 (diamonds) and 55.3 (triangles down)) as well as for the adsorption on planar surfaces (crosses), as a function to the distance from the surface. Dashed line shows a power law of $-4/3$	105
4.8	Variation of the average energy per adsorbed chain ($\langle H_{mf} \rangle$) with the sphere size.	105
4.9	Variation of the adsorbed end-distribution for different sizes of sphere ($R/l = 1.36$ (circles), 5.08 (squares) and 55.3 (triangles down)) as well as for the adsorption on plane surfaces (crosses), with respect to the distance from the surface. Dashed line shows a power law of -0.532	106
4.10	Loop volume fraction profiles as a function of sphere radius ($R/l = 1.36$ (circles), 8.8 (diamonds), 18.1 (stars), 36.7 (triangles left) and 55.3 (crosses)). System conditions: $N = 100$, $\varepsilon = -0.35 kT$ and $\phi^0 = 0.001$	108
4.11	Tail volume fraction profiles as a function of sphere radius ($R/l = 1.36$ (circles), 8.8 (diamonds), 18.1 (stars), 36.7 (triangles left) and 55.3 (crosses)). System conditions: $N = 100$, $\varepsilon = -0.35 kT$ and $\phi^0 = 0.001$	108

4.12	Variation of the crossover distance z^* with the sphere size. Full line shows the crossover distance (z_w^*) obtained in the adsorption on flat surfaces. System conditions: $N = 100$, $\varepsilon = -0.35 kT$ and $\phi^0 = 0.001$	109
4.13	Variation of z^*/z_w^* as a function of the ratio R/z_w^* for two chain lengths ($N = 100$ (triangles) and 200 (circles)), $\phi^0 = 0.001$ and $\varepsilon = -0.35 kT$. The values of z_w^*/l are 6.08 and 7.86 for $N = 100$ and 200 , respectively.	109
4.14	Variation of the loop (triangles) and tail (circles) <i>rms</i> thickness with the sphere radius. System conditions: $N = 100$, $\phi^0 = 0.001$ and $\varepsilon = -0.35 kT$	110
4.15	Variation of the <i>rms</i> thickness with the sphere radius. System conditions: $N = 100$, $\phi^0 = 0.001$ and $\varepsilon = -0.35 kT$	110
4.16	Variation of the adsorbance (number of monomers per l^2) with the sphere size. System conditions: $N = 100$, $\phi^0 = 0.001$ and $\varepsilon = -0.35 kT$	111
4.17	Variation of the loop (circles) and tail (squares) adsorbance (number of monomers per l^2) with the sphere size. System conditions: $N = 100$, $\phi^0 = 0.001$ and $\varepsilon = -0.35 kT$. .	112
4.18	Variation of the loop (circles) and tail (squares) adsorbance (number of monomers per l^2) with the sphere size. System conditions: $N = 200$, $\phi^0 = 0.001$ and $\varepsilon = -0.35 kT$. .	112
4.19	Histogram of loops for three sphere sizes ($R/l = 1.36$ (full line), 5.08 (dash dot line) and 55.3 (short dash line)). System conditions: $N = 100$, $\phi^0 = 0.001$ and $\varepsilon = -0.35 kT$. . .	114
4.20	Histogram of tails for three sphere sizes ($R/l = 1.36$ (full line), 5.08 (dash dot line) and 55.3 (short dash line)). System conditions: $N = 100$, $\phi^0 = 0.001$ and $\varepsilon = -0.35 kT$. . .	114
4.21	Histogram of loops for two values of ε ($-0.35 kT$ (full line) and $-1 kT$ (dashed line)) considering the sphere size $R/l = 1.36$, $N = 100$ and $\phi^0 = 0.001$	115
4.22	Histogram of tails for two values of ε ($-0.35 kT$ (full line) and $-1 kT$ (dashed line)) considering the sphere size $R/l = 1.36$, $N = 100$ and $\phi^0 = 0.001$	115
4.23	Contour plot of tails for the sphere size $R/l = 1.36$. System conditions: $N = 100$, $\phi^0 = 0.001$ and $\varepsilon = -0.35 kT$. We name the shortest tail as n_1 and the largest as n_2 . . .	116
4.24	Contour plot of tails for the sphere size $R/l = 1.36$. System conditions: $N = 100$, $\phi^0 = 0.001$ and $\varepsilon = -1 kT$. We name the shortest tail as n_1 and the largest as n_2	117
5.1	Adsorption of polymers onto colloidal particles: large sphere (case a) and small sphere (case b).	124
5.2	Star-shaped complex ($q=2$, $p=4$)	127

List of Tables

3.1	Values of radius of gyration and end-to-end distances corresponding to self-avoiding walk as well as markovian chains, obtained from Single Chain Mean Field method (SCMF), for different chain lengths. The coefficient A and the exponent ν are the results of a fit of the data of Fig. 3.3, for $N \geq 100$, of the form $R_{g,end}/l = AN^\nu$	66
3.2	Characteristic lengths of the adsorbed layer obtained from Single Chain Mean Field method (SCMF). For $N = 100$, the bulk monomer volume fraction is 0.058, and 0.033 for $N = 200$ monomers. In both cases, $\varepsilon = -0.35kT$	69
3.3	Volume fraction at contact with the wall for different bulk monomer volume fractions. The results correspond to an adsorption energy $\varepsilon = -1kT$, being obtained by means of Single Chain Mean Field (SCMF) for polymer lengths $N = 100$ and $N = 200$, as well as for Monte Carlo (MC) simulations for chains $N = 200$	74
3.4	Characteristic dimensions of the adsorbed layer, in units of l , obtained from Single Chain Mean Field (SCMF) and Monte Carlo (MC) methods, for various bulk volume fractions.	76
4.1	Characteristic lengths of the adsorbed layer obtained from Single Chain Mean Field method (SCMF) for sphere radii ranging from $R = 1.36l$ to $R = 55.3l$ and for plane wall case. System conditions: $N = 100$, $\phi^0 = 0.001$ and $\varepsilon = -0.35kT$	104
4.2	Average number of adsorbed chain ends at distances $r \geq R$ and $r \geq 2R$, being r the distance from the center of the colloidal particle. System conditions: $N = 100$, $\phi^0 = 0.001$ and $\varepsilon = -1kT$	106

Chapter 1

Introduction

A *polymer* is a large molecule constructed from many smaller structural units called *monomers* joined together by covalent bonds. Polymers have existed in natural form since life began and those such as DNA, RNA, proteins and polysaccharides are some of the most important macromolecules found in plant and animal life. From the earliest times, the man has used many of these polymers as materials for providing clothing, decoration, tools, weapons and other requirements. However, the origins of today's polymer industry commonly are accepted as being in the nineteenth century when important discoveries were made concerning the modification of certain natural polymers, as cellulose and Gutta-percha. In our days, the name polymer is mostly used for molecules with a few repeating monomeric units, usually artificially made. [1]

The use of synthetic and natural polymers as stabilisers for colloid systems (sols, dispersions, microemulsions, etc.) is becoming more important everyday in contemporary life. Polymer additives can be applied in preconcentrations and dehydration of suspensions in mineral processing, purifications of drinking and wastewater and even in nutritional and pharmaceutical emulsions. These properties are controlled by the manipulation of a very large number of variables, which will determine the molecular composition and the morphology of the material. Examples of these variables can be the molecular architecture of homopolymer (linear, star, long-branched), the molecular weight distribution or the processing conditions used as, for example, the temperature-pressure history or the flow field. However, in industrial practice is frequent to find problems in materials design in both their synthesis and processing. These problems have to be solved subject to strong financial and time constraints, which are crucial factors in the success and survival of a given industry. An example of the kind of problems to be solved is the search for chemical modifications to reduce the permeability of a semicrystalline plastic in order to increase the shelf-life of beverage bottles, made with this polymer, without affecting their mechanical properties. Traditionally, these problems are solved experimentally studying a

large sets of homologous systems, helped by phenomenological correlations (systematized in convenient algebraic forms) between chemical constitution, morphology and physico-chemical properties, but with large remains of trial-and-error procedures.

In the mid-1980s, the importance of the design of new polymeric materials in addition to the use of quantum, statistical theories and simulations, in order to help or replace these phenomenological correlations, suffered an important rise. These kinds of modelling approaches, based on a fundamental molecular description, present many advantages over phenomenological correlations, based on macroscopic observations. On the one hand, these theories can be used in situations in which the experimental data are scarce and difficult to be obtained, or even prohibitively expensive. On the other hand, they give the possibility to study a very wide range of properties using a minimal set of model parameters.

However, the use of these molecular methods also present disadvantages. Computer simulations are limited to small systems by the excessive demand of computer time when the number of degrees of freedom to be described is large. In molecular simulations the conformations of polymer chain are generated via many random moves, where the interactions present in the systems as well as the consideration of self-avoidance chains are taken into account. In all many-body simulations, it is essential to perform an adequate sampling of the phase space of the model system, which is an important problem for systems of long chain molecules, particularly at high densities, when the number of conformations grows exponentially with the number of monomers of the chain. As far as molecular simulation methods are concerned, it can be mentioned the *Monte Carlo* methods (MC) and *Molecular dynamics* (MD). The original MC algorithm was developed by Metropolis *et al.* in 1953 [2] and has been applied in various areas of statistical physics including polymer physics problems [3, 4, 5]. MC method uses a statistical sampling of the conformation space, where only energetically significant conformations are taken into account. Thus, many properties of the system as, for example, the polymer density profile, are calculated as an average over all the sampled conformations with its statistical weight. Many MC schemes have been proposed to sample the configuration space in both homogenous and confined polymeric system. Among these methods, we can distinguish the *Configurational-Bias Monte Carlo* (CBMC) technique, developed by Siepmann and Frenkel [6], which has been used in many applications such as the simulation of phase equilibria of chain molecules [7] or the simulation of polymer adsorption on surfaces [8]. Molecular dynamics simulations solves the integration of Newton's equations of motion in real space for each particle that constitutes the polymer chain, and whose interactions are directly taken into account by means of inter-atomic potentials. However, important computational limitations are found due to its difficult to study *slow* processes that need large time frames (larger than hundreds of picoseconds), such as the dynamics of polymer adsorption and relaxation. Despite of these drawbacks, MD models have been succesful in gaining physical insight in various areas of polymer science. Thus, applying MD simulations,

polymer adsorption phenomena have been studied, for example, by Murat *et al.* [9] and Kramarenko *et al.* [10], among others.

Together with the simulation method, many analytical theories have been developed to describe the structure of adsorbed polymeric layer. Most of these theories are based on a classical *mean-field approximation* [11, 12] or on a phenomenological *scaling* approach [13]. Such theories do not take into account directly the details of the chain chemical structure and the nature of the intermolecular potentials. Mean-field theories essentially describe one chain in an effective potential field, known as the mean-field potential, which is self-consistently determined from the solution of the mean field problem, taking into account all the segment-segment interactions found in the system. The application of the mean-field theories is limited by the assumption that it is assumed that spatial fluctuations in the local segment density are negligible. From a general point of view mean-field theories for polymer adsorption extended the standard Flory-Huggins picture of polymer solutions allowing the calculation of free energies in systems with concentration gradients.

In the early 80's, de Gennes analyzed the behaviour of polymers adsorbed at interfaces considering a mean-field approach. The properties of the adsorbed polymeric layer are obtained by the minimization of an appropriate surface free energy functional constructed including a local swelling of the chain and the proper functional form of the osmotic pressure, such that the adequate scaling laws are obtained. This approach is very illustrating since, as the work done in chapters 2, 3 and 4 of this thesis, shows that proper scaling laws are compatible with a mean-field treatment. The approach of de Gennes has been used, through one order parameter theory, to analyze polymer layers under different solvent conditions [14, 15, 16, 17]. Previous approaches were based on Edwards treatment [18] in the *Ground State Dominance approximation* [19] and reproduce the scaling laws proper of ideal chains. However, all these approximations based on one-order parameter theories give no description of finite size effects. It is thus only valid for extremely long chains and restricted to the region close to the surface. More recently, Semenov *et al.* [20] presented a theoretical description based on a mean-field approximation within the framework of ideal chains but going beyond the standard ground state dominance approximation. Thus, in this approach using two coupled order parameters, the finite size of the polymer chains is taken into account as well as the relative contributions of loops, tails and free chains to the polymer concentration at a given distance from the adsorbing layer.

However, the mean-field theory based on ideal chain behavior breaks down under good solvent conditions. The ideal chain mean-field description is correct under the so-called marginal solvency conditions, in which the excluded volume is weak and can be treated perturbatively. To include the effect of these excluded volume correlations in an analytical theory, it is necessary to introduce the ideas used by renormalization group theory, which was originally developed to study of critical phenomena. The basic idea of this theory is to see the change observed in the macroscopic properties of the system when the basic

scales of the model are altered. The scaling approach presented by de Gennes [13] is also reminiscent of critical phenomena in this sense. De Gennes argued that, in a good solvent, long flexible chains strongly adsorbed on a solid wall build a self-similar diffuse layer with no characteristic length. Thus, the local correlation length, depending on the local monomer concentration, should scale as the distance to the wall. De Gennes found that the overall concentration profile falls off from the wall as $c(z) \sim z^{-4/3}$, in contrast to the mean field prediction where $c(z) \sim z^{-2}$. In the mid-1990s, Semenov and Joanny [21] presented another version of the scaling theory in which the structure of the adsorbed layer is considered as separated into two regions being the inner dominated by loops while the tails dominate the region beyond a characteristic distance $z^* \sim N^{1/d-1}$, where N is the polymerization index and d the space dimension. The existence of a characteristic length in the adsorbed layer is the most important theoretical results of these authors. Later, also a mean-field theory based on the statistics of ideal chains was developed to account for the new structure of the layer [20, 22].

All the theoretical approaches discussed previously have their applicability limited to very long chains. In this context, an important complement to the analytical theories is the use of computers to solve the statistical mechanical problem of polymers near interfaces, which yield results far from the asymptotic regimes studied by the analytical treatments. One of the most known techniques is the numerical lattice *Self-consistent Field* (SCF), which offers a numerical solution of the mean-field problem for chains of finite size. In this direction, the first works developed in adsorption of polymers were done by DiMarzio and Rubin [23, 24], being extended by Scheutjens and Fleer [25, 26]. The SCF solves the Schrödinger or modified diffusion equation due to Edwards [18], giving the propagator or statistical weight of one chain in a self-consistent field, from which all other physical properties are derived. The main characteristic in the use of this theory is the markovian nature of the chains, i.e. without excluded volume correlations along the chain, since they are considered as being ideal chains embedded in a mean-field.

This work aims at developing appropriate numerical and analytical modelling techniques, which can describe the structure of a polymeric layer adsorbed on a solid surface, taking into account the excluded volume correlations along the chain. In the first place, the methodology known as *Single Chain Mean Field* (SCMF), originally developed by Ben-Shaul, Szleifer and coworkers [27, 28], has been modified to include an importance sampling methodology, suitable for polymer adsorption problems. In this way, it has been possible to numerically calculate properties that can be experimentally measured, such as monomer volume fraction profiles, adsorbance or thickness of the adsorbed polymer layer, and compare with the results issued from other methodologies. The theoretical background concerning the use of this importance sampling method and a review of the SCMF theory is given in chapter 2.

To check the efficiency of our method, firstly, we concentrated our attention in the study of polymer adsorption on flat surfaces. The SCMF results with self-avoiding chains

have been compared with lattice multi-chain Monte Carlo simulations, for the same values of the chain length, adsorption energy and bulk concentrations. In this part of the work, presented in chapter 3, we have calculated the properties of the adsorbed layer such as the total, loop and tail monomer density profiles, adsorbance and thickness obtaining, in all these cases, the same density dependence for both methods, SCMF and MC. For completeness, the results obtained with our method, employing ideal chains in the sampling of the phase space, were compared with those obtained from self-consistent method of Scheutjens and Fleer (SCF) [26]. The results found are in very good agreement with the calculations in each case.

In spherical surfaces, the influence of the curvature on the structure of grafted polymer layers has been the subject of numerous studies from theoretical and numerical point of view [29, 30]. In the case of the adsorption, we can mention theoretical and experimental works [31, 32, 33, 34]. However, there are only a few studies [35] that analyse the structure of the layer, studying the total density profile, adsorbance or the thickness of the adsorbed layer for a wide range of radii, from a numerical point of view. Thus, up to the best of our knowledge no detailed analysis of the structure of the adsorbed layer formed by relatively short polymers on spherical particles has been given. Hence, our results, obtained from the modified SCMF method, are the first giving quantitative predictions about the structure adsorbed polymeric layers onto spherical particles. We present this analysis in chapter 4.

Finally, chapter 5 is devoted to the introduction of an scaling analysis suitable for the treatment of polymer-colloid mixtures, which complements the studies done in previous chapters. In this latter chapter the scaling point of view adopted in ref. [21] for flat surfaces is used as an starting point for adsorption of polymers onto small particles [36]. In particular, we have paid special attention to the interaction between different particles mediated by polymers as well as the structure of a system of isolated particles and many polymers adsorbed on them. One of the key problems of polymer-colloid systems is the prediction of the types of structures formed as a result of interaction of macromolecules with the particles. It has been shown experimentally [37] that if the density of colloids and polymers is sufficiently large, the adsorption onto the colloidal surface can lead to physical crosslinking and to the formation of a gel. The analytical theory developed in this work has been focussed to study the formation of star-shaped complexes from the dilute polymer-colloid solutions as well as the formation of this gelation transition, produced in semidilute conditions from the formation of similar complexes.

Summarizing, this dissertation can be naturally divided into three parts. The first part is this introduction, which includes a review of general aspects of polymer solutions and polymer adsorption, as well as of the other theoretical treatments of polymer solutions in general, which will serve to grasp the context in which our work is inserted. The reader familiar with the phenomenology and theoretical background of polymer adsorption can skip the rest of this chapter. The second part is related to the development and application of the new SCMF theory, which embraces chapters 2, 3 and 4. The third part, which only

contains chapter 5, corresponds to a scaling description of the polymer adsorption on colloidal particles in colloid-polymer mixtures. Finally, in chapter 6 we propose possible applications of the developed methodology as suggestion of future work.

1.1 Polymers in solution

1.1.1 General aspects

Polymer chains can be characterized by their degree of flexibility. It is possible to find flexible macromolecules, in which a substantial bend can be formed over a length of several links (Fig. 1.1.a), as a result of the rotation around the backbone bonds. Stiff-chain macromolecules are those in which bend needs much greater lengths to become appreciable (Fig. 1.1.b) and macromolecules without any kind of flexibility behave as stiff rods or rigid general conformations (Fig. 1.1.c).

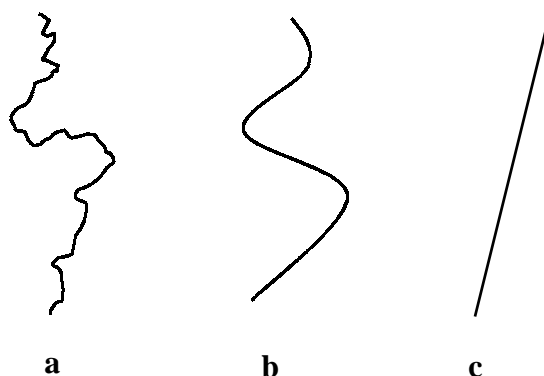


Figure 1.1: Representation of different types of polymers depending on their degrees of flexibility. **a.** Flexible chain; **b.** Stiff chain; **c.** Rigid chain.

Each polymer molecule in solution is bombarded by the solvent molecules and the other polymers, due to the thermal energy of the system. Thus, polymers not only diffuse in solution and rotate but also move through a huge range of conformations, whose number increases exponentially with the number of segments of the chain. The average conformation is neither fully extended nor fully compressed, since both are highly ordered states, but polymers present in solution a high conformational entropy thus adopting a fuzzy coil-like structure. In the presence of interfaces as, for instance, an adsorbing wall, the resulting structure will be given by the competition between the tendency to a maximal disordered state and the energetic gain that implies be in contact with the adsorbing wall.

Therefore, due to their configurational entropy, polymers in solution would tend to adopt, on average, an intermediate conformation called *random coil*, more or less spherical, with a relatively high concentration of monomer units in the central region and a more dilute periphery. The monomer-monomer interactions, however, introduce a configurational constraint, preventing the monomers to overlap, due to a high energy penalty

issued from the repulsive molecular potentials. This effect is known as the *excluded-volume* interaction, which plays a crucial role in the understanding of polymer solutions. The excluded volume interaction is a collective effect that depends on the relative intensity of the mutual monomer-monomer and monomer-solvent interactions. If the monomer-solvent attraction is dominating, then the polymer dissolves well in the solvent and the latter is referred to as *good solvent*. As such, the excluded volume interaction is dependent on the temperature. The temperature at which the second virial coefficient vanishes is known as the θ -temperature, and the conformational entropy of the polymer determines its behavior. If the excluded volume interaction is independent of the temperature, in a given range, then the solvent is referred to as *athermal* [13, 38, 39].

Ideal Chains

There are several theories whose main objective is to explain those physico-chemical properties depending on the overall polymer structure. These properties are universal in the sense that, apart from the values of certain coefficients, the qualitative behavior is the same independently of the chemical structure. We will briefly discuss how the models are constructed. We will start with the simple case, in which the excluded volume interactions are neglected.

The simplest model considers the polymer as an ideal chain whose the bonds between atoms in the backbone are treated as vectors connecting volumeless points without interaction with each other. Therefore the polymer is modelled as a freely jointed chain of N segments each of length l . Each segment, known as Kuhn segment, does not correspond to a chemical monomeric unit, but to a sequence of monomers which reflect the local intrinsic stiffness of the backbone [40]. An example would be the model used by Szleifer [41] to study the adsorption of protein molecules on PEO grafted surfaces, in which each segment represents a $(CH_2 - CH_2 - O)$ group with an effective length l .

In the *random flight model*, the polymer is modeled as a sequence of N segments whose orientation in space is completely random. There is no restriction on the direction of each segment and on the overlap, so that the conformation resembles the trajectory of a particle diffusing under the action of a random force or Brownian movement. The chain is Markovian, in the sense that dividing the chain into two parts, each part is statistically independent of the other. This Markovian property is inherent to all the self-consistent field theories based on Edwards equation, which will be discussed later on [39].

It is interesting to derive some simple properties from the random flight model, which will serve us to introduce properties of ideal chains in solution. The conformation of a chain can be represented by $N + 1$ position vectors $\{\mathbf{R}_n\}$ with $n = 0 \dots N$, or also by the set of bond vectors $\{\mathbf{r}_n\}$ where

$$\mathbf{r}_n = \mathbf{R}_n - \mathbf{R}_{n-1} \quad (1.1)$$

In the random flight model the bond lengths have to be fixed ($|\mathbf{R}_n - \mathbf{R}_{n+1}| = l$). The distance between the end points of the chain is the *root mean square end-to-end distance*, R_{end} .

$$R_{end}^2 \equiv \langle (\mathbf{R}_0 - \mathbf{R}_N)^2 \rangle = \left\langle \left(\sum_{n=1}^N \mathbf{r}_n \right)^2 \right\rangle \quad (1.2)$$

where the brackets represent the average over all configurations that the chain may adopt. The mean *end-to-end distance*, R_{end} , is a measure of the size of the chain and, in fact, could be considered as being the mean coil diameter. Since there is no correlations between segments, then one has

$$\mathbf{r}_n \cdot \mathbf{r}_m = \delta_{nm} \quad (1.3)$$

where δ_{nm} stands here for the Kronecker δ symbol, being its value 1 if $n = m$ and zero otherwise. The mean square displacement is proportional to N , the index of polymerization. Thus,

$$R_{end}^2 = \sum_{n,m=1}^N \langle \mathbf{r}_n \cdot \mathbf{r}_m \rangle = \sum_{n=1}^N \langle \mathbf{r}_n^2 \rangle + 2 \sum_{n>m} \langle \mathbf{r}_n \cdot \mathbf{r}_m \rangle = Nl^2 \quad (1.4)$$

as \mathbf{r}_m and \mathbf{r}_n are statistically independent, according to eq. (1.3). Thus, the end-to-end distance corresponding to the ideal chains satisfies a power-law behavior in the polymer size N , with an exponent 1/2, which is characteristic of the ideal chain behavior.

The size of the coil can be also measured in terms of the *radius of gyration*, R_g , which is the root mean-square distance of the segments from the centre of mass of the chain, $\mathbf{R}_{cm} = (\sum_{i=0}^N \mathbf{R}_i)/(N+1)$.

$$R_g^2 = \left\langle \frac{\sum_{i=0}^N (\mathbf{R}_i - \mathbf{R}_{cm})^2}{N+1} \right\rangle = \left\langle \frac{\sum_{0 \leq i < j \leq N} (\mathbf{R}_i - \mathbf{R}_j)^2}{N+1} \right\rangle \quad (1.5)$$

The radius of gyration of a polymer in solution can be obtained experimentally by elastic light scattering. Thus, the radius of gyration of a gaussian coil is related with end-to-end distance by the relation

$$R_g^2 = (R_{end}^2/6) = \frac{1}{6}Nl^2 \quad (1.6)$$

Therefore, the both measures of the overall size of the chain obey a square root law with the index of polymerization. This exponent, known as *exponent of Flory*, ν [42], is independent of the type of polymer considered and the only condition is that the chain has to be very flexible, no excluded volume interactions present, and sufficiently long. Furthermore, since the model does not incorporate microscopic details on the nature of the monomers, such a behavior is universal and independent of the chemical composition, provided that the just mentioned properties of the chain are given.

The statistical distribution of the end-to-end vector of an ideal polymer is gaussian

Again, it is considered a freely jointed chain of independent N vectors randomly oriented. If the length of the chain is very large ($N \rightarrow \infty$), since all the segments are statistically independent and according to the central limit theorem, the probability distribution function, corresponding to the end-to-end vector ($P_N(\mathbf{R}_{end})$), is a Gaussian distribution, i.e.

$$P_N(\mathbf{R}_{end}) = (2\pi Nl^2/3)^{-3/2} \exp[-3\mathbf{R}_{end}^2/(2Nl^2)] \quad (1.7)$$

where the factor $(2\pi Nl^2/3)^{-3/2}$ is obtained from the normalization condition,

$$\int P_N(\mathbf{R}_{end})d\mathbf{R}_{end} = 1 \quad (1.8)$$

In general, for any pair of monomers n and m , the probability distribution of the vector $\mathbf{R}_m - \mathbf{R}_n$ is also Gaussian, provided that $|m - n| \gg 1$ [39].

Since the polymer chain is an object bearing a large number of degrees of freedom, we can assign a conformational entropy per chain. Effectively, fixing the end-to-end distance, as a measure of the overall size of the polymer, one can use Boltzmann formula to write

$$S(\mathbf{R}_{end}) \simeq k \ln P_N(\mathbf{R}_{end}) \simeq S_0 - \frac{3k\mathbf{R}_{end}^2}{2Nl^2} \quad (1.9)$$

where S_0 is a residual entropy independent of the extension of the chain, and k is Boltzmann's constant. From this entropic consideration, it is also possible to regard the chain

as a Hooke spring, whose tension is the product of the entropy reduction associated to the decrease of the conformations compatible with a large R_{end} , times the temperature. This apparent elasticity of the polymer coil has been used as a base of simple statistical mechanical models of polymers [38, 39]. Let us write the free energy F as

$$F(\mathbf{R}_{end}) = U_0 - TS(\mathbf{R}_{end}) = F_0 + \frac{3kT}{2Nl^2} \mathbf{R}_{end}^2 \quad (1.10)$$

where U_0 and F_0 are contributions independent of the chain extension. Thus, the effective spring constant can be identified as being

$$H = -\frac{3kT}{Nl^2} \quad (1.11)$$

which depends on the temperature. This simple argument has been used to give an explanation of the temperature dependence of rubber elasticity [1].

Excluded volume

In the ideal chain model, the volume of the segments and the solvency effects are ignored. It gives a reasonable description in poor solvents, where the segments do not experiment a net preference for the solvent molecules (the second virial coefficient is very small), hence more compact conformations are energetically preferred. However, as mentioned, in the case of solutions of polymers in good solvents the excluded volume becomes important. In these conditions, the interaction between monomers and solvent molecules is favourable in front of the monomer-monomer interactions, which becomes effectively repulsive. The excluded volume interactions cause a swelling of the polymeric coil, which prefers to sacrifice some entropy to reduce the monomer-monomer interactions. However, when this interaction is relevant, there appear significant changes in the statistical behavior of polymers. Effectively, the overall size of the polymer no longer scales as $N^{1/2}$, but with a different Flory exponent ν [13]. The Markovian nature of the ideal chain is lost due to the fact that two segments of the chain can be correlated if they meet close in space, regardless how far are along the chain backbone. These excluded volume correlations are crucial in the understanding of the properties of polymers in good solvents.

Flory was the first to understand the influence that excluded volume plays in polymer solutions. He devised an easy way to obtain the exponent ν for all dimensionalities, by means of simple arguments. We can begin considering an isolated polymer coil in solution of a certain unknown radius, R . Then, the internal monomer concentration would scale as

$$c_{int} = \frac{N}{R^d} \quad (1.12)$$

where d is the dimensionality of the space. There is a certain repulsive energy inside of the coil due to the segments repel each other. This energy, of the order of kT per contact, is proportional to the number of contacts present inside of the coil. An estimate of the number of monomer-monomer contacts is given by the product of the total excluded volume of the chain (proportional to vN , being v , the excluded volume per monomer) with the local monomer concentration c . Hence, this repulsive energy would be proportional to

$$U_{rep} \sim \frac{1}{2}kTvcN \sim kTv\frac{N^2}{R^d} \quad (1.13)$$

The excluded volume parameter is assumed to be of the order of the volume of one monomer, $v \sim l^d$. The arguments presented are *mean field* in nature since all the correlations between monomers are ignored.

The repulsive energy leads to coil expansion. But this swelling may be too large and unfavorable for the entropic contribution of the coil. Flory considered the two opposite effects, writing

$$\frac{F(R)}{kT} = U - TS \sim \frac{vN^2}{R^d} + \frac{R^2}{Nl^2} \quad (1.14)$$

The minimum of this free energy gives us the dependence between the size and polymerization index of the polymer, yielding

$$\frac{\partial F}{\partial R} = 0 \implies R \sim lN^\nu \quad (1.15)$$

being the exponent $\nu = \frac{3}{d+2}$. As we can see, the value of this exponent ν will depend on the dimensionality of the space. Hence, in the case of ideal (gaussian) chains, where $\nu = 1/2$, the value of d would be 4. Thus $d = 4$ is the critical dimension for the excluded volume problem in polymer solutions, at which the contact between monomers is *irrelevant*. At $d = 3$, then, the excluded volume interaction becomes important. In this case, the exponent ν would be $3/5$. Because swelling of the chain, its spatial dimensions are proportional to a higher power of N than $1/2$ (ideal chains), so the radius of gyration would scale with N as $R_g/l \sim N^{3/5}$. The value of ν given by Flory calculations is only approximate in $d = 3$ although exact at $d = 4$ and $d = 2$. Group of Renormalization

theories give a value of ν around $0.588 \sim 0.6$ after an ϵ expansion up to a second order. These values of the exponent have been experimentally verified [43]

In the Flory notation $v = (1 - 2\chi)l^d$ where l^d is the monomer volume and χ is the Flory-Huggins interaction parameter, which measures the excess affinity of segments for each other over that of the solvent, in the Flory-Huggins equation of state. If the value of $\chi = 0$ (or with small χ), we refer to a solution of polymers in good solvents. If $\chi = 1/2$ the behaviour of the polymer molecule is ideal. At these conditions the net excluded volume that causes an expansion of the coil is balanced by the unfavourable polymer-solvent interactions so the polymer chain adopt unperturbed dimensions. This condition is known as θ point, as mentioned.

1.1.2 Semidilute polymer solutions

Scaling theory

In the previous section we have analyzed solutions of polymers in conditions such that whose monomer concentration is low enough so that, on average, the distance between molecules is greater than the radius of gyration of a single molecule (Fig. 1.2.a). In such a dilute regime, all the monomers of the chain are correlated due to excluded volume interactions. Moreover, the concentration fluctuations become important. Thus, it is expected that, in these situations, mean-field calculations fail in properly describing the properties of the system. However, if the polymer concentration is increased, the coils will end up being forced to interpenetrate. The concentration at which the molecules begin to overlap is called *overlap concentration* and is symbolized by c^* (see Fig. 1.2.b). At this concentration, by definition, the polymer coils in solution just fill the available volume without overlapping. Thus, if we consider a polymer of polymerization index N , with a radius of gyration R_g , the value of c^* can be assigned by the equation

$$c^* = \frac{3N}{4\pi R_g^3} \quad (1.16)$$

Thus, the overlap concentration scales, using the Flory result for the radius of the chain, as $N^{-4/5}$ for non-ideal chains (N^{-1} if the chains are ideal), and is a decreasing function of the polymer size. If we increase the concentration beyond c^* , the fluctuations of segment concentration become less important. However, mean field treatments still fail in this regime, known as *semidilute concentration regime*, due to the fact that excluded volume correlations are still present at distances smaller than the bulk correlation length (ξ^0). However, since the relationship established by de Gennes between polymeric solutions and critical phenomena, the dilute and semidilute regime can be studied by the *scaling theory*

[13]. Hence, mean field treatments only provide a qualitative picture of the problem but can give values of the coefficients. Scaling laws are able to provide the correct power-law behavior of the magnitudes of interest, but can neither produce values for the coefficients nor crossover behaviors.

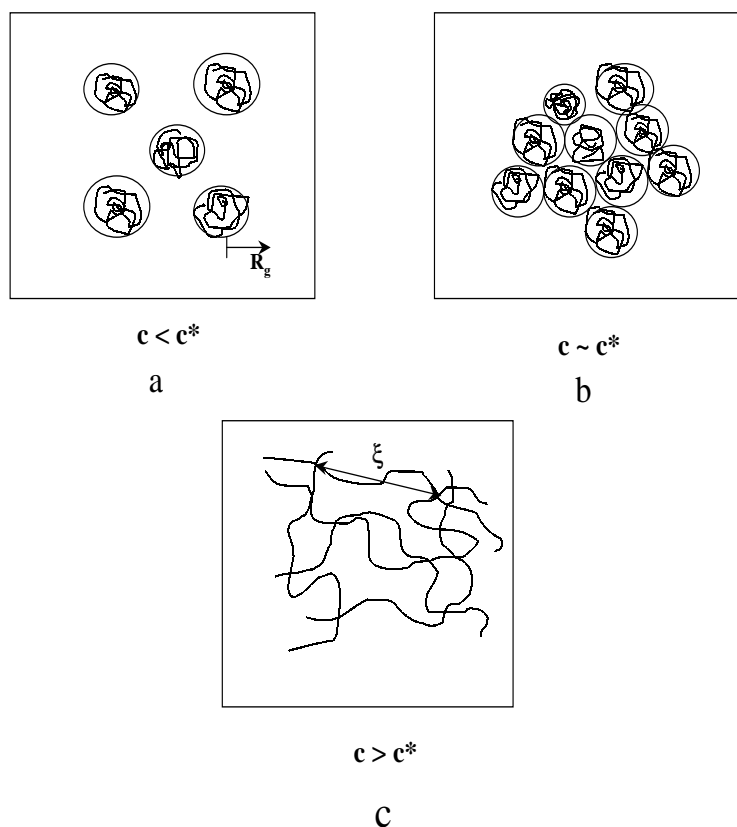


Figure 1.2: Crossover between dilute and semidilute solutions: **a.** corresponds to the dilute conditions, **b.** overlap threshold and **c.** semidilute concentration.

From a scaling point of view, in the semidilute regime the solution resembles a transient network with an average mesh size proportional to the bulk correlation length ξ (see Fig. 1.2.c). If we select one of the chains corresponding to the network of Fig. 1.2.c and increase the magnification, it is possible to see a mesh volume of size ξ^3 that contains a number of monomers g of length l , belonging to a same chain. Thus, our selected molecule can be viewed as a sequence of *blobs* of diameter ξ (see Fig. 1.3), inside which excluded volume correlations prevail. Thus, one can write

$$\xi \sim l g^{3/5} \quad (1.17)$$

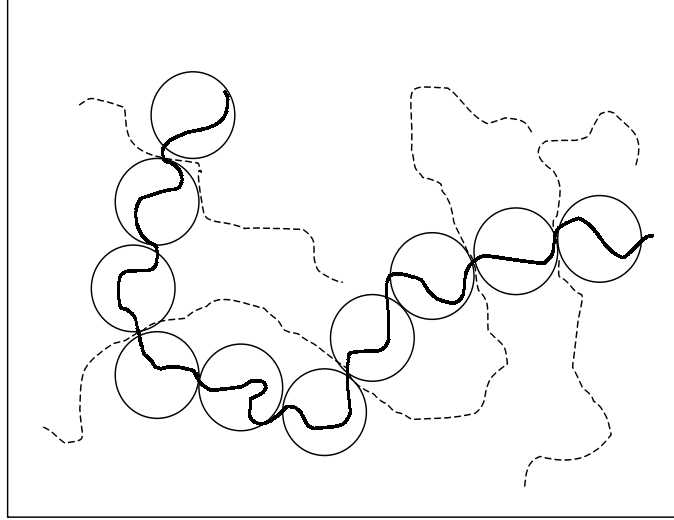


Figure 1.3: The *blob* picture of a chain in a semidilute solution; some of the interacting chains are shown as dashed lines.

With the increase of the polymer concentration, the size of the blobs (i.e. ξ) becomes smaller. Therefore, in semidilute solutions, it is expected that the correlation length does not depend on the chain length, but only on the concentration, if $N \rightarrow \infty$. Thus, using *scale invariance* together with the fact that $\xi \sim N^0$, one ends up writing [13]

$$\xi(c) \sim R_g \left(\frac{c}{c^*} \right)^m \quad (1.18)$$

where R_g is the size of the coil in dilute solutions that depends on the degree of polymerisation according to $R_g \sim l N^\nu$, and the ratio c/c^* is invariant under a redefinition of the number of segments of the chain and the length of each segment. From the eq.(1.16) and considering that ξ does not depend on N , it is possible to find the value of the exponent m in good solvents, yielding $m = -3/4$. Thus, arrives at the non-trivial result

$$\xi(c) \sim c^{-3/4} \quad (1.19)$$

The bulk correlation length is the more important length in semidilute polymer solutions. Some properties can also be deduced from scaling arguments, as for instance, the variation of the global size of a polymer coil as the concentration is varied. To see this, let us assume that the renormalized chain of blobs has a Gaussian distribution since excluded volume correlations are screened beyond ξ . Hence, treating the blob chain as a gaussian chain then

$$R_g^2 \sim \frac{N}{g} \xi^2 \quad (1.20)$$

where ξ plays here the role of the size of the effective monomer, and N/g is the number of these effective monomers in the chain, g being defined from eq. (1.17). By replacing g from eq.(1.17) and taking into account eq.(1.19), we obtain

$$R_g^2 \sim N l^2 c^{-1/4} \quad (1.21)$$

Therefore, the main conclusion is that the radius of gyration as well as the correlation length decrease with the increasing of the concentration for semidilute conditions. Furthermore, if we are in melt conditions, the monomer concentration is $c \simeq 1$. Thus, according to this, we obtain that the chains are ideal in melts. Eq. (1.21), therefore, permits an appropriate crossover between the excluded volume statistics of isolated chains in solution and the ideal behavior of chains in a melt. Due to the fact that the density fluctuations are small in a melt, is precisely in this regime where mean-field approaches may be used without error because all the segments experience, on average, the same force field.

To end this section, it is interesting to note that the eq. (1.15) predicts that the chains in a spatial dimensionality $d = 4$ are ideal. Thus, scaling arguments can also be used to predict the behavior of chains in $d = 4$ since the expected results issued from mean-field theories based on ideal Markovian chains will be in agreement with these scaling laws predicted in this dimensionality, provided that the length of the chains is sufficiently large, eventually $N \rightarrow \infty$.

Effectively, if the ideal behavior is assumed, then the Flory exponent is $\nu = 1/2$, so that we can write

$$c_4^* \sim \frac{N}{R_g^4} \quad (1.22)$$

for the overlap concentration, with $R_g \sim lN^{1/2}$, and

$$\xi_4 \sim lg^{1/2} \quad (1.23)$$

for the correlation length. Here, the subscript 4 is introduced to emphasize that this corresponds to a higher dimensionality space. Then, the dependence of the correlation length with the concentration gives

$$\xi_4(c) \sim R_g \left(\frac{c}{c^*} \right)^m \sim N^0 \Rightarrow \xi_4(c) \sim c^{-1/2} \quad (1.24)$$

which is a different dependence in the concentration than that found in the case of chains with excluded volume interactions in $d = 3$. Finally, the radius of gyration of the chain becomes independent of the concentration in four dimensions, in contrast with the weak dependence given in eq. (1.21).

Markovian self-consistent field theory

After having reviewed a few aspects of the behavior of polymers in solution, here we introduce more in detail the self-consistent mean-field theory due to Edwards, in which chains in solution are treated as ideal chains in an external field that reflects the excluded volume repulsion due to the local presence of monomers. The main aspects of this theory is the Markovian nature of the chains, as far as connectivity is concerned, and the self-consistent determination of the concentration profile from the solution of the one-chain problem. This theory is at the base of the so-called Scheutjens-Fleer numerical procedure that will be described more in detail in the next section.

In inhomogeneous systems, the imposition of composition gradients affects the free energy, essentially in the case where the composition gradients are on the level of the polymer radius of gyration. In 1965, Edwards [18] presented an interesting analogy between the problem of interacting polymers and the classical problem of interacting electrons, where the paths are assimilated to polymer conformations. This analogy was the base to the development of the self-consistent field theory that we are going to describe.

A polymer in solution is characterized by the magnitude $G(\mathbf{r}, \mathbf{r}'; N)$, namely the propagator, which is the statistical weight of a chain of length N that starts at a position \mathbf{r}' and ends at \mathbf{r} . The analogy between an ideal polymer conformations and random walk trajectories of a Brownian particle, makes that the propagator or an ideal, isolated chain (without excluded volume interactions) obeys a diffusion equation of the form

$$\frac{\partial G_0}{\partial N} = \frac{l^2}{6} \nabla^2 G_0 \quad (1.25)$$

where $l^2/6$ is the analogous of the *diffusion coefficient* in Brownian movement. The formal solution of this equation can be expressed as a path integral over all the conformations of the chain with fixed end-points. That is

$$G_0(\mathbf{r}, \mathbf{r}'; N) = \int_{\mathbf{r}_1[\gamma]=\mathbf{r}'}^{\mathbf{r}_N[\gamma]=\mathbf{r}} \mathcal{D}\gamma \exp \left[-\frac{3}{2l^2} \int_1^N dn \left(\frac{\partial \mathbf{r}_n[\gamma]}{\partial n} \right)^2 \right] \quad (1.26)$$

where the symbol $\mathcal{D}\gamma$ stands for a sum over all the conformations. In an interacting system, the random walk is not free, but is affected by a spatially varying field $U(\mathbf{r})$. Thus, statistical weights of the different steps are not equivalent because their dependence on the Boltzmann factor. Thus, the formal solution for the propagator takes the form

$$G(\mathbf{r}, \mathbf{r}'; N) = \int_{\mathbf{r}_1[\gamma]=\mathbf{r}'}^{\mathbf{r}_N[\gamma]=\mathbf{r}} \mathcal{D}\gamma \exp \left[-\frac{3}{2l^2} \int_1^N dn \left(\frac{\partial \mathbf{r}_n[\gamma]}{\partial n} \right)^2 - \frac{1}{kT} \int_1^N dn U(\mathbf{r}_n[\gamma]) \right] \quad (1.27)$$

where $U(\mathbf{r})$ is the potential energy per segment. Considering this latter expression, the diffusion equation is then modified as

$$\frac{\partial G}{\partial n} = \frac{l^2}{6} \nabla^2 G - U(\mathbf{r})G \quad (1.28)$$

This is the basic equation of the self-consistent field theory, which has the same form as the Schrödinger equation. The first term of the equation takes into account the connectivity of the chain, the second corresponds to the tendency of entropic effects to disperse the segments and the third accounts for the action of the potential $U(\mathbf{r})$. If $U(\mathbf{r}) = 0$, the balance between the first and the second term of the equation determines the propagator. If the value of $U(\mathbf{r}) > 0$ then the density of configuration is locally reduced, excluding the chain from that region of space; if $U(\mathbf{r}) < 0$, we have the opposite case.

Eq. (1.28) is however empty if the functional form of $U(\mathbf{r})$ is not given. In the self-consistent field approach, the energetic contribution is due not only to the action of external fields, but also to the repulsion due to excluded volume interactions from the local monomer density. Therefore, one writes

$$U(\mathbf{r}) = vc(\mathbf{r}) + U_{ext}(\mathbf{r}) \quad (1.29)$$

where U_{ext} is the external field and $c(\mathbf{r})$ stands for the average monomer concentration. Furthermore, the average local monomer density is an implicit function of the propagator, which must be self-consistently determined. Thus, the monomer concentration at the space point \mathbf{r} is given by

$$\begin{aligned} c(\mathbf{r}) &= \mathcal{N}_p \frac{\int_1^N dn \int d\mathbf{r}' d\mathbf{r}'' G(\mathbf{r}, \mathbf{r}'; n) G(\mathbf{r}'', \mathbf{r}; N - n)}{\int \int d\mathbf{r}'' d\mathbf{r}' G(\mathbf{r}'', \mathbf{r}'; N)} \\ &= \frac{c^0 e^{vNc^0}}{N} \int dn Z(\mathbf{r}, n) Z(\mathbf{r}, N - n) \end{aligned} \quad (1.30)$$

where the magnitude \mathcal{N}_p is the number of polymer chains in the solution volume, c^0 is the bulk monomer concentration, and $Z(\mathbf{r}, n)$ is the partial partition function obtained from the propagator or Green function by means of the integral

$$Z(\mathbf{r}, n) \equiv \int d\mathbf{r}' G(\mathbf{r}, \mathbf{r}'; n) \quad (1.31)$$

The partial partition function is the statistical weight of a chain segment with length n in which one of the terminal links (indexed 1) is fixed in space while the another one is anywhere. From this new magnitude, the diffusion-type eq.(1.28) is rewritten as

$$\frac{\partial Z}{\partial n} = \frac{l^2}{6} \nabla^2 Z - \left(\frac{v c^0 e^{vNc^0}}{N} \int Z(\mathbf{r}, n) Z(\mathbf{r}, N - n) dn + U_{ext} \right) Z \quad (1.32)$$

obtained by the integration of the eq.(1.28) with respect to \mathbf{r} , using the definition of eq. (1.31) and the relation eq.(1.30). Finally, the denominator in eq. (1.30) has to be explicitly considered. Effectively, the double integral of the propagator gives the total statistical weight of a polymer chain in the system, that is the total partition function. Thus, the following relation holds

$$\int \int d\mathbf{r}' d\mathbf{r}'' G(\mathbf{r}'', \mathbf{r}'; N) = \mathcal{N}_p e^{-\mu_p/kT} = \frac{\mathcal{N}_p N}{v c^0} e^{-vNc^0} \quad (1.33)$$

where the polymer chemical potential is given by

$$\frac{\mu_p}{kT} = \ln \frac{v c^0}{N} + v c^0 N \quad (1.34)$$

as it follows from eq. (1.33) and the solution of eq. (1.28) for an homogeneous system of fixed concentration c^0 .

Along this work we will often refer to what we have denoted as *Markovian connectivity*, which has been already mentioned several times. This intrinsic property of a given chain model can be stated as

$$G(\mathbf{r}'', \mathbf{r}; N) = \int d\mathbf{r}' G(\mathbf{r}', \mathbf{r}; n) G(\mathbf{r}'', \mathbf{r}'; N - n) \quad (1.35)$$

In a more intuitive way, this property indicates that the number and the statistical weight of the conformations of a segment of chain of n monomers is independent of the conformations taken by the rest of the $N - n$ monomers of the chain. This property, expressed in eq. (1.35), is implicitly used in the relationship established between the average monomer density and the propagator, as given in eq. (1.30). Obviously, if excluded volume interactions are exactly taken into account (not in mean), this property is not going to be satisfied. In the literature it is customary to associate mean field calculations with the so-called Gaussian statistics. However, we will demonstrate along this work that the mean-field nature of the calculations is not the most distinctive aspect to explain the qualitative different results found in scaling calculations and Edwards self-consistent field findings. What makes the difference is in fact whether in the calculations the excluded volume correlations are taken into account or not, that is, whether the connectivity of the chain is Markovian or not. Therefore, along this work we will refer to Markovian and non-Markovian mean field theories, to make clear such a distinction.

1.1.3 Other theories

Although the analytical simplicity of the Markovian self-consistent field theories make them widely used, we have already pointed out that the methodology fails in describing the quantitative behavior of dilute and semidilute solutions. The explicit consideration of the many-body correlations into the description is done by means of the Renormalization Group techniques [43]. However, the calculations involved in this procedure are significantly more complex. Going beyond the merely asymptotic regime is an almost impossible task. From a more numerical point of view, the Monte Carlo (MC) method permits the explicit treatment of the inter and intra chain correlations in an explicit way. Thus, the MC results are widely used. However, the large number of conformations of relatively small chains makes this method to be very expensive when applied to polymeric systems. Thus, results on the behavior of isolated chains can be found but data on polymer adsorption are, for instance, very scarce. However, the interest of this methodology is that it supposes a complete solution of the statistical mechanical problem.

In the case of melts, Flory and Huggins devised an equation of state for the thermodynamic behavior of polymers. This equation of state is implicit in the treatment of Edwards of inhomogeneous systems and suffers from the same drawback when applied to

semidilute solutions.

1.2 Polymer adsorption

After the description of general properties and modelisation of polymer solutions, in the following a brief of the different theories on polymer adsorption will be given. In particular, we will center our attention on the so-called Scheutjens and Fleer numerical method [26] and the analytical treatment known as the *two order parameter theory* due to Semenov, Joanny and coworkers [20, 22]. Furthermore, we will also discuss some of the properties that can be experimentally measured.

1.2.1 Scaling Theory of polymer adsorption

In 1981 de Gennes [44] used scaling arguments to characterize the concentration profile at an adsorbing interface. The concepts of the scaling theory for homogeneous solutions were also applied to polymers in a good solvent next to the adsorbing surface. The main conditions needed for the scaling view to be valid are that an important fraction of the adsorbed layer stays in the semidilute regime. From this point of view, for very long polymers it is possible to derive power laws for the different regimes in which the structure of the layer can be divided. The first one, known as **proximal regime**, is the nearest region to the surface and its extension is similar to the size of the monomer l . In this region the density profile is dominated by the segment-surface contacts (depends only on the adsorption strength) and should be treated by means of especial methods[45]. The second region is the **central regime**, characterized by being far from surface as well as from the edge of the layer. In this region and due to the overlapping of the chains due to the presence of the adsorbing wall, that makes the local concentration be higher than the overlap concentration, one can define a local correlation length, according to eq. (1.19), depending on the position through $c(z)$. The main assumption of the scaling argument then states that since the adsorbed layer has no characteristic length (the edge of the layer is very far) any length should be proportional to the distance to the wall, the only relevant length. Thus, one can write $\xi \sim z$ or, in other words, the profile is self-similar (Fig. 1.4). Therefore, making use of eq. (1.19) one can write

$$c(z) \sim \xi(z)^{-4/3} \sim z^{-4/3} \quad (D < z < \xi^0) \quad (1.36)$$

where the distance D is determined by the adsorption strength and is larger than the size of the segment l and ξ^0 is the bulk correlation length

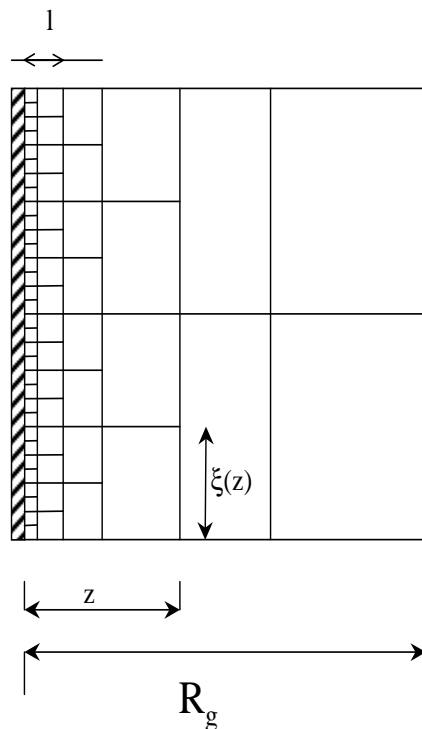


Figure 1.4: Presentation of the adsorbed polymer layer as a *self-similar mesh* in the semidilute regime. At a distance z from the adsorbing surface, the size of the correlation length, ξ , is itself of order z .

The last region described by de Gennes is the **distal regime**. It is the outer part of the profile for $c(z)$ being again characterized by a single length scale, the correlation length of the bulk solution in this approach. It should decay exponentially towards c^0 as

$$c(z) = c^0(1 + e^{-z/\xi^0}) \quad (z > \xi^0) \quad (1.37)$$

The scaling and Markovian self-consistent field approaches to polymer adsorption are very different in philosophy, and both give different predictions for the relevant power-laws in good solvents in the central regime of the layer. De Gennes predicts that the concentration profile decays with a power law regime of the form $c(z) \sim z^{-4/3}$, independently of the bulk density c^0 and of the dimension of the chain length N . However, from scaling arguments we can also infer the predictions of theories based on ideal chains, that is, of Markovian mean-field theories. To this end, we have to assume that the space dimensionality is $d = 4$ in which, according to the discussion in the paragraph after eq. (1.15), the chains behave as ideal and, therefore, satisfy a Markovian connectivity since the excluded volume correlations along the chain can be ignored. Thus, in four dimensions, it is found

that the correlation length depends on the inverse square root of concentration, according to eq. (1.24). Therefore, the concentration profile would scale like the inverse square of the distance

$$c(z) \sim z^{-2} \quad (1.38)$$

This scaling law was effectively obtained from self-consistent field calculations from Edwards equation (1.28) [19] as well as using the Scheutjens and Fler self-consistent method [46], described later on. In the latter, the predictions indicated, in the limit of infinitely long chains and vanishing bulk volume fraction, a power law similar to the eq. (1.38) but with corrections for finite size of the chains and non-zero bulk concentrations. Hence, working in a cubic lattice, these authors found the following value for the exponent of the decay of the concentration profile in the central regime

$$\alpha = -2 + 1.87(\ln(\phi^0))/N^{0.5} \quad (1.39)$$

being α the exponent of the expression $c(z) \sim z^\alpha$ and N the degree of polymerization.

1.2.2 Markovian self-consistent field description of polymer adsorption

After having reviewed the main features of polymer adsorption onto plane walls, we will briefly discuss the predictions found from the solution of Edwards equation (1.28) or, equivalently, eq. (1.32). In particular, we will introduce the description in terms of two order parameters that has served to introduce a new view in the internal structure of the adsorbed polymeric layer. The elements of this description will be often used in our Single Chain Mean Field analysis of forthcoming chapters.

Ground State Dominance

The Edwards eq. (1.28) is still valid for inhomogeneous systems being, moreover, the starting point of the pioneering works on polymer adsorption. As mentioned, the mean field treatment, based on the Markovian nature of the chain propagator (eq. (1.35)), is able to give a qualitative picture of the problem, although the power-law behaviors will differ from scaling predictions.

The treatment of confined systems, as it is the case in adsorption, permit some simplifications in the analytical solution of the mean-field problem described by eqs. (1.28)

or (1.32). Effectively, taking into account the mapping between n in Edwards equations onto an imaginary time it of the analogous Schrödinger equation, if the energy spectrum is discrete, the behavior is dominated by the ground state [19]. The time evolution of the eigenfunctions in the latter equation, $|e^{iE_s t}| = 1$, becomes exponentially decreasing function in the former, $e^{-E_s n}$, making this approximation possible for polymers. More in detail, this approximation known as *Ground State Dominance* starts with the spectral decomposition of the propagator in terms of its eigenfunctions and eigenvalues, i.e.

$$G(\mathbf{r}, \mathbf{r}'; N) = \sum_{s=0}^{\infty} \psi_s(\mathbf{r}) \psi_s(\mathbf{r}') e^{-E_s N} \simeq \psi_0(\mathbf{r}) \psi_0(\mathbf{r}') e^{-E_0 N} \quad (1.40)$$

being E_s the eigenvalues and ψ_s the corresponding eigenfunctions, which only depend upon the position. Notice that if there is a confining potential, E_0 is negative, so that the exponent is positive. Thus, from this approximation and the eq. (1.30), the monomer volume fraction, $\phi = \nu c$ is equal to

$$\phi(\mathbf{r}) \sim \phi^0 \psi_0^2 \quad (1.41)$$

Therefore, under this approximation the Edwards equation can be rewritten as

$$\frac{l^2}{6} \nabla^2 \psi_0 - \phi^0 \psi_0^3 - E_0 \psi_0 = 0 \quad (1.42)$$

where ψ_0 is referred to as *order parameter* [19, 13], in analogy with critical phenomena. This last equation embeds an eigenvalue problem since the energy E_0 is not known a priori, and has to be found to match boundary conditions usually at the wall and at the infinity. This approach has been used to analyze the behaviour of polymers adsorbed at interfaces under Θ [15] and poor solvent [17] conditions. Under good solvent conditions, de Gennes [14] introduced a similar equation but that takes into account the local swell of the chain due to excluded volume correlations, based on Widom's trick. Such a treatment is essentially mean field but is able to reproduce the appropriate scaling behavior. However, all one parameter theories give no description of finite size effects, and as such are valid for extremely long chains and near the walls, in which the tails are greatly outnumbered by loops. Thus, this theory only describes the region close to the surface.

Description in terms loops and tails: Two order parameters theory

The description of the adsorbed layer in terms of trains, loops and tails (Fig. 1.5) have been analyzed from mean field [20, 22] and scaling (will be explained with more detail in

the chapter 5) points of view [21]. Semenov *et al.* used a self-consistent approach based on the Edwards propagator equation (1.28), which was worked out to introduce two coupled order parameters to describe the concentration profile in the adsorbed layer. The finite size of the polymer chain is taken into account in the framework of this theory.

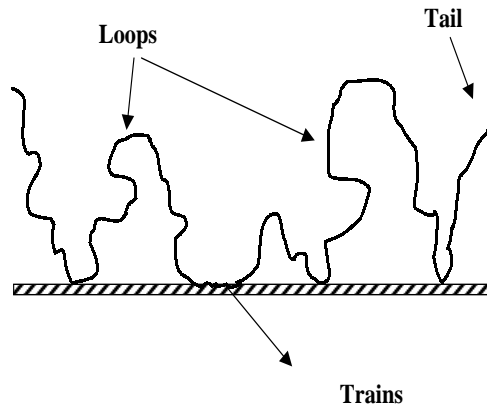


Figure 1.5: Loops-tails-trains conformations of a homopolymer adsorbed on a plane surface

One of the results from this two order parameters approach is that the adsorbed layer has a double layer structure with an inner layer dominated by loops and an outer layer dominated by tails, in agreement with the numerical results obtained by Scheutjens and Fleer [25, 26], in their approach to the full solution of Edwards equation. The change from loop-dominant to tail-dominant region is produced at a distance z^* from the surface (referred to as *crossover distance*, from now on, see Fig. 1.6). The distance z^* , for very long chains, is much longer than the monomer size, but much shorter than the coil size R_g . It depends, only, on the polymerization index and the dimension of space, and scales as $z^* \sim 1/N^{d-1}$ in the limit $N \rightarrow \infty$.

The two coupled equations that describe the two order parameter can be derived from Edwards equation which, for convenience, we rewrite here. That is,

$$\frac{\partial Z}{\partial n} = \frac{l^2}{6} \nabla^2 Z - U(\mathbf{r})Z \quad (1.43)$$

where mean-field potential, $U(\mathbf{r})$, is calculated (compare with eq. (1.30)) from the equation

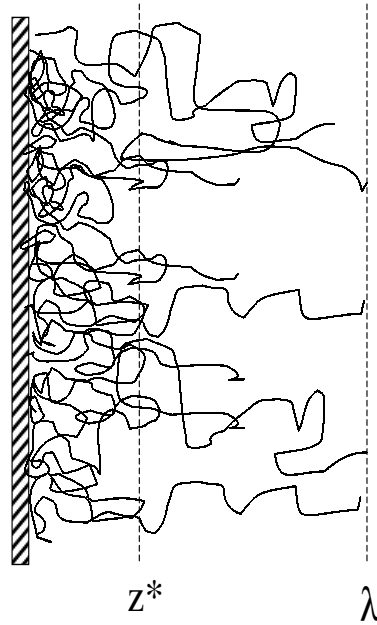


Figure 1.6: Division of the adsorbed polymeric layer on loops and tails regions. z^* is the crossover distance and λ is the thickness of the adsorbed layer being of the order of the radius of gyration of the polymer, $Rg \sim lN^\nu$, in a dilute solution.

$$U(\mathbf{r}) = U_{ads}(\mathbf{r}) + \frac{\phi^0}{N} \int Z(\mathbf{r}; n) Z(\mathbf{r}; N - n) dn - \phi^0 \quad (1.44)$$

where ϕ^0 is the bulk volume fraction and $Z(\mathbf{r}; n)$, the partition function corresponding to a portion of the chain of length n with one of its ends at \mathbf{r} and the other one anywhere. Here we have redefined the partition function introduced in eq. (1.31) according to the transformation $Z \rightarrow \exp(-\phi^0 n)Z$, for simplicity's sake. The first term on the right hand side of this equation is the adsorption potential of the surface and the second term proportional to the local concentration of monomers. The third term is the background bulk potential that has appeared due to the redefinition of the partition function.

The wall potential is not negligible only in a thin layer close to the wall. The effect of a local potential $U_{ads}(\mathbf{r})$ can be reduced to an effective boundary condition for the propagator that reads [13]

$$\left. \frac{\partial G}{\partial \mathbf{r}} \right|_{z=0} = -\frac{1}{b} G|_{z=0} \quad (1.45)$$

where b is the extrapolation length, which in strong adsorption conditions, it is of the order of the monomer size l .

Due to the analogy between the Edwards equation and a Schrödinger equation (Sturm-Liouville problem), we can introduce an expansion in eigenfunctions, which satisfy the set of equations which, in general, take the form

$$-E_s \psi_s = \frac{l^2}{6} \nabla^2 \psi_s - U(\mathbf{r}) \psi_s \quad (1.46)$$

where ψ_s are the eigenfunctions and E_s , its corresponding eigenvalues. Thus, the solution of the eq. (1.43) may be formally rewritten in terms of the eigenfunctions and eigenvalues as

$$Z(\mathbf{r}; n) = \sum_s e^{-E_s} K_s \psi_s(\mathbf{r}) \quad (1.47)$$

where K_s is an amplitude that satisfies

$$K_s = \int \psi_s(\mathbf{r}) d\mathbf{r} \quad (1.48)$$

according to the relations between the propagator and the partial partition function. The spectrum E_s is in general formed by a continuous branch $E_s = q^2 \geq 0$ and by a set of discrete levels ($E_s < 0$), issued by the confinement of the chain due to a potential well. In the adsorption problem, the discrete levels depend on the local attraction to the wall and domain the adsorption. This part of the spectrum may contain only one bound state if the adsorption potential is a Dirac's δ well. Thus, $E_0 \equiv -\varepsilon$ corresponds to the effective adsorption energy per monomer, which will be in addition related to the thickness of the adsorbed layer. Thus, it is necessary, inside the strong adsorption condition, that $\varepsilon N \gg kT$.

Therefore, taken into account the division of the energy spectrum on discrete and continuous, the partition function (eq. 1.47) can be separated into

$$Z(\mathbf{r}; n) = K_o \psi_o e^{\varepsilon n} + \sum_q K(q) \psi(\mathbf{r}; q) e^{-q^2 n} \equiv Z_a(\mathbf{r}; n) + Z_f(\mathbf{r}; n) \quad (1.49)$$

where $Z_a(\mathbf{r}; n)$ and $Z_f(\mathbf{r}; n)$ can be identified as the partition functions corresponding to the adsorbed and free chains, respectively.

Loops and tails concentration

From the distinction of the partition function between adsorbed chains, which have at least one monomer in contact with the surface, and free chains, without monomers in contact with surface, we can calculate, self-consistently, the expressions corresponding to the monomer volume fraction belonging to loops, tails and free chains. Thus, if the total monomer volume fraction may be split in three contributions, $\phi(\mathbf{r}) = \phi_l(\mathbf{r}) + \phi_t(\mathbf{r}) + \phi_f(\mathbf{r})$, considering the eq. (1.49) (see Fig. 1.7), we can write

$$\phi_l(\mathbf{r}) = \frac{\phi^o}{N} \int dn Z_a(\mathbf{r}, n) Z_a(\mathbf{r}, N - n) \quad (1.50)$$

$$\phi_t(\mathbf{r}) = \frac{2\phi^o}{N} \int dn Z_f(\mathbf{r}, n) Z_a(\mathbf{r}, N - n) \quad (1.51)$$

$$\phi_f(\mathbf{r}) = \frac{\phi^o}{N} \int dn Z_f(\mathbf{r}, n) Z_f(\mathbf{r}, N - n) \quad (1.52)$$

If we develop the integrals from the eq. (1.49), we have for the first two contributions that

$$\phi_l(\mathbf{r}) = \phi^0 K_o^2 e^{\varepsilon N} \psi_0^2(\mathbf{r}) \equiv \psi(\mathbf{r})^2 \quad (1.53)$$

$$\phi_t(\mathbf{r}) = \frac{2}{N} \phi^0 K_o \psi_0(\mathbf{r}) \int e^{\varepsilon(N-n)} Z_f(\mathbf{r}; n) dn \equiv B\varphi(\mathbf{r})\psi(\mathbf{r}) \quad (1.54)$$

where

$$B = \frac{2}{N} \sqrt{\phi^0} e^{\frac{\varepsilon N}{2}} \quad (1.55)$$

$$\varphi(\mathbf{r}) = \int e^{-\varepsilon n} Z_f(\mathbf{r}; n) dn \quad (1.56)$$

The mean field potential, in terms of the two order parameters introduced, is rewritten as

$$U(\mathbf{r}) = \psi^2(\mathbf{r}) + B\psi(\mathbf{r})\varphi(\mathbf{r}) - \phi^0 \quad (1.57)$$

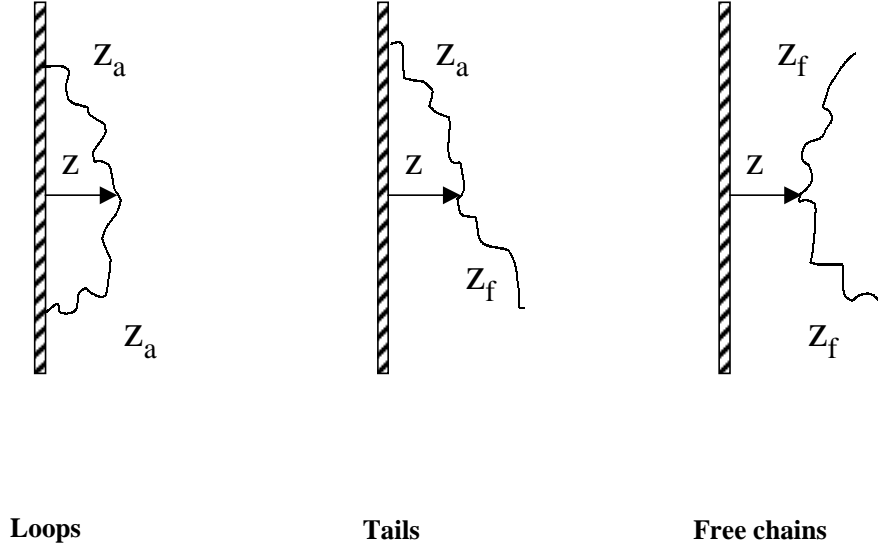


Figure 1.7: Representation of the loops (ϕ_l), tails (ϕ_t) and free chains (ϕ_f) of the adsorbed layer, as a function of their corresponding partition functions. In this picture the variable z is the distance to the wall.

where $\psi(\mathbf{r})$ and $\varphi(\mathbf{r})$ are the two order parameters whose variation with the distance will give us the density profiles of monomers corresponding to loops and tails. The normalization constant B is obtained from the conservation of the end points, being its dimension inversely proportional to the length. Because of the full theory is restricted to distances from the wall smaller than the free chain radius, the theory does not consider the free chains at the level presented here.

Taking into account that $\psi(\mathbf{r})$ is a solution of the Edwards Schrödinger-like equation (1.43), this parameter satisfies

$$\frac{l^2}{6} \nabla^2 \psi - (U(\mathbf{r}) + \varepsilon) \psi = 0 \quad (1.58)$$

whose boundary conditions are

$$\psi'|_{z=0} = -\frac{1}{b} \psi|_{z=0} \quad \psi(z \rightarrow \infty) \rightarrow 0 \quad (1.59)$$

The order parameter $\varphi(\mathbf{r})$ is related with the partition function corresponding to the free chains, which also satisfies the Edwards equation

$$\frac{\partial Z_f}{\partial n} = \frac{l^2}{6} \nabla^2 Z_f - U(\mathbf{r}) Z_f \quad (1.60)$$

Thus, considering eq. (1.49), the equation that satisfies the order parameter $\varphi(\mathbf{r})$ is obtained upon integration of both members of eq. (1.60) with respect to n and neglecting the term proportional to $\exp(-\varepsilon N)$

$$-\frac{l^2}{6} \nabla^2 \varphi + (U(\mathbf{r}) + \varepsilon) \varphi = 1 \quad \varphi(z \rightarrow 0) \rightarrow 0 \quad (1.61)$$

where it has been considered the initial condition $Z(n \rightarrow 0) \rightarrow 1$. Therefore, the two coupled differential equations that describe the structure of the adsorbed layer are

$$\frac{l^2}{6} \nabla^2 \psi - (\psi^2 + B\psi\varphi + \varepsilon - \phi^0) \psi = 0 \quad (1.62)$$

$$-\frac{l^2}{6} \nabla^2 \varphi + (\psi^2 + B\psi\varphi + \varepsilon - \phi^0) \varphi = 1 \quad (1.63)$$

The two order parameter theory is the first able to give a comprehensive explanation of the structure of polymer layers and is often used in the interpretation of the data obtained either experimentally or by means of simulations. Furthermore, in ref. [22] Johner and collaborators have developed a two order parameter theory beyond the Gaussian approximation, using again the Widom's trick, as in the original paper of de Gennes [44] aiming at the recovery of the proper scaling laws from an intrinsically mean-field theory. Such a theory produces proper scaling laws for the majority of the profiles. However, the theory also produces a value for the so-called susceptibility exponent γ different from that obtained by means of Renormalization Group procedures [43, 47].

The SCF theory of Scheutjens and Fler

The task of solving the non-linear integro-differential equation (1.28) has been numerically carried out by Scheutjens, Fler and collaborators, and their methodology is widely used nowadays to obtain a qualitative insight about the behavior of polymers near interfaces [48]. It is thus worth to give a few words about it.

The self-consistent method, referred to as SCF theory, was developed around 1980 by J.M.H.M Scheutjens and G.J. Fler, in which a generalized lattice model for the adsorption

of interacting chains is considered [25, 26]. This theory can be viewed as an extension of DiMarzio-Rubin model for isolated chains [23, 24], and is equivalent to the continuum space Edwards equation for the propagator (1.28), as mentioned. The result is obtained here by a set of implicit equations which are solved numerically to obtain the self-consistent solution for the full propagator of the chain. The system is thus Markovian.

In the SCF model developed by Scheutjens and Flerer, the system is formed by two kinds of molecules: the polymer and solvent molecules. Each polymer segment or solvent molecule is assumed to occupy one lattice site. Each chain is subdivided into segments with ranking number $s = 1, 2, \dots, N$, and these segments can take only discretized positions with respect to the surface. Therefore the space is subdivided in lattice layers, numbered $z = 1, 2, \dots$, of spacing l equal to the bond length a (for simplicity we express all distances in units of l). In the calculations it has usually been considered a simple cubic lattice, where each lattice site has six neighbours. Polymer segments can be adsorbed and the corresponding volumen fraction profile $\phi(z)$ develops perpendicular to the surface. All inhomogeneities parallel to the surface are ignored. The surface is located at $z = 0$ so that polymer segments occupy discrete positions from $z = 1$, where the adsorption takes place, until $z = M$, being M a layer far away from the surface and far enough to ensure that the bulk values are reached.

The potential $u_i(z)$ felt by a segment of a molecule of type i (where i is either polymer or segment), is considered in a local mean-field approximation

$$u_i(z)/kT = u'(z) + \chi_{ij} (\langle \phi_j(z) \rangle - \phi_j^0) - \delta_{1,z} \chi_s \quad (1.64)$$

for both types of molecule i and j in the system (solvent or polymer). In the equation we can distinguish, the first term $u'(z)$ is the *excluded volume field* which ensures that every layer is completely filled; the second term contains the Flory-Huggins interaction parameter, χ , which takes into account the polymer-solvent interaction. The $\langle \phi_j(z) \rangle$ is a neighbour average of the volume fraction $\phi_i(z)$. In the case of a cube lattice, this average takes the form

$$\langle \phi_i(z) \rangle = (\phi_i(z-1) + 4\phi_i(z) + \phi_i(z+l)) / 6 \quad (1.65)$$

The quantity ϕ_i^0 is the bulk volume fraction of the i^{th} species (polymer or solvent). The third term corresponds to the interaction between the polymer segments and the wall which contains the Silberberg χ_s parameter [49, 50]. This parameter indicates a favourable adsorption energy for a polymer segment over that for a solvent molecule (so $\chi_s = 0$ for the solvent). Therefore it can be defined as

$$\chi_s = (U_1 - U_2)/kT \quad (1.66)$$

where U_i is the adsorption energy of species i , 1 being solvent and 2 a polymer segment. According to this definition χ_s is counted positive if there is a net segment-surface attraction. The Kronecker delta, $\delta_{1,z}$, is unity for $z = 1$ and zero elsewhere: only adsorbed segments experience the adsorption energy.

The statistical weight of any conformation is generated from $\prod \lambda_i G_i(z)$, where λ is the fraction of nearest neighbour lattice cells occupied by the polymer segment in layer i and $G_i(z)$ is the one-segment weighting factor (also called *free segment distribution function*) in layer i to a distance z from surface

$$G_i(z) = \exp [u_i(z)/kT] \quad (1.67)$$

When the polymer is built in a lattice, we must consider that such chain is formed by segments connected among them. In the case of a segment s placed in the layer z , the next segment, $s + 1$, may be in the layer $z - 1$, or in layer z , or in layer $z + 1$. Thus, from recurrence relations,

$$G_i(z, s|1) = G_i(z) \langle G_i(z, s - 1|1) \rangle \quad (1.68)$$

$$G_i(z, s|N) = G_i(z) \langle G_i(z, s + 1|N) \rangle \quad (1.69)$$

one can ensure the chain connectivity for segment s in layer z . The quantities $G(z, s|1)$ and $G(z, s|N)$ are the *end-segment distribution functions* ($G(z, s)$) starting from the first and last segment, respectively. Due to the fact that end points do not have a preceding segment, these functions are related with the *free segment distribution functions* $G(z) = G(z, 1|1) = G(z, N|N)$ (eqs. 1.68 and 1.69). The angular brackets indicate a weighted average over the neighboring lattice layers (a segment has a fraction of its contacts in the same layer and the others in each of the adjoining layers).

The volume fraction profile can be expressed in $u_p(z)$ and $G(z, s)$ which constitutes the closure relation in the SCF equations. Combining these definitions we obtain the equation known as *the composition law*

$$\phi(z) = \sum \phi(z, s) = \frac{\phi^o}{N} \sum e^{u_p(z)} G(z, s|1) G(z, s|N) = \frac{\phi^o}{N} \sum \frac{G(z, s|1) G(z, s|N)}{G(z)} \quad (1.70)$$

where the Markovian nature of the chains is used, as in eq. (1.30). The factor $e^{u_p(z)}$ corrects for the double counting of segment s . This equation relates $\phi(z)$ with the potential, $u(z)$, which is also related with the volume fraction profile by eq. (1.64). The result is obtained by a self-consistent method where the set of coupled equations is solved numerically under the volume filling constraint, i.e. $\sum_i \phi_i(z) = 1$ for any z . More details are contained in the Chapter 5 of the book by J. Lyklema [51].

1.2.3 Other theories

Renormalization Group methods have been also used to study polymer adsorption, although the double layer structure has never been described within this theory [47, 43]. Again, Monte Carlo simulations offer a way to numerically solve the full many body problem. However, due to the fact that the conformational space of merely a few chains is overwhelmingly large, if the number of monomers is large, only a few simulations of relatively short chains are found in the literature, which will be analyzed more in depth in forthcoming chapters.

The most interesting alternative to the mean-field theories previously discussed is the approach of Aubouy, Guiselin and Raphaël [52], based on an heuristic free energy where the entropy of the loop distribution was explicitly considered. Although there is not an explicit treatment of the tails, their method is able to correctly reproduce the scaling behavior of different properties of the layer (not involving tails). We will go back to this discussion in chapter 4.

1.3 Experimental characterization of polymer interfaces

The structure of adsorbed polymers is of fundamental importance in understanding the mechanisms of steric stability of colloidal dispersions. From this point of view, much experimental work is reported to obtain the conformations of polymers at interfaces using several experimental techniques. However, it is important to take into account the dependence of these results in these techniques since different results can be obtained when different measuring methods are used.

The structural properties of an adsorbed polymer layer can be described in terms of four static properties. First, the total adsorbed mass, Γ , or surface coverage θ . Second, the layer thickness, λ , which can be experimentally obtained from ellipsometric measurements [53] (based on the principle that light undergoes a change in polarizability when it is reflected at a surface), from measurements in flow [54] or from photon correlation

spectroscopy (PCS) experiments [55, 56]. The third property is the average bound fraction of polymer segments, p being obtained from magnetic resonance [57] or FT-IR [58] measurements. The last property is the polymer volume fraction profile normal to the interface, $\phi(z)$, which is obtained experimentally by small-angle neutron scattering (SANS) [59], in systems of stable particulate dispersions with high interfacial areas, or also by the neutron reflectometry [60] measurements.

Another interesting property that will often be discussed in this work is the loops and tail size distributions. An example of measurement of these distributions is the work presented by Patel and collaborators [61] about the adsorption of the polydimethyl siloxane onto silica in solutions of hexane. In this case it is described the relative importance of loops and tails due to the difference in adsorption, from a good solvent, between cyclic and linear forms of polydimethyl siloxane, since cyclic polymers do not form tails. In this case the conformational energy change on adsorption is lower at low relative molecular masses and small surface concentration. When the relative molecular masses is increased, the cyclic species form larger loops, thus reducing the entropy change during adsorption. However, in the linear polymer the behaviour is different due to the fact that the tails contribution to the entropy change becomes diluted at higher relative molecular masses. One should keep in mind, however, the fact that ring polymers have additional topological constraints (polymeric rings remain linked or unlinked during all the process of adsorption) that can strongly affect the entropic properties of the adsorbed layer and, therefore, the structure.

1.3.1 Layer thickness

Various methods have been proposed to measure the thickness of an adsorbed layer. However, different properties of the layer may be determined depending upon the method used. Thus, the results obtained by hydrodynamic and electrokinetic techniques may exceed considerably the average thickness obtained from ellipsometry or neutron radiation, because they are influenced by the effect of the tails.

The small-angle neutron scattering (SANS) and wave methods have been used to determine directly the first and second statistical moments corresponding to the volume fraction profile normal to the interface or, what is the same, the mean distance of polymer segments (belonging to adsorbed chains) from the surface.

The first moment λ_1 and the second moment λ of the profile are given by the equations

$$\lambda_1 = \frac{\int_0^\infty z\phi_a(z)dz}{\int_0^\infty \phi_a(z)dz} \quad (1.71)$$

$$\lambda^2 = \frac{\int_0^\infty z^2 \phi_a(z) dz}{\int_0^\infty \phi_a(z) dz} \quad (1.72)$$

where z is the distance to the surface and $\phi_a(z)$ is the density profile of the adsorbed polymer chains.

The quantify λ is also known as the *root mean-square* thickness of the adsorbed layer.

In the case of the measurements of the layer thickness by light ellipsometry not only are measured reflected intensities, but also the changes in polarization upon reflection. A flat bare surface usually reflects light of all polarizations. But when the measurements are carried out at the *Brewster angle*, i. e., the angle of incidence for which the intensity of reflected parallel polarisation is a minimum, the reflectance coefficient vanishes. This cancellation is suppressed as soon as the surface is covered by an adsorbed layer [62]. Thus, the residual reflectance at the Brewster angle will depend on the number of segments per unit of area. There are several equations to link the quantity that is measured by ellipsometry to the theoretical volume-fraction profile. The definition chosen by Flerer *et al.* [48] was

$$\lambda_{ellip} = \frac{(\int_0^\infty \phi_a(z) dz)^2}{\int_0^\infty (\phi_a(z))^2 dz} \quad (1.73)$$

This is in contrast with the result obtained analytically by de Gennes [14] who concluded that λ_{ellip} corresponds to the first moment of the profile λ_1 .

Other technique to measure the thickness of the adsorbed polymer layer is through hydrodynamic methods. They are based on the fact that the adsorbed layer affects the flow of solvent along the surface, comparing it with flow past the bare surface. To determine the effective thickness, it is necessary to know the exact shape of the velocity profile which depends on the shape of the surface (usually simple geometries are chosen as smooth cylindrical channels or spherical colloidal particles) under scrutiny and on its orientation with respect to the flow field.

In order to find the relation between the segment density profile and the hydrodynamic thickness (λ_{hydr}), the Debye-Brinkman hydrodynamic model was developed for flow past a porous layer [48]. The velocity profile in the direction normal to the surface $v(z)$ satisfies the differential equation $d^2v/dz^2 - v/k^2 = 0$, where k is a permeability function which depends on $\phi(z)$. Therefore, the $v(z)$ is described by the next equation of movement,

$$\frac{d^2v}{dz^2} = v \frac{\phi_a(z)}{C_h(1 - \phi_a(z))} \quad (1.74)$$

where C_h is a permeability constant (whose value is of the order of the unity). For the resolution of this equation is taken into account the extrapolation to zero of the linear part of the solution for $v(z)$ and the obtained z is taken as the thickness of the adsorbed layer.

The comparison of both methods (ellipsometry and hydrodynamic) shows that λ_{hydr} is much bigger than λ_{ellip} . This difference is due to the latter is mainly determined by the loops, where the density of the layer is large enough to affect the refractive index, while the hydrodynamic thickness senses the segment density of the tails that extend beyond the bulk of the layer.

1.3.2 Adsorbed amount

The adsorbed mass, Γ , is one of the basic parameters in the description of polymer adsorption. Adsorbed mass represents the total number of monomers belonging to adsorbed chains per unit of area; therefore it is possible to say that the adsorbed amount is mainly determined by the loops and trains in a flat interface. We will show that this is not the case in curved interfaces, where the amount due to tails can modify this view. From simulation data, it is possible to calculate this parameter by the equation

$$\Gamma = \int_0^{\infty} c_a(z) dz \quad (1.75)$$

Adsorbed amounts are usually presented in the form of an adsorption isotherm as a function of the equilibrium bulk polymer concentration at a given temperature. A typical adsorption isotherm of a monodisperse polymer solutions is shown in the Fig. 1.8. As we can see, there is a high adsorption even in diluted conditions. However, in higher concentrations, the isotherm shows an horizontal region, known as *pseudo-plateau*, which indicates the saturation of the adsorbing surface in these conditions (For more details read the ref. [48]).

1.3.3 Volume fraction profile

The determination of volume fraction profiles for adsorbed polymers is important to the understanding and manipulation of colloidal dispersions. Small-Angle Neutron Scattering (SANS) has led to the direct determination of the volume fraction profile, $\phi(z)$, in these systems. However, the SANS method is restricted in its applicability on the one hand because the samples must be particulate and of the order of 100-500 nm diameter and on the other hand in that these dispersions must be stable. Therefore, the experiment

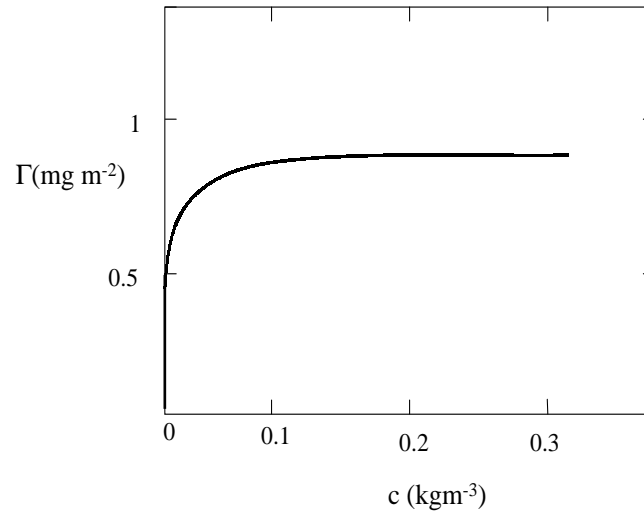


Figure 1.8: An adsorption isotherm for a monodisperse polymer solution.

of nonaqueous dispersions below full polymer coverage cannot be possible if flocculation occurs [60].

Inside of comparison between theory and scattering experiment, it is interesting the work presented by Auvray *et al* [63] in which was compared the prediction of the scaling theory developed by de Gennes [13] to the results obtained from neutron-scattering experiments. These experiments were performed on a high-molecular weight chains of polydimethylsiloxane (PDMS with MW=270000), adsorbed on silica in presence of pure cyclohexane (good solvent). The results obtained were consistent with the scaling laws, predicting the structure of the polymer layer as self-similar, while the concentration profile decreases as a function $z^{-4/3}$. In contrast, measurements made with shorter polymers have not shown the same behaviour, indicating the limitations of the scaling laws to $N \rightarrow \infty$. Thus, we can mention neutron reflectivity measurements of polystyrene (MW=50000) adsorbed on mica in which the best fits with polymer concentration profiles presented the form of an exponential decay [60].

In the next section, a non-technical overview of SANS technique is presented.

Small Angle Neutron Scattering

A SANS experiment on polymer layers proceeds as follows. A dilute dispersion of colloidal particles is prepared. The scattering length density of the solvent is matched to that of the substrate particles, a condition commonly referred to as *contrast matched*. This process consists on the selective suppression of the scattering from the particles by adjusting the isotopic composition of the solvent in which the particles are dispersed. Thus, the measured scattering is only produced by the adsorbed layer, with no contribution from the substrate particles.

In a SANS experiment, the scattering intensity is measured as a function of the scattering vector Q , which can be calculated from adjustment of the wavelength of the incident radiation λ and the scattering angle, θ , being defined by

$$Q = \frac{4\pi\mu}{\lambda} \sin \frac{\theta}{2} \quad (1.76)$$

where the neutron refractive index, μ , is a derivative of the scattering lengths in the materials.

The scattering intensity which describes the scattering from a polymer-coated particle can be understood in terms of the scattering due to the average concentration in the layer [59], thus

$$I(Q) = \frac{cte}{Q^2 r_o} \left(\int_0^\infty c(z) \sin(Qr_o + Qz) dz \right)^2 \quad (1.77)$$

where r_o is the particle radius.

The last equation describes the scattering from the layer assuming that the adsorbing particle is monodisperse and that the scattering instrument has an infinite Q resolution. In earlier work, it was assumed that neither of both criteria could be considered, so using certain assumptions this equation was simplified, obtaining

$$I(Q) = \frac{cte}{Q^2 r_o} \left(\int_0^\infty c(z) e^{iQz} dz \right)^2 \quad (1.78)$$

due to the difficulty on obtaining $c(z)$ from this equation, two methods have been used to resolve it. The first one considers the functional nature of $c(z)$ and a self-consistent fitting procedure is used [64], while the latter does not invert the eq.(1.78) but analyzes the data directly for certain features that would be consistent with a predicted layer structure [65]

Bibliography

- [1] F. Rodríguez, *Principles of Polymeric Systems*, (Taylor and Francis, 1996).
- [2] M. Metropolis, A. W. Rosenbluth, M. N. Rosenbluth, A. N. Teller and E. J. Teller, *J. Chem. Phys.* **21**, 1087 (1953).
- [3] K. Binder, *Monte Carlo and Molecular Dynamics Simulations in Polymer Sciences*, (Oxford University Press, Oxford, New York, 1995).
- [4] R. Zajac and A. Chakrabarti, *J. Chem. Phys.* **104**, 2418 (1996).
- [5] Jianwen Jiang, Honglai Liu and Ying Hu, *Macromol. Theory Simul.* **7**, 105 (1998).
- [6] J. I. Siepmann and D. Frenkel, *Mol. Phys.* **75**, 59 (1992).
- [7] G. C. A. M. Mooij, D. Frenkel and B. Smit, *J. Phys.: Condens. Matter* **4**, 255 (1992).
- [8] J. de Joannis, *Equilibrium properties of polymer solutions at surfaces: Monte Carlo simulations*, PhD. thesis, University of Florida, (2000).
- [9] M. Murat and G. S. Grest, *Macromolecules* **22**, 4054 (1989); M. Murat, *Macromolecules* **28**, 5928 (1995).
- [10] E. Y. Kramarenko, R. G. Winkler, P. G. Khalatur, A. R. Kohkhlov and P. Reineker, *J. Chem. Phys.* **104**, 4806 (1996).
- [11] A. K. Dolan and S. F. Edwards, *Proc. Roy. Soc. London* **337 A**, 509 (1974).
- [12] G. J. Fleer, J. M. H. M. Scheutjens and M. A. Cohen Stuart, *Colloids Surf.* **31**, 1 (1998).
- [13] P. G. de Gennes, *Scaling Concepts in Polymer Physics*, (Ed. Cornell University Press, Ithaca, NY, 1979).
- [14] P. G. de Gennes, *Macromolecules* **15**, 492 (1982).
- [15] K. Ingersent, J. Klein and P. A. Pincus, *Macromolecules* **23**, 548 (1990).

- [16] J. Klein and P. A. Pincus, *Macromolecules* **15**, 1129 (1982).
- [17] K. Ingersent, J. Klein and P. A. Pincus, *Macromolecules* **19**, 1374 (1986).
- [18] S. F. Edwards, *Proc. Phys. Soc.* **85**, 613 (1965).
- [19] I. S. Jones and P. Richmond, *J. Chem. Soc. Faraday Trans. II* **73**, 1062 (1977).
- [20] A. N. Semenov, J. Bonet i Avalos, A. Johner and J. F. Joanny, *Macromolecules* **29**, 2179 (1996).
- [21] A. N. Semenov and J. F. Joanny, *Europhysics Letters* **29** (4), 279 (1995).
- [22] A. Johner, J. Bonet i Avalos, C. C. van der Linden, A. N. Semenov and J. F. Joanny, *Macromolecules* **29**, 3629 (1996).
- [23] E. A. Di Marzio, *J. Chem. Phys.* **42**, 2101 (1965).
- [24] R. J. Rubin, *J. Chem. Phys.* **43**, 2392 (1965).
- [25] J. M. H. M. Scheutjens and G. J. Fleer, *J. Phys. Chem.* **83**, 1619 (1979).
- [26] J. M. H. M. Scheutjens and G. J. Fleer, *J. Phys. Chem.* **84**, 178 (1980).
- [27] A. Ben-Shaul, I. Szleifer and W.M. Gelbart, *J. Chem. Phys.* **83**, 3597 (1985).
- [28] M. A. Carignano and I. Szleifer *J. Chem. Phys.* **98**, 5006 (1992).
- [29] A. Chakrabarti, P. Nelson and R. Toral, *Physical Review A* **46** (8), 4930 (1992).
- [30] I. Szleifer and M. A. Carignano, in *Advances in Chemical Physics*, edited by I. Prigogine and S.A. Rice (John Wiley and Sons, New York, 1996).
- [31] P. A. Pincus, C. J. Sandroff and T. A. Witten, *J. Physique* **45**, 725 (1984).
- [32] C. M. Marques and J. F. Joanny, *J. Phys. France* **49**, 1103 (1988).
- [33] M. Aubouy and E. Raphaël, *Macromolecules* **31**, 4357 (1998).
- [34] T. Cosgrove, P. C. Griffiths and P. M. Lloyd, *Langmuir* **11**, 1457 (1995).
- [35] C. M. Wijmans, F. A. M. Leermarkers and G. J. Fleer, *Langmuir* **10**, 1331 (1994).
- [36] A. Johner, J. F. Joanny, S. Díez Orrite and J. Bonet Avalos, *Europhys. Lett.* **56** (4), 549 (2001).
- [37] B. Cabane and R. Duplessix, *J. Phys. France* **48**, 651 (1987).
- [38] M. Doi, *Introduction to Polymer Physics*, (Clarendon Press, Oxford 1996).

- [39] M. Doi and S. F. Edwards, *The theory of Polymer Dynamics*, (Clarendon Press, Oxford 1986).
- [40] W. Khun, *Kolloid Z.* **68**, 2 (1968).
- [41] I. Szleifer, *Biophysical Journal* **72**, 595 (1997).
- [42] P. F. Flory, *Principles of Polymer Chemistry*, (Cornell University Press: Ithaca, N. Y., 1953).
- [43] J. des Cloizeaux and G. Jannink, *Les polymères en solution: leur modélisation et leur structure*, (Les éditions de Physique, Les Ulis, 1988).
- [44] P. G. de Gennes, *Macromolecules* **14**, 1637 (1981).
- [45] E. Eisenriegler, *Polymers near surfaces*, (World Scientific: Singapore, 1993).
- [46] P. G. van der Linden and F. A. M. Leermakers, *Macromolecules* **25**, 3449 (1992).
- [47] B. Duplantier, *J. Stat. Phys.* **54**, 581 (1989).
- [48] G. J. Fleer, M. A. Cohen Stuart, J. M. H. M. Scheutjens, T. Cosgrove and B. Vincent, *Polymers at Interfaces*, (Chapman and Hall; London, 1993).
- [49] A. Silberberg, *J. Chem. Phys.* **48**, 2835 (1968).
- [50] R. J. Roe, *J. Chem. Phys.* **60**, 4192 (1974).
- [51] J. Lyklema, *Fundamentals of Interface and Colloid Science, Volumen II: Solid-Liquid Interfaces*, (Academic Press, 1995).
- [52] M. Aubouy, O. Guiselin and E. Raphaël, *Macromolecules* **29**, 7261 (1996)
- [53] A. Takahashi, M. Kawaguchi, K. Kayashi and T. Kato, *ACS Symp. Ser.* **39**, 240 (1984).
- [54] Y. Cohen, *Macromolecules* **21**, 494 (1988).
- [55] M. A. Cohen-Stuart, F. H. W. H. Waajen, T. Cosgrove, B. Vincent and T. L. Crowley, *Macromolecules* **17**, 1825 (1984).
- [56] Victoria S. Stenkamp and John C. Berg, *Langmuir* **13**, 3827 (1997).
- [57] T. Cosgrove, B. Vincent, M. A. Cohen-Stuart, K. G. Barnett and D. S. Sissons, *Macromolecules* **14**, 1018 (1981).
- [58] T. Cosgrove, C. A. Prestidge and B. Vincent, *J. Chem. Soc., Faraday Trans.* **86**, 1337 (1990).

- [59] J. H. E. Hone, T. Cosgrove, M. Spanhiannikova, T. M. Obey, J. C. Marshall and T. L. Crowley, *Langmuir* **18**, 855 (2002).
- [60] T. Cosgrove, T. G. Heath, J. S. Phipps and R. M. Richardson, *Macromolecules* **24**, 94 (1991).
- [61] A. Patel and T. Cosgrove, *Macromolecules* **28**, 8621 (1995).
- [62] R. Azzam and N. Bashara, *Ellipsometry and Polarized Light*, (North Holland 1977).
- [63] L. Auvray and J. P. Cotton, *Macromolecules* **20**, 202 (1987).
- [64] T. Cosgrove, *J. Chem. Soc. Faraday Trans.* **86**, 1323 (1990).
- [65] P. Auroy and L. Auvray, *J. Phys. II (Paris)* **3**, 227 (1993).

Chapter 2

Theoretical approach

The theoretical treatment that we will discuss here is based on the *Single Chain Mean Field* theory (SCMF), originally developed by Ben-Shaul, Szleifer and coworkers [1], to study the structure of micellar aggregates in the absence of solvent molecules, and later generalized for longer chains in the presence of solvent [2, 3]. The conformational and thermodynamic behaviour of the grafted polymeric layers has been analysed in great detail by means of this theory. The details of the SCMF and a comparison with Monte Carlo simulations devoted to grafted polymeric layers and surfactant aggregates are given elsewhere [4, 5].

The SCMF theory may be placed between the full-scale computer simulations (Monte Carlo and Molecular Dynamics) and that of simple analytical approaches based on order-parameter theories (cf. chapter 1). From the latter, it is possible to obtain information about *universal* properties of the system, independent of molecular details. However, aiming at a quantitative comparison with experimental data or even large-scale simulations, the microscopic information hidden in the value of the coefficients appearing in the analytical theories, becomes relevant. In the case of computer simulations, they provide the exact solution of the model system yielding the equilibrium collective properties. The choice of the model depends on the application. However, in order to obtain these average properties, it is necessary to compute in detail all the interactions between the different species (polymer segments and solvent molecules) present in the simulation box, which dramatically reduces the size of the systems to be studied. In addition, due to this size limitation, one is forced to deal with one thermodynamic condition at one time.

In the SCMF approach, the main idea is to build a mean field theory centered in the chain as the reference state, with intramolecular interactions described exactly while interactions with other molecules (other polymers and solvent) are calculated in a self-consistent mean-field approximation. Such a procedure differs from the self-consistent

field approximations based on Edwards equation (1.28), which take an ideal chain as a reference state. Hence, the ideal chain reference state is Markovian (according to eq. (1.35)) and has no correlations between segments of the chain, as it has been discussed in Chap.1.

The application of the SCMF theory does not assume any particular statistical behavior of the chain, which can be non-Markovian in the sense that distant segments of the chain can be correlated due to the direct excluded volume interactions. Therefore, the calculation of any average property of the system requires the knowledge of all possible, or a representative sample of single-chain configurations of the chain model. Once obtained the set of configurations and assuming the incompressibility condition, the probability distribution function for the full configuration (usually referred to as *pdf*) is calculated as a function of the thermodynamic variables of the system. From the knowledge of the pdf, any desirable average property can be obtained.

Thus, the main difference between the SCF and the SCMF theories is the implicit assumption of ideal chains with Markovian connectivity in the former, according to eq. (1.35). The propagator, in the spirit of the SCMF theory, would be given by a sum over the *self-avoiding* conformations of the chain, weighted with a mean-field Hamiltonian H_{mf} (to be described later), keeping the chain ends fixed in space. That is

$$G(\mathbf{r}, \mathbf{r}'; N) = \int_{\mathbf{r}_0=\mathbf{r}'}^{\mathbf{r}_N=\mathbf{r}} \mathcal{D}\gamma e^{-H_{mf}[\gamma]/kT} \neq \int d\mathbf{r}'' G(\mathbf{r}'', \mathbf{r}'; n) G(\mathbf{r}, \mathbf{r}''; N-n) \quad (2.1)$$

where γ is a given conformation and the sum $\mathcal{D}\gamma$ here runs only on the self-avoiding conformations of the chain. Obviously, this is not a Markovian connectivity due to the fact that the number of available conformations of a given portion of the chain of n monomers depends on the conformations of the rest of the chain, with $N - n$ monomers. The propagators of the two portions of the chain are thus correlated. The computational advantage of the Markovian assumption is that the one-chain conformational space does not need to be explicitly sampled, and then very long chains can be numerically considered if the correlations due to excluded volume interactions along the chain are sacrificed.

In this work, we have applied the basic ideas underlying the theory to analyze polymer adsorption, especially the structure of the adsorbed layer. However, due to the narrow and deep adsorbing well, an optimal sampling of the polymer configurational space has been developed for the sampling to be statistically significant for the properties that we want to describe. Previous versions of the SCMF theory use an homogeneous sampling of the one-chain conformational space, a strategy that gives good results in situations such as micellar aggregates of short molecules [5], as well as in tethered polymeric layers [4]. However, in polymer adsorption problems, where bulk as well as the interfacial properties have to be properly described, an homogeneous sampling for chains of about 100 monomers

already required an overwhelmingly large number of conformations. In this chapter we will review the mathematical framework of the SCMF theory and introduce our importance sampling strategy that permitted us to obtain results with a personal computer, due to the small number of samples required. The price that we pay is the computer time involved in the construction of the biased sample that we will use.

2.1 The Single Chain Mean Field theory

The starting point of the theory is to consider that all polymer molecules are equivalent so the state of the system is completely characterized by the knowledge of the one-chain configurational probability distribution, $P[\gamma]$, together with the solvent molecules number density field $c_s(\mathbf{r})$, considered as a continuum. From the probability distribution function, $P[\gamma]$, one can obtain the polymer density profile and all other average conformational and thermodynamic properties, together with the solvent density profile. A given configuration of the polymer is denoted by γ , standing for the set of vectors, $\{\mathbf{r}_i[\gamma]\}$, indicating the position of the centers of the monomers of the chain, with $i = 1 \dots N$, N being the polymerization index.

The next step is to write the Helmholtz free energy functional of the system in term of the probability distribution function of one single chain and the density profiles of polymers and solvent molecules. Then the minimization of the free energy will provide the functional form of these quantities. The term corresponding to the internal energy takes into account the inter and intramolecular interactions including the interactions of the polymer segment with the adsorbing surface. The entropic contribution contains the conformational entropy of the chains as well as the dispersion of the solvent molecules. Hence, the mean-field free energy functional of the system polymers-solvent, in a given volume of space, is given by the expression [3]

$$\begin{aligned}
 F[P[\gamma], c_s(\mathbf{r})] &= kT\mathcal{N}_p \int \mathcal{D}\gamma (P[\gamma] \ln P[\gamma]) \\
 &+ kT \int_V d\mathbf{r} c_s(\mathbf{r}) \ln \phi_s(\mathbf{r}) + \int \mathcal{D}\gamma P[\gamma] U[\gamma, c_s(\mathbf{r}), c(\mathbf{r})] \quad (2.2)
 \end{aligned}$$

In this equation, k is the Boltzmann's constant, and \mathcal{N}_p is the number of polymers in the volume. The local volume fraction of solvent molecules is given by $\phi_s(\mathbf{r}) = v_s c_s(\mathbf{r})$, where $c_s(\mathbf{r})$ is the local solvent number density. Moreover, the symbol $\mathcal{D}\gamma$ denotes here an integration with respect to *all the allowed configurations* of the chain, which may be both ideal or self-avoiding configurations, depending on the model used. The independent macroscopic variables in the free energy functional eq. (2.2) are T , \mathcal{N}_p and V , since the

system is considered as incompressible. Hence, the volume accessible is filled either by solvent molecules or by polymer segments. Thus, if N_s denotes the total number of solvent molecules in the volume, the incompressibility assumption implies that,

$$V = v_p N \mathcal{N}_p + v_s N_s \quad (2.3)$$

where v_p and v_s are the volume of a polymeric and solvent molecule, respectively.

In eq. (2.2), $U[\gamma, c_s(\mathbf{r}), c(\mathbf{r})]$ is the energy of a given configuration γ in a solvent density field $c_s(\mathbf{r})$ and local monomer density $c(\mathbf{r})$. Thus, here we assume that, not only, the interaction energy can explicitly depend on the configuration, but also through the local monomer number density,

$$c(\mathbf{r}) \equiv \int \mathcal{D}\gamma P[\gamma] \sum_{i=1}^N \delta(\mathbf{r} - \mathbf{r}_i[\gamma]) \quad (2.4)$$

as well as on the solvent density $c_s(\mathbf{r})$. This interaction energy can include both intra-chain and inter-chain interactions, as well as interactions with external fields (as for example, adsorbing surfaces). Hence, the energy term can be further decomposed into three contributions, according to

$$U[\gamma, c_s(\mathbf{r}), c(\mathbf{r})] = U_{intra}[\gamma] + U_{inter}[\gamma, c_s(\mathbf{r}), c(\mathbf{r})] + U_{ext}[\gamma] \quad (2.5)$$

The first term on the right hand side of this equation corresponds to the intra-chain monomer-monomer interactions, which is a function only of every configuration. The second term stands for the interactions of the chain with the solvent as well as with monomers of other chains. The third term in eq. (2.5) corresponds to the interaction with external fields (for example, interaction with adsorbing surfaces).

In the case of the short-range hard-core repulsions, they are taken into account by means of both the generation of self-avoiding configurations of the chains, as well as through the *volume filling* constraint, describing the repulsive interaction with the molecules of the environment. This condition has to be satisfied at every point in the volume (volume filling constraint), and is stated as

$$\phi(\mathbf{r}) + \phi_s(\mathbf{r}) = 1 \quad (2.6)$$

where the average monomer volume fraction is given by

$$\phi(\mathbf{r}) \equiv \int \mathcal{D}\gamma P[\gamma] \sum_{i=1}^N v_p \delta(\mathbf{r} - \mathbf{r}_i[\gamma]) = v_p c(\mathbf{r}) \quad (2.7)$$

Hence, the mean-field interaction is non-homogeneous and varies depending on the distribution of the monomers of polymer and solvent as a function of the distance from the surface.

Thus, introducing the constraint as a Lagrange multiplier field $\pi(\mathbf{r})$, one can finally write

$$\begin{aligned} F[P[\gamma], c_s(\mathbf{r})] &= kT \mathcal{N}_p \int \mathcal{D}\gamma (P[\gamma] \ln P[\gamma]) + kT \int_V d\mathbf{r} c_s(\mathbf{r}) \ln \phi_s(\mathbf{r}) \\ &+ \int \mathcal{D}\gamma P[\gamma] U[\gamma, c_s(\mathbf{r}), c(\mathbf{r})] + \int_V d\mathbf{r} \pi(\mathbf{r}) \{\phi(\mathbf{r}) + \phi_s(\mathbf{r}) - 1\} \end{aligned} \quad (2.8)$$

The free-energy functional described by eq. (2.8) deserves some comments. In the first place, our description involves some degree of coarse graining. Effectively, eq. (2.6) is meaningful only in a coarse-grained sense since it cannot be strictly satisfied at a length scale smaller than the size of the monomers and solvent molecules. Therefore, according to eqs. (2.6) and (2.7), our formulation is *local*, in the terminology of density functional theories, due to the fact that in the definition of the volume fraction, monomers as well as solvent molecules are considered as point particles, and no excluded volume correlations are described. Hence, phenomena such as the oscillatory density profile near an attractive hard wall, with a wavelength of the order of the monomer (solvent) size, will lie beyond the scope of this work [6]. In the second place, since inter-chain interactions will be considered only throughout the local average monomer density, both in the expression of $U_{inter}[\gamma, c_s(\mathbf{r}), c(\mathbf{r})]$ as well as in the volume-filling constraint eq. (2.6), the inter-chain correlations will be ignored. It is then expected that our formalism reproduces mean-field results in properties such as the dependence of the critical density with the temperature in polymer phase separation. However, on one hand, our theory is suitable for the description of properties related to the long length scale features of the polymers, in the spirit of the usual mesoscopic description of polymers in solution. On the other hand, it is important to realize that, due to the fact that our formulation keeps up the connectivity and self-avoidance of the chain into account, it is expected that the description of properties related to one-chain features will yield the appropriate exponents, unlike mean-field theories based on Markovian connectivity. We will show the differences with respect to the explicit consideration of ideal chain conformations in some of the properties analyzed and shown in the next chapter.

Density Functional theories (DFT) for polymeric liquids have formal similarities with

our description [6, 7, 8]. Instead of the volume-filling constraint, in DFT the repulsive interactions are introduced by means of an excess free-energy depending on local averages of the monomer densities [9]. Not only, these theories can describe density oscillations near attractive surfaces with short-range potentials, but also disregard inter-chain correlations, described only through a local monomer density.

In this work, we will concentrate our attention to the description of the structure of polymer adsorption onto planar and curved surfaces, for flexible and moderately long polymers. In the following chapters, the results produced by this method will be further compared with the results of Monte Carlo simulations as well as with scaling results. To simplify the forthcoming analysis, it is convenient to introduce here the specific model that we will use along the next chapters. We will consider here polymers of N monomers, the latter being described by spherical particles exerting hard-core repulsions between them and with the solvent molecules. Thus, the intra-chain contribution of the energy is zero. As far as attractive intermolecular interactions are concerned, we make no distinction between the solvent molecules and polymer segments (they are similar energetically), thus the interactions solvent-solvent and solvent-segment of polymer can be ignored. Therefore, in the right hand side of eq. (2.5) only the contribution due to the interaction with external fields will be non-zero. In particular, we will consider an attractive square well potential, of an energy depth ε and a range d , of the order of the monomer size, at the surface of the adsorbing wall, to model the adsorption of monomers at its surface. Therefore, the energetic contribution is simply given by the expression

$$U[\gamma, c_s(\mathbf{r}), c(\mathbf{r})] = U_{ext}[\gamma] = \varepsilon \int d\mathbf{r} \theta(d - |z - z_0|) \sum_{i=1}^N \delta(\mathbf{r} - \mathbf{r}_i[\gamma]) \quad (2.9)$$

where z_0 is the position of the solid repulsive surface and θ is the Heaviside function, $\theta(x)$, which is 0 when the argument x is negative and 1 elsewhere.

From eq (2.2) by evaluating

$$\frac{\delta F}{\delta P[\gamma]} = 0 \quad (2.10)$$

$$\frac{\delta F}{\delta c_s(\mathbf{r})} = 0 \quad (2.11)$$

one obtains the equations satisfied by the fields that minimize the free energy eq. (2.2) subject to the constraint given in eq. (2.6). The solution of eq. (2.10) yields the probability distribution of a given conformation γ ,

$$P[\gamma] = A e^{-H_{mf}[\gamma]/kT} \quad (2.12)$$

The second equation, eq. (2.11), gives the solvent density profile

$$c_s(\mathbf{r}) = B e^{-v_s \pi(\mathbf{r})/kT} \quad (2.13)$$

In eq. (2.12), A is a normalization constant issued from the condition

$$\int \mathcal{D}\gamma P[\gamma] = 1, \quad (2.14)$$

and $H_{mf}[\gamma]$ is the mean-field Hamiltonian for a given conformation γ

$$H_{mf}[\gamma] \equiv \int d\mathbf{r} [v_p \pi(\mathbf{r}) + \varepsilon \theta(d - |z - z_0|)] \sum_{i=1}^N \delta(\mathbf{r} - \mathbf{r}_i[\gamma]) \quad (2.15)$$

In eq. (2.13), the constant B is given by the condition

$$N_s = \int d\mathbf{r} c_s(\mathbf{r}) \quad (2.16)$$

where N_s is the total number of solvent molecules in the volume.

Equations (2.12) and (2.13) explicitly depend on the yet unknown Lagrange multiplier field $\pi(\mathbf{r})$. This field can be determined by using the expressions for the probability distribution as well as the solvent concentration into the constraint equation (2.6), which provides an equation in which the only unknown is the Lagrange multiplier. We then obtain

$$v_s N_s \frac{e^{-v_s \pi(\mathbf{r})/kT}}{\int d\mathbf{r} e^{-v_s \pi(\mathbf{r})/kT}} + v_p \mathcal{N}_p \frac{\int \mathcal{D}\gamma e^{-H_{mf}[\gamma]/kT} \sum_{i=1}^N \delta(\mathbf{r} - \mathbf{r}_i[\gamma])}{\int \mathcal{D}\gamma e^{-H_{mf}[\gamma]/kT}} = 1 \quad (2.17)$$

The solution of the previous equation permits the calculation of the Lagrange multiplier field $\pi(\mathbf{r})$, which completely determine the mean-field probability distributions and, from the latter, all relevant properties of the system.

2.1.1 Calculation at a fixed chemical potential

As it has been mentioned, the choice of the total number of chains in the system \mathcal{N}_p and the volume V is required to obtain the solution of the mean-field $\pi(\mathbf{r})$ from eq. (2.17). However, since we want to describe inhomogeneous systems, fixing a priori the total number of chains in the volume does not give us any knowledge of the bulk polymer density. Thus, it is convenient to eliminate \mathcal{N}_p in eq. (2.17) in favor of the bulk polymer density, through the chemical potential μ .

With this purpose let us consider the partition function of one chain in the mean field, as given by the configurational integral

$$\mathcal{Z}_p \equiv \frac{1}{l^D} \int \mathcal{D}\gamma e^{-H_{mf}[\gamma]/kT} \quad (2.18)$$

where l stands for a characteristic length of the elementary volume of the chain configurational space, being D the dimensionality of such a space. From the mean-field point of view, we can relate the statistical weight of one chain with the chemical potential from the relation

$$\mathcal{Z}_p = \mathcal{N}_p e^{-\mu_p/kT} \quad (2.19)$$

where μ_p is the polymer chemical potential. For the solvent field, one has

$$\mathcal{Z}_s \equiv \frac{1}{l^3} \int_V d\mathbf{r} e^{-\pi(\mathbf{r})v_s/kT} = N_s e^{-\mu_s/kT} \quad (2.20)$$

where here μ_s corresponds to the solvent chemical potential. In an incompressible system, however, the only independent chemical potential is the so-called *exchange chemical potential* μ due to the fact that the addition of one chain to the system has to be compensated with the removal of the equivalent volume of solvent molecules. Thus, in our context μ is given by

$$\mu = \mu_p - N \frac{v_p}{v_s} \mu_s \quad (2.21)$$

Therefore, without loss of generality, we can choose $\mu_s = 0$ in eq. (2.20), which fixes the scale of the chemical potential of the polymer, and identify μ_p with the exchange chemical potential μ in eq. (2.19). In addition, it follows that

$$\frac{1}{l^3} \int_V d\mathbf{r} e^{-\pi(\mathbf{r})v_s/kT} = N_s \quad (2.22)$$

We will further consider that our system is in thermodynamic equilibrium with an homogeneous system of the same volume. Hence, both systems share the same chemical potential. For such an homogeneous system, the one-chain partition function Z_p^0 can also be evaluated from eq. (2.18), with the corresponding mean-field hamiltonian given by

$$H_{mf}^0[\gamma] \equiv \int d\mathbf{r} v_p \pi^0(\mathbf{r}) \sum_{i=1}^N \delta(\mathbf{r} - \mathbf{r}_i[\gamma]) = v_p \pi^0 N \quad (2.23)$$

where no interface has been introduced. The second equality follows from the fact that π^0 is a constant if the system is macroscopically homogeneous. Thus, the equilibrium condition between the inhomogeneous and the homogeneous systems allows us to write

$$e^{-\mu/kT} = \frac{Z_p}{\mathcal{N}_p} = \frac{Z_p^0}{\mathcal{N}_p^0} \quad (2.24)$$

with

$$\frac{Z_p^0}{\mathcal{N}_p^0} = \frac{N v_p}{l^D \phi^0 V} e^{-v_p \pi^0 N/kT} \int \mathcal{D}\gamma = \frac{N v_p}{l^D \phi^0 V} \left[\frac{l^3}{v_s} (1 - \phi^0) \right]^{N v_p/v_s} \int \mathcal{D}\gamma \quad (2.25)$$

where we have defined the bulk monomer volume fraction, from the properties of the homogeneous system as being $\phi^0 \equiv v_p N \mathcal{N}_p^0/V$. The second equality follows after eliminating $e^{-\pi^0}$ using eq.(2.22), together with the incompressibility condition eq. (2.6). Hence, the constraint equation to be solved after the introduction of the bulk monomer density as an independent parameter is

$$\frac{v_s}{l^3} e^{-v_s \pi(\mathbf{r})/kT} + \frac{V \phi^0}{N} \left[\frac{v_s/l^3}{1 - \phi^0} \right]^{v_p N/v_s} \frac{\int \mathcal{D}\gamma e^{-H_{mf}[\gamma]/kT} \sum_{i=1}^N \delta(\mathbf{r} - \mathbf{r}_i[\gamma])}{\int \mathcal{D}\gamma} = 1 \quad (2.26)$$

Notice the conformational space volume included in the denominator of the second term on the left hand side of this last expression. This volume too has to be sampled by means of Monte Carlo techniques, as we will see in the next subsection.

2.1.2 Importance sampling of the phase space of one single self-avoiding chain

The solution of the constraint equation, eq. (2.26), involves integrations over the one-chain configurational space. These integrations can, in principle, be analytically done for ideal chains, where monomers can overlap. However, in the case of self-avoiding chains, such an analytic evaluation is virtually impossible for chains with more than a few monomers. One way to overcome this difficulty is to evaluate the configurational integrals by means of the Monte Carlo method (appendix A) of sampling of the configurational space, generating self-avoiding conformation of chains. It is crucial to realize at this point that the exact description of the self-avoiding chain conformations permits to keep excluded volume correlations along the chain despite the fact that the interchain interactions and the effect of the solvent is taken at the mean-field level. The use of ideal chain conformations in the evaluation of the configurational space integrals transfers all the intrachain excluded volume repulsions to the mean field $\pi(\mathbf{r})$, smoothing out these intrachain correlations. Thus, properties depending on one-chain statistics will be sensitive to the method of evaluation of the configurational space integrals, something that will be seen in the values of the exponents in the power-law behavior of the different properties that we will discuss later on. On the other hand, the numerical nature of the generation of self-avoiding chain conformations restricts the length of the chains that can effectively be treated in the framework of SCMF in several orders of magnitude, when compared with calculations based on Markovian statistics that do not rely on an explicit generation of polymer conformations [10].

It has been customary to use a uniform sampling of the polymer conformation space in the calculations based on the SCMF theory, in the case of systems with planar geometry, or a biased sampling with a weight proportional to $1/r^2$, in the case of micelle formation with spherical geometry [5]. In our case, the presence of an adsorbing potential of strength of the order of kT and a narrow width, of the order of the monomer size, makes the uniform sampling uneficient, since the most of the configurations generated in this way have an irrelevant statistical weight when monomer densities as well as end monomer density profiles are computed. Therefore, here we will develop the theory for a general biased sampling and discuss the *optimal sampling* for a given situation of interest.

To evaluate the integral of a given function $f[\gamma]$ over the configurational space of a chain by means of the Monte Carlo method, we use the well known formula [11]

$$\int \mathcal{D}\gamma f[\gamma] \simeq \frac{1}{\Lambda} \sum_{\alpha=1}^{\Lambda} \frac{f[\gamma_{\alpha}]}{\mathcal{P}_B[\gamma_{\alpha}]} \quad (2.27)$$

where Λ is the total number of sampling points in the configurational space and $\mathcal{P}_B[\gamma]$ is

the probability distribution of the biased sampling. It is convenient for our purposes to relate $\mathcal{P}_B[\gamma]$ with a statistical weight $w[\gamma]$, to which we will refer later on

$$\mathcal{P}_B[\gamma] = \frac{w[\gamma]}{\int \mathcal{D}\gamma w[\gamma]} \quad (2.28)$$

Notice that $\mathcal{P}_B[\gamma]$ has dimensions of inverse volume of the configurational space, so that the right hand side of eq. (2.27) has the proper dimensions.

Therefore, aiming at a numerical evaluation of the constraint equation, the conformational space integrations in the second term on the right hand side of eq. (2.26) can be rewritten in terms of a sum over the Monte Carlo samples, giving

$$\frac{\int \mathcal{D}\gamma e^{-H_{mf}[\gamma]/kT} \sum_{i=1}^N \delta(\mathbf{r} - \mathbf{r}_i[\gamma])}{\int \mathcal{D}\gamma} = \frac{\sum_{\alpha=1}^{\Lambda} e^{-H_{mf}[\gamma_{\alpha}]/kT} \sum_{i=1}^N \delta(\mathbf{r} - \mathbf{r}_i[\gamma_{\alpha}])/w[\gamma_{\alpha}]}{\sum_{\alpha=1}^{\Lambda} 1/w[\gamma_{\alpha}]} \quad (2.29)$$

Notice that the phase space volume in the denominator has also been calculated by means of the same biased Monte Carlo sampling, so that the normalizing factors $\int \mathcal{D}\gamma w[\gamma]$ cancel out.

The averages of a given variable $A(\mathbf{r}, \mathbf{r}_i[\gamma])$ can then be performed in a similar way

$$\langle A(\mathbf{r}) \rangle = \frac{\int \mathcal{D}\gamma e^{-H_{mf}[\gamma]/kT} A(\mathbf{r}, \mathbf{r}_i[\gamma])}{\int \mathcal{D}\gamma e^{-H_{mf}[\gamma]/kT}} \simeq \frac{\sum_{\alpha=1}^{\Lambda} e^{-H_{mf}[\gamma_{\alpha}]/kT} A(\mathbf{r}, \mathbf{r}_i[\gamma_{\alpha}])/w[\gamma_{\alpha}]}{\sum_{\alpha=1}^{\Lambda} e^{-H_{mf}[\gamma_{\alpha}]/kT}/w[\gamma_{\alpha}]} \quad (2.30)$$

Finally, to end this section, it is important to also realize that the most efficient sampling of the conformational space is that done with a distribution given by the absolute value of the integrand itself, i.e. [11]

$$w[\gamma] = |f[\gamma]| \quad (2.31)$$

Hence, the choice $w[\gamma] = e^{-H_{mf}[\gamma]/kT}$, although not optimal for a specific property, will be a convenient choice to make the samples relevant for the problems at hand.

Considering the eq. (2.29), the constraint equation (2.26) is rewritten as

$$\frac{v_s}{l^3} e^{-v_s \pi(\mathbf{r})/kT} + \frac{V \phi^0}{N} \left[\frac{v_s/l^3}{1 - \phi^0} \right]^{v_p N/v_s} \frac{\sum_{\alpha=1}^{\Lambda} e^{-H_{mf}[\gamma_{\alpha}]/kT} \sum_{i=1}^N \delta(\mathbf{r} - \mathbf{r}_i[\gamma_{\alpha}])/w[\gamma_{\alpha}]}{\sum_{\alpha=1}^{\Lambda} 1/w[\gamma_{\alpha}]} = 1 \quad (2.32)$$

To numerically find the lateral pressures $\pi(\mathbf{r})$, the space will be discretized in layers of finite thickness δ in order to obtain a set of coupled nonlinear equations. Then, the integrals over the variable \mathbf{r} are converted into sums over different finite layers.

2.2 Appendix A

2.2.1 Monte Carlo simulation

A standard Monte Carlo simulation (MC) is essentially an iterative process in which a set of independent configurations is generated for a system of N particles that interact through a known potential $\Phi(\mathbf{R}^N)$. By different random movements, new configurations are generated which are accepted or not so that the simulation efficiently explores the space of possible configurations. Hence, the generation of the configurations is following a probability distribution according to the chosen ensemble.

One of the fundamental tasks of statistical mechanics is to link the microscopic (atomic-scale) description of a particular substance to its equilibrium macroscopic (thermodynamic) properties. Therefore, physical properties are measured as configurational averages over the sequence of equilibrium configurations of the model system. Thus, knowing the probability density function, the average value of some observable A can be formulated as

$$\langle A \rangle = \int A(\mathbf{r}^N) P(\mathbf{r}^N) d\mathbf{r}^N \quad P(\mathbf{r}^N) = \frac{e^{\Phi(\mathbf{R}^N)}}{\int \dots \int e^{\Phi(\mathbf{R}^N)} d\mathbf{R}^N} \quad (\text{A-1})$$

where $A(\mathbf{r}^N)$ denotes the instantaneous value of the observable corresponding to the configuration \mathbf{r}^N and $P(\mathbf{r}^N)$ is the probability density to find the system in a configuration around \mathbf{r}^N . From this point of view, the Monte Carlo method in equilibrium statistical mechanics starts from the idea of approximating the exact equation (A-1), where one integrates over all configurations \mathbf{r}^N with their proper weights $P(\mathbf{r}^N)$, by an integration using a characteristic subset of configurations $(\{\mathbf{r}_1^N, \mathbf{r}_2^N, \mathbf{r}_3^N, \dots, \mathbf{r}_M^N\})$ generated randomly in configuration space according to the probability distribution $P(\mathbf{r}^N)$; this subset of configurations is used as a statistical sample. Hence, if one considers $M \rightarrow \infty$, the discrete sum

$$\langle A \rangle \sim \sum_{\{\mathbf{r}^N\}} A(\mathbf{r}^N) \quad (\text{A-2})$$

must approximate (A-1).

The main problem is to find an appropriate method which generates randomly points in configuration space according to the probability distribution $P(\mathbf{r}^N)$. One of the solutions to this problem is the method proposed by Metropolis *et al.* [12]. From this method, the

states of the system are sampled with a relative probability proportional to the Boltzmann factor, $e^{-U(\mathbf{r}^N)/kT}$ (being $U(\mathbf{r}^N)$ the interaction energy of the conformation \mathbf{r}^N). First, it is necessary to define a chain or a set of chains, which we denote by o (old) and with a Boltzmann factor equal to $e^{-U(o)/kT}$. A new conformation of the system is generated by flipping or rotating one or more bonds chosen randomly. This new conformation is denoted as n (new) and its Boltzmann factor is equal to $e^{-U(n)/kT}$. Now, the next step is decide if we accept or reject this new configuration. This decision is based on the detailed balance condition which requires that the frequency of moves from the state o to the state n should be equal to the frequency of moves out from the state n to the state o . If the move probabilities are symmetric we obtain that

$$P(o)acc(o \rightarrow n) = P(n)acc(n \rightarrow o) \Rightarrow \tag{A-3}$$

$$\frac{acc(o \rightarrow n)}{acc(n \rightarrow o)} = \frac{P(n)}{P(o)} = e^{-\beta[U(n)-U(o)]}$$

In the case of the energy change, $-\beta[U(n) - U(o)]$, is less than zero, then the trial move would be accepted. However, if $-\beta[U(n) - U(o)] > 0$ the decision about accepting or rejecting the trial move is through the generation of a random number, α , from an uniform distribution in the interval $[0, 1]$. Thus, we would accept the trial move if $\alpha < e^{-\beta[U(n)-U(o)]}$ while it would be rejected in the case of $\alpha \geq e^{-\beta[U(n)-U(o)]}$. If it happened the system would be returned to its original state and this state would be counted again, otherwise we would bias the sampling scheme [13].

The Metropolis rule is a Markov stochastic process, since the probability of a random move is independent of the history of the system, only on the actual situation. In this case, the detailed balance condition for the transition probabilities ensures that the proper thermodynamic equilibrium probability distribution is reached after a large number of steps.

There are other methods based on the Rosenbluth method of chain regrowth. These methods have their window of practical applications and may have advantages and disadvantages with respect to the Metropolis rule. In this problem, using chain growth would appreciably fast the process of sampling, since the statistical weight of the samples is known just after the growth. However, for long chains in complex geometries is possible that the Metropolis algorithm would lead the conformations to the optimal sampling condition. The difference between the two methods will be studied in the future.

Bibliography

- [1] A. Ben-Shaul, I. Szleifer and W. M. Gelbart, *J. Chem. Phys.* **83**, 3597 (1985).
- [2] M. A. Carignano and I. Szleifer *J. Chem. Phys.* **98**, 5006 (1992).
- [3] I. Szleifer, *Biophys. J.* **72**, 595 (1997).
- [4] I. Szleifer and M. A. Carignano, in *Advances in Chemical Physics*, edited by I. Prigogine and S.A. Rice (John Wiley and Sons, New York, 1996).
- [5] A. D. Mackie, A. Z. Panagiotopoulos and I. Szleifer, *Langmuir* **13**, 5022 (1997).
- [6] A. Yethiraj and C. E. Woodward, *J. Chem. Phys.* **102**, 5499 (1995).
- [7] A. Yethiraj, *J. Chem. Phys.* **109**, 3269 (1998).
- [8] S. Sen, J. M. Cohen, J. D. McCoy and J. G. Curro, *J. Chem. Phys.* **101**, 9010 (1994).
- [9] S. Nordholm, M. Johnson and B. C. Freasier *Aust. J. Chem.* **33**, 2139 (1980).
- [10] G. J. Fleer, M. A. Cohen-Stuart, J. M. H. M. Scheutjens, T. Cosgrove and B. Vincent, *Polymers at Interfaces* (Chapman and Hall, London, 1993) and references there in.
- [11] W. H. Press, B. P. Flannery, S. A. Teukolsky and W. T. Vetterling, *Numerical Recipes: Fortran Edition* (Cambridge University Press, Cambridge, UK, 1986).
- [12] M. Metropolis, A. W. Rosenbluth, M. N. Rosenbluth, A. N. Teller and E. J. Teller, *J. Chem. Phys.* **21**, 1087 (1953).
- [13] D. Frenkel and B. Smit, *Understanding Molecular Simulation* (Academic Press, San Diego, 1996).

Chapter 3

Adsorption on flat surfaces

Polymer adsorption has been extensively studied in recent years from both experimental and theoretical points of view [1]. Together with the practical applications of polymer adsorption there is also a more fundamental interest since they are a good example of confined polymer system, together with polymers in pores, grafted layers, microstructures in polymer blends and copolymer solutions, among many others.

The internal equilibrium structure of polymers reversibly adsorbed is a matter of some debate that still needs of much experimental work to reveal all its internal complexity. Pioneering works on this topic have been those of Jones and Richmond [2] which, starting from the mean-field treatment of Edwards [3], introduced the so-called *ground-state dominance* approximation (cf. chapter 1). In this formalism, a free energy functional for one order parameter is constructed from which the structure of the layer as well as the density profiles are obtained. Later, de Gennes [4], who used a similar functional properly modified, was able to reproduce the proper scaling laws that he had already obtained from more heuristic arguments.

However, subsequent numerical [1] and theoretical [5, 6, 7] work, based on the self-consistent field approach of Edwards, indicated that the structure of the layer is more complex than suggested by the one order parameter approaches mentioned. This complexity is due to the important finite size effects that give a particular importance to the polymer end-points, completely disregarded in one order parameter theories (c.f. chapter 1). Results from the self-consistent field numerical method of Scheutjens and Fleer on polymer adsorption onto flat surfaces confirm two different aspects. On the one hand, the complexity of the structure of the layer, decomposed into a loop and tail sublayers, is in agreement with the theoretical approaches based on two order parameters [7]. On the other, confirm the validity of the two order parameter approach in the description of the central and proximal regions of the adsorbed layer.

As far as the effect of the excluded volume correlations are concerned, one can say that the Markovian nature of Edwards approach is responsible for the exponents obtained in the different power law regimes disagree with scaling results [5] and experimental data [8]. Thus, in addition with the aforementioned self-consistent field calculations, more detailed theoretical analysis, based on the Renormalization Group [9, 10], and computational work, such as Monte Carlo simulations (MC), have been required [11, 12, 13, 14, 15], aiming at a more quantitative comparison with the experimentally observable power-law decay of the profiles. In addition, scaling laws are concerned with very long polymers $N \rightarrow \infty$, often lying out of the range of experimentally accessible polymer sizes. Thus, it is also of crucial interest analyze the behaviour of shorter polymers. Monte Carlo simulations of polymer adsorption are very difficult due to the large energetic barriers to be overcome by polymers in the sampling of its configurational space. The relaxation of the structural details of the adsorbed layer is a difficult matter that has been responsible for the fact that only a few MC analysis have been done on relatively long polymer adsorption (hundreds of segments). In fact, MC results are found only from the beginning of the last decade. One has, for instance, short polymers of $N = 32$ [12] adsorbed onto a flat wall, or results for longer chains [11] that disagree with the most of the modern MC data [15]. In this context, the SCMF theory appears as a suitable tool to analyze long polymer adsorption. The advantages of this method are, on the one hand, that includes excluded volume correlations along the chain and thus proper scaling laws are expected to be found in the long chain limit. On the other, the sampling of the configurational space of one single chain in a mean field is much simpler than many body MC simulations and, thus, can be more efficiently carried out.

In this chapter, we will apply the SCMF theory, with the importance sampling developed in the previous chapter, to polymer adsorption onto a plane wall. The results obtained will be compared with Monte Carlo simulations under the same conditions to analyze the differences between the two methods and prove the predictive nature of the method. Moreover, SCMF results with generation of overlapping chains will be compared with SCF data obtained from the application of the Scheutjens-Fleer theory. This comparison will serve us to study the importance of the excluded volume correlations along the chain and thus the role of the Markovian/non-Markovian connectivity of the chain in the reference state as far as the layer properties are concerned.

The chapter is organized as follows. In section 3.1, we will give the numerical details used in our calculations considering the adsorption of polymers on flat surfaces. In section 3.2, the structure of the adsorbed layer will be analyzed taking into account two different polymer lengths $N=100, 200$ and bulk volume fractions $\phi^0(N = 100) \sim 0.058$ and $\phi^0(N = 200) \sim 0.033$. The value of the adsorption energy in both cases will be $\varepsilon = -0.35 kT$. The comparison of the SCMF results with MC simulations data for different bulk volume fractions will be done in the section 3.3. Finally, in section 3.4, we will also analyze the structure of the adsorbed layer but considering Markovian chains of length $N = 200$.

The results will be compared with results issued from the Scheutjens and Fler method, obtained with the same set of parameters.

3.1 Numerical calculation details

The solution of the SCMF problem has been done from a sampling of the configurational space of *off-lattice* polymers of 100 and 200 monomers, in a cubic box of size $L = 115.32l$ and $L = 226.92l$, respectively, being l the monomer length. The adsorbing wall has a thickness of $2.72l$ and it is located at $z = 0$, occupying the center of the simulation box. Hence, the repulsive hard surfaces are at the planes $z \pm 1.36l$. The wall is rigid and cannot be penetrated by the chain beads. Adsorption takes place because we have introduced a square well potential at the surface of the plane, according to eq. (2.9), whose width available to monomers is $d = 1.86l$ and different values of ε of the order of kT have been considered. Since periodic boundary conditions (see Appendix A) are considered, the size of the box has been chosen such that the chains never reach two surfaces at one time, even at the state of full extension.

The chains are modeled as pearl necklaces of non-overlapping beads of diameter l , whose centers are separated a fixed distance equal to its diameter. The excluded volume per monomer has been taken as being independent of the conformation of the chain, and estimated to be $v_p = 1.86l^3$, assumed as constant all over this work. This value corresponds to an estimate of the net volume excluded per monomer in a chain.

Due to the translational symmetry of the system in the directions parallel to the wall, the mean-field constraint $\pi(\mathbf{r})$ is considered as being a function of the coordinate z only. Hence, the box has been divided into layers of thickness $1.86l$, parallel to the plane, inside which π is taken as constant. On the one hand, this choice permits us to have a reasonable precision on the spatial variation of π and, on the other hand, the volume of the layer is large enough for eq. (2.6) to make sense.

In view of the Monte Carlo evaluation of the configurational space integrals, as in eqs. (2.29) and (2.30), a *configurational file* is created. In this file, the coordinates of all monomers of the polymer corresponding to a large number of different configurations (usually 2×10^4), are stored together with the numerical value of its bias weight $w[\gamma]$. Then, the sums over all the configurations in the averages will simply be replaced by sums over the sample of configurations stored in the configurational file. In the beginning of the simulation, this configurational file is filled by an uniform distribution, $w[\gamma] = 1$, of conformations. It contains a collection of statistically independent self-avoiding chains whose first monomer is randomly located inside the simulation box. It is clear that in eqs.(2.29) and (2.30) the direct use of this initial sample, stored in the configurational file, will be rather uneficient. Effectively, due to the narrow and deep adsorbing well, only a few

of these configurations will be statistically relevant for the adsorption problem (especially those that will have monomers in the adsorbing well). To overcome this difficulty a bias field is introduced aiming at gathering a large number of configurations around the most relevant part of the chain configurational space. Once the bias field has been fixed, the configurational file is transformed so that the chains are distributed according to the selected bias $w[\gamma]$. To obtain this new configurational file, a chain is randomly chosen and its configuration modified by an elementary movement (crankshaft, reptation or simple overall translation of the chain, according to a random number that permits us to choose one of these movements). The statistical weight of the new configuration with respect to the bias field is then compared with the old one, and accepted or rejected according to the Metropolis rule [16]. The procedure is repeated a large number of times, until indicators such as the sum of the energy with respect to the bias field of the conformations in the configurational file (Fig. 3.1), or that of the conformations in contact with the adsorbing well, is stationary in a statistical sense (see Fig. 3.2). Once this point is reached, the stored configurations are distributed according to the prescribed statistical weight $w[\gamma]$. With respect to multi-chain Monte Carlo simulations, the acceptance rate is much larger since the topology of the energy space is smoother for a chain in a mean field than in a multi-chain system.

With the purpose of obtaining a configurational file statistically significant, we have chosen the Boltzmann weight,

$$w[\gamma] \propto e^{-H_{mf}[\gamma]/kT} \quad (3.1)$$

where $H_{mf}[\gamma]$ is given in eq. (2.15), as the appropriate bias. Of course, since $\pi(\mathbf{r})$ is not known a priori, an iterative procedure has to be used to recalculate the field while relaxing the conformations of the configurational file, until a stationary value is obtained. In Figs. (3.1) and (3.2) are shown, respectively, the evolution of two indicators of the relaxation of the configurational file, as functions of the MC steps. Notice the sharp jumps due to the recalculation, in the iterative procedure, of the mean-field Hamiltonian used as a bias field .

Since the configurations are recorded and the probability distribution of every one is known, performing averages by means of sums over the configurations in the configurational file has some advantages with respect to the usual procedure used in Monte Carlo simulations. Effectively, once the samples are correctly distributed in the configurational file, thus eq. (2.26), making use of eq. (2.29), can be solved for different values of the parameters that define physical problem, i.e. the adsorption energy ε and the bulk density ϕ^0 . This produces a new Lagrange multiplier field $\pi(\mathbf{r})$ from which the mean-field Hamiltonian $H_{mf}[\gamma]$ as well as the physical probability distribution $P[\gamma]$ are determined for the new conditions. Hence, the range of applicability of a given sampling is only limited by its statistical relevance for the physical conditions that one wants to analyze.

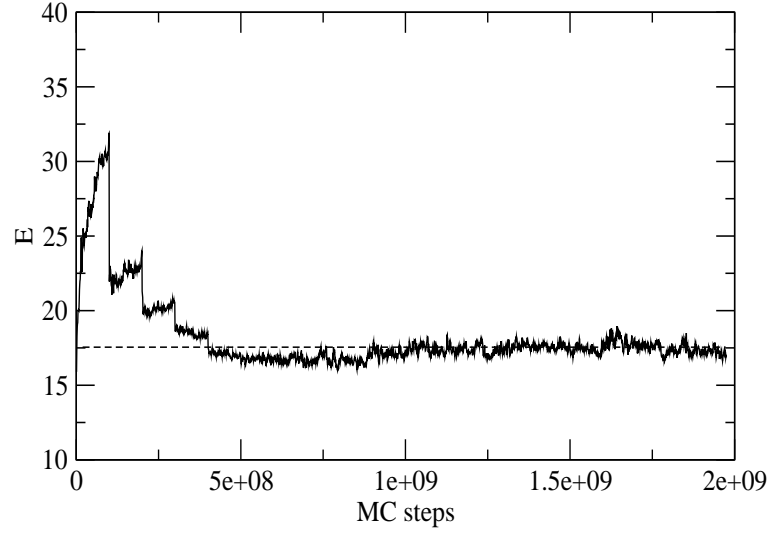


Figure 3.1: Variation of the energy of the configurational file, $E = -\sum_{\gamma} H_{mf}(\gamma)$, with Monte Carlo (MC) steps for a system with $N = 100$, $\phi^0 = 0.058$ and $\varepsilon = -0.35 kT$.

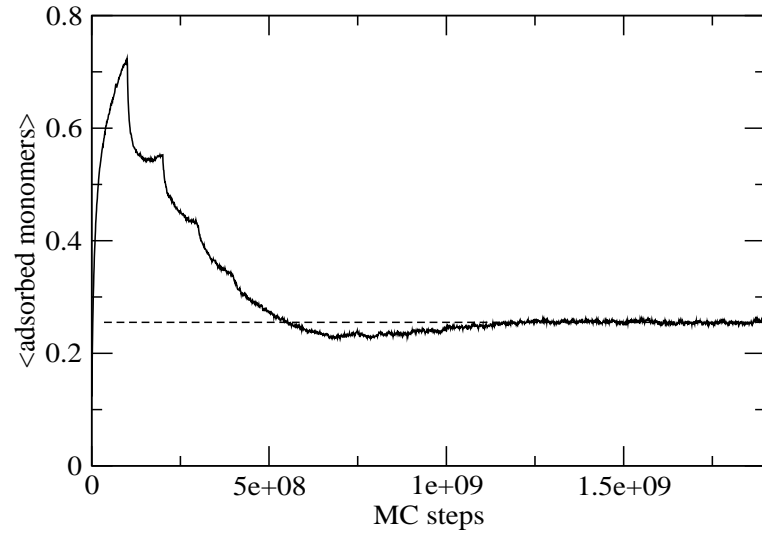


Figure 3.2: Variation of the average number of adsorbed monomers of the configurational file with respect to Monte Carlo (MC) steps for a system with $N = 100$, $\phi^0 = 0.058$ and $\varepsilon = -0.35 kT$.

Effectively, a sampling suitable for a dilute bulk solution may not be statistically relevant when concentrate solutions are used, although it could still be relevant at intermediate concentrations.

In the case that ideal instead of self-avoiding chains are generated in the sampling, the procedure followed is the same except for the fact that there is no energy penalty if monomers overlap. Notice that the generation of ideal chains in the sampling effectively eliminates the excluded volume correlations along the chains, due to the fact that the intra chain excluded volume repulsions are incorporated into the mean field $\pi(\mathbf{r})$. This fact leads to a sampling with more compact conformations that will produce a different behaviour. This effect will be discussed later on.

3.2 Structure of the adsorbed layer as predicted by SCMF.

Let us introduce the characteristic lengths in polymer adsorption onto flat walls. Firstly, the bulk correlation length ξ defines the distance at which density perturbations die out. The numerical value that we will use in this section will be calculated from the expression (see eq. 1.18)

$$\xi \equiv R_g \left(\frac{\phi^0}{\phi^*} \right)^{-3/4} \quad (3.2)$$

as obtained from scaling arguments for excluded volume chains [17], with ϕ^0 , the volume fraction of monomers in the bulk, and ϕ^* the monomer volume fraction at the overlap (see also chapter 1). The overlap concentration c^* is defined as (c.f eq. 1.16)

$$c^* \equiv \frac{3N}{4\pi R_g^3} \quad (3.3)$$

where R_g is the radius of gyration of the chain numerically obtained in a homogeneous system. In the case of ideal chains, we will still use eq. (3.2) but with exponent $-1/2$ and the radius of gyration corresponding to that of the markovian chain. The overlap volume fraction is thus, $\phi^* = v_p c^*$.

Secondly, the thickness of the layer that we will use along this work will be obtained from the expression

$$\lambda^2 \equiv \frac{\int z^2 \phi_a(z) dz}{\int \phi_a(z) dz} \quad (3.4)$$

where ϕ_a is the volume fraction monomers belonging to adsorbed chains (cf. eq. 1.72). Similarly, from the volume fraction of monomers belonging to loops and tails their corresponding root mean square thickness λ_t and λ_l respectively, are obtained.

As far as the inner structure of the adsorbed layer is concerned, it is customary to define *loops* as being portions of the adsorbed chain between two monomers in contact with the wall, *tails* are portions of the chain between the last adsorbed monomer and an end, while *trains* are sequences of monomers all in contact with the wall [1]. Here, however, we will make no distinction between trains and loops. The density profiles of monomers belonging to loops and to tails are, therefore, indicators of this internal structure. Then, third and last, the crossover length z^* is defined in this work as the distance at which loop and tail monomer concentration profiles, c_l and c_t , respectively, cross each other [5], separating the adsorbed layer into a loop and a tail sublayers. This can be formally stated as

$$c_l(z^*) = c_t(z^*) \quad (3.5)$$

With regard to the bulk concentration, also different regimes are usually distinguished. We have already defined the overlap concentration c^* in eq. (3.3). Since the thickness of the layer scales as the size of the polymeric coil, R_g , the layer starts to be significantly affected by the presence of free chains in its vicinity when the bulk concentration approaches the overlap concentration, that is, when $\xi \sim \lambda$. In the second place, the concentration c_1 is defined as the concentration at which $\xi \sim z^*$ so that the loop layer starts to merge into the bulk free polymers [6]. At higher polymer densities a concentration c_2 can also be introduced [18], but its analysis lies beyond the scope of this work.

Let us first consider the predictions of one-chain properties for an homogeneous system. In Fig. 3.3 we show the functional dependence of the end-to-end distance of the chains with respect to the number of segments N , in a system with a homogeneous polymer density, as obtained from our SCMF methodology. We compare both, the self-avoiding (or non-markovian) chains and the markovian chains, that is, non-markovian and markovian connectivity, respectively. The numerical results of end-to-end distance as well as radius of gyration for both kinds of chains are listed in Table 3.1.

Notice that the physical problem posed in both cases is exactly the same, but the methodology differs in the allowed conformations of the chains in the mean field, that is, in the choice of the reference state on which the mean field is build. The power law behaviour found for the radius of gyration with self-avoiding chains in the sampling is

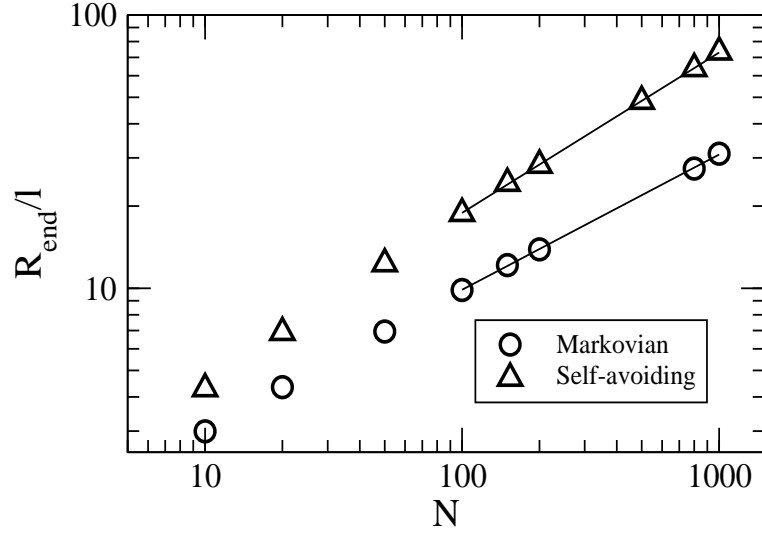


Figure 3.3: End-to-end distance corresponding to self-avoiding and markovian chains, obtained from SCMF method, as a function of chain length. Solid lines show the fitted power law, $N \geq 100$: $R_{end}/l = 1.27N^{0.587}$, for the case of self-avoiding walk chains (triangles), and $R_{end}/l = 1.02N^{0.495}$ for markovian chains (circles).

N	32	100	200	1000	A	ν
R_g^{SAW}/l	3.69	7.45	11.29	29.34	0.49	0.593
R_{end}^{SAW}/l	9.33	18.79	28.22	73.28	1.27	0.587
R_g^{Markov}/l	2.32	4.06	5.70	12.92	0.41	0.499
R_{end}^{Markov}/l	5.52	9.85	13.88	31.07	1.02	0.495

Table 3.1: Values of radius of gyration and end-to-end distances corresponding to self-avoiding walk as well as markovian chains, obtained from Single Chain Mean Field method (SCMF), for different chain lengths. The coefficient A and the exponent ν are the results of a fit of the data of Fig. 3.3, for $N \geq 100$, of the form $R_{g,end}/l = AN^\nu$

very close to that observed in excluded volume statistics, $R_g \sim lN^\nu$, with $\nu \simeq 3/5$ [19, 9]. On the other hand, the results for ideal chains are compatible with Gaussian (ideal chain) statistics, yielding an exponent $\nu \simeq 1/2$.

It is important to mention that the results found for R_g as well as for R_{end} , by means of the SCMF calculations for both, self-avoiding and ideal chains, are independent of the bulk monomer concentration c^0 used in the calculations. Therefore, already at this stage, two main conclusions can be drawn with respect to the SCMF method and its comparison with Markovian SCF as well as MC simulations. On the one hand, due to the fact that the characteristic size of the chain in the bulk is independent of monomer concentration, the expected crossover between the excluded volume statistics in very dilute solution and the ideal behaviour of chains in melts, as given by the scaling expression

$$R_g \sim l(l^3 c^0)^{-1/8} N^{1/2} \quad (3.6)$$

is not described by the SCMF formulation. Thus, the theory cannot properly predict the screening of the excluded volume correlations along the chain backbone by the local monomer concentration [17]. Thus, the chains are excessively swollen even at large bulk concentrations [20]. This effect is especially noticeable when long chains in semi-dilute solutions are considered. However, it is irrelevant for short chains, where the SCMF method has received the major field of application [21], since the overlap concentration is then much higher. The second conclusion, on the other hand, is that there are significant qualitative and quantitative differences between solving the mean-field problem by summing either over self-avoiding or over overlapping configurations, in the description of the one-chain properties [22]. In the first case, excluded volume correlations along the chain are preserved, while, in the second, all excluded volume effects are accounted for the mean field $\pi(\mathbf{r})$, yielding in general to more compact conformations. This difference will have significant effects on the description of adsorption that we will later discuss.

Let us consider only self-avoiding chains from now on unless the contrary is indicated. Fig. 3.4 shows typical results of the internal structure of the layer obtained by means of SCMF. In this case, we present results for loops, tails and adsorbed monomer volume fractions for two different chain lengths, $N = 100$ and $N = 200$, at bulk monomer fractions $\phi^0(N = 100) \simeq 0.058$ and to $\phi^0(N = 200) \simeq 0.033$, corresponding roughly to half of the overlap concentration in each case. The adsorption energy is $\varepsilon = -0.35kT$, above the threshold adsorption energy, the latter estimated to be around $\varepsilon = -0.28kT$ [23]. In Fig. 3.5, we have represented the adsorbed monomer volume fraction profile of the previous systems in a logarithmic scale. The figure shows that there is a regime near the wall that can be considered as following a power-law decay. The exponent obtained from the fit is -1.26 for $N = 100$ and -1.23 for $N = 200$, both very close to the scaling exponent $-4/3 \simeq -1.33$, obtained in the limit $N \rightarrow \infty$ [4].

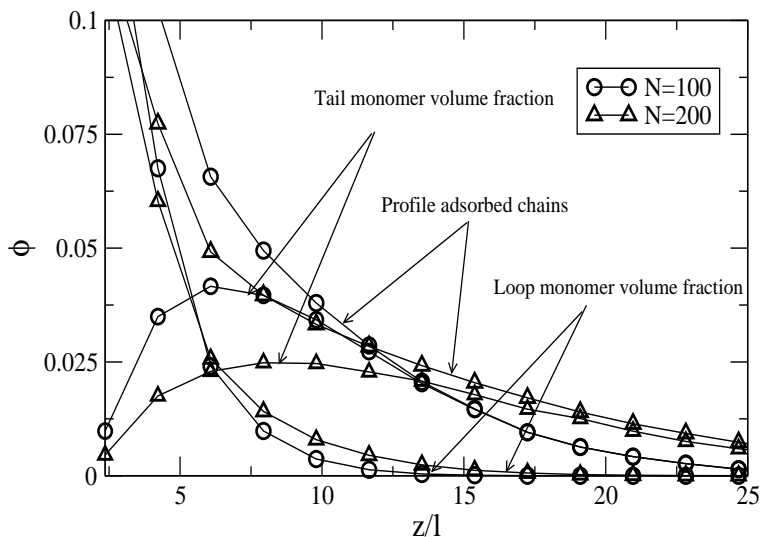


Figure 3.4: Representation of loop, tail and adsorbed monomer volume fraction profiles, obtained from Single Chain Mean Field method (SCMF), corresponding to chains of $N = 100$ (circles) and $N = 200$ (triangles) at bulk monomer volume fractions $\phi^0 \simeq 0.058$ and $\phi^0 \simeq 0.033$, respectively. In both cases $\varepsilon = -0.35 kT$.

Although there is a reasonable agreement between our numerical exponent and the scaling results under the conditions of concentrations near the crossover, we find that the initial apparent power-law decay depends on the bulk concentration in this regime of chain lengths, indicating that we are not in the asymptotic long chain scaling regime. This fact has already been pointed out in refs. [15, 24].

The characteristic lengths of the adsorbed layers under these representative conditions are listed in the following table 3.2.

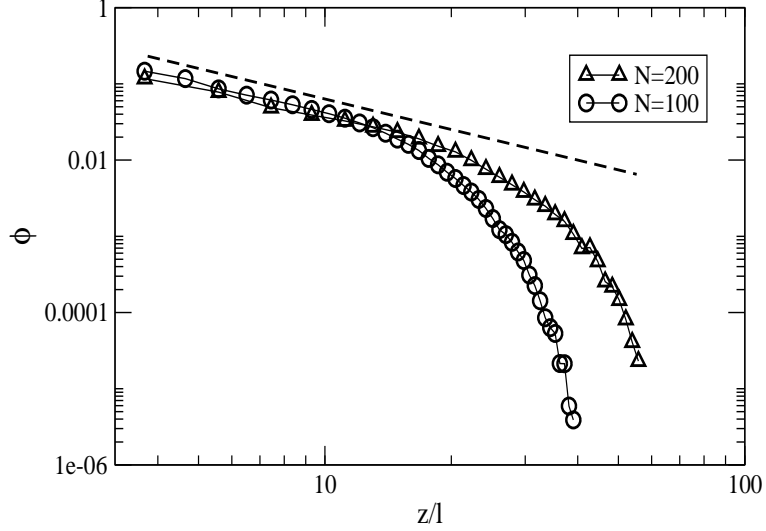


Figure 3.5: Representation of the adsorbed monomer volume fraction profiles corresponding to chains of $N = 100$ (circles) and $N = 200$ (triangles), obtained from Single Chain Mean Field approach (SCMF), at bulk monomer volume fractions $\phi^0 \simeq 0.058$ and $\phi^0 \simeq 0.033$, respectively. In both cases, $\varepsilon = -0.35 kT$.

N	z^*/l	λ/l	ξ/l	R_g/l
100	5.43	7.55	11.87	7.45
200	6.46	11.27	17.98	11.29

Table 3.2: Characteristic lengths of the adsorbed layer obtained from Single Chain Mean Field method (SCMF). For $N = 100$, the bulk monomer volume fraction is 0.058, and 0.033 for $N = 200$ monomers. In both cases, $\varepsilon = -0.35 kT$.

Since λ is close to z^* , these results correspond to the so-called *starved* regime, as it has been defined in references [6, 7]. In this regime, the central region of the adsorbed layer is dominated by the loops, the tails being important only near the cutoff of the layer. The situations that are analyzed in this work all lie in the starved regime. To go beyond the starved regime and have a neat distinction between the proximal, central and distal regions (cf. Chapter 1), it is necessary that $z^* \ll \lambda$ which implies that $N^{1/10} \gg 1$ (conversely, $N^{1/6} \gg 1$ in the Markovian mean-field), something that requires very long

chains. In the starved regime, the scaling length for the central region is precisely the thickness of the layer λ instead of z^* [7, 25].

It is of particular interest the decay of the tail monomer profile, since it offers a way to compare the intrinsic behaviour of the models analyzed here. The thickness of the tail monomer volume fraction profile should scale as the thickness of the whole layer which, in turn, should be proportional to the radius of gyration of the chain at a given concentration. In the example that we are analyzing here, one obtains

$$\frac{\lambda_t(N = 200)}{\lambda_t(N = 100)} = \frac{15.37}{10.12} = 1.52 \simeq \frac{R_g(N = 200)}{R_g(N = 100)} = 1.53 \simeq \left(\frac{200}{100}\right)^{3/5} \quad (3.7)$$

It is rather clear from the previous result that in this particular case the extension of the tails follows excluded volume statistics. Hence, according to the unscreened nature of the excluded volume correlations in the SCMF model, such a scaling will be expected all over the concentration range studied.

Together with the monomer volume fraction profiles, we have also obtained the end-monomer distribution profile, which is shown in Fig. 3.6 in logarithmic scale. The end-monomer distribution is a quantity difficult to obtain from simulations, since the sample points scale as the number of chains in the sample, instead of as the number of monomers. This number is usually too small to obtain good statistical meaning for a reasonable computer time. The quality of our data indicates the adequacy of the importance sampling method introduced in this work in the solution of the SCMF problem. The end-monomer distribution is of special theoretical interest since its decay near the adsorbing wall involves the so-called *magnetic susceptibility* exponent $\gamma \simeq 1.162$ in $d = 3$ (or $\gamma = 1$ in $d = 4$, which is also the value corresponding to the Markovian mean-field), which is independent of the Flory exponent ν [17]. Scaling arguments predict a decay of the form

$$c_{end}(z) \sim z^{-\beta/\nu} \quad (3.8)$$

where $\beta = (d\nu - \gamma)/2$. The numerical value obtained here is $\beta/\nu \simeq 1.4$ and $\beta/\nu \simeq 1.18$ for $N = 100$ and $N = 200$, respectively, while the scaling predictions are $\beta/\nu \simeq 0.532$. For this particular magnitude, the asymptotic predictions and the numerical SCMF results in the initial decay rate are more disparate than in the case of the total monomer density. Again, this apparent power-law behaviour is a function of the concentration, giving a less steeper decay as concentration increases. Again, this fact indicates that our results cannot be directly compared with scaling predictions because the latter are only valid in the asymptotic limit $N \rightarrow \infty$.

To end this section, the end-monomer distribution for different bulk concentrations is

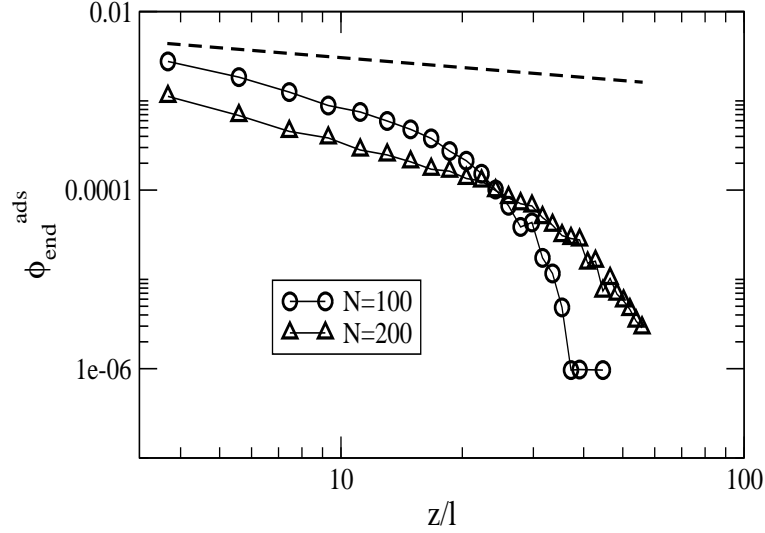


Figure 3.6: End-monomer distribution profile, corresponding to the adsorbed chains obtained from Single Chain Mean Field method (SCMF), for $N = 100$ (circles) and $N = 200$ (triangles) at bulk monomer volume fractions $\phi^0 \simeq 0.058$ and $\phi^0 \simeq 0.033$, respectively. Dashed line corresponds to a power law of -0.532 . In both cases $\varepsilon = -0.35 kT$.

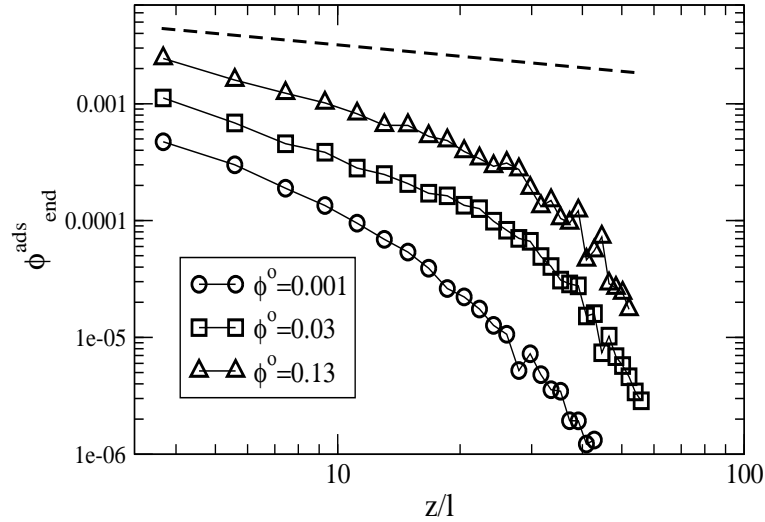


Figure 3.7: End-monomer distribution profile, corresponding to the adsorbed chains obtained from Single Chain Mean Field method (SCMF), for different bulk monomer volume fractions ($\phi^0 = 0.001, 0.03, 0.13$) considering $N = 200$ and $\varepsilon = -0.35 kT$. Dashed line corresponds to a power law of -0.532 .

represented in Fig. 3.7, in which $N = 200$ and $\varepsilon = -0.35 kT$. As already observed in the case of the monomer profiles, the initial power-law decay depends on the concentration and, therefore, we can again conclude that such short chains do not display the asymptotic regime expressed by the scaling exponents.

3.3 Comparison with Monte Carlo simulations

Since one of the main objectives of this work is to check the ability of the SCMF method in producing reliable data on polymer adsorption, in what follows we will focus our analysis on the behaviour of polymer adsorption as a function of the bulk concentration considering only a chain length $N = 200$. The comparison is done with data obtained from multi-chain lattice Monte Carlo simulations as given in refs. [15, 23]. There are, however, intrinsic difficulties in the comparison due to the different nature of the models. We have chosen to identify the spacing of the cubic lattice defined in these references with our monomer length l . With this identification, the obtained radius of gyration from both methods for isolated chains are rather close, $R_g(MC)/l = 9.37$ as compared with $R_g(SCMF)/l = 11.29$ (one can also compare the parameters of the fitting $R_g/l = 0.42N^{0.594}$ given in ref. [24], with those given in Table 3.1). Furthermore, we will compare the monomer volume fraction by simply multiplying our monomer concentration by the monomer volume $1.86l^3$, according to eq. (2.7). For chains of 200 monomers, the overlap concentration is obtained from eq. (3.3), giving $\phi^*(SCMF) = 0.061$ and $\phi^*(MC) = 0.051$ [24]. In addition, the adsorption energy is chosen to be the same in both models and equal to $\varepsilon = -1 kT$. To compare the profiles we have chosen that the layer 1 in the MC simulations coincides with the external border of the adsorbing well. Obviously, this choice of monomer length and excluded volume parameter can distort the one to one comparison of the data. However, in our analysis we will center our attention in intrinsic properties of the layer, expressed in the natural lengths in each case in order to be independent of the particular values chosen. In addition, aiming at a finer comparison with MC data, we have introduced a finer division in the simulation box, with layers of thickness $0.93l$, inside which the value of the Lagrange multiplier field $\pi(z)$ has been calculated from the SCMF equation (2.32).

In Figs. 3.8, 3.9 and 3.10 we show the comparison between monomer fraction profiles obtained from SCMF and MC simulations. In both methods the bulk monomer fraction is $\phi^0 = 0.0026$, corresponding to a very dilute solution. Despite the fact that the models used are rather different, the results for the total monomer volume fraction are very good, as can be seen in Fig. 3.8. The difference in the volume fraction of monomers at contact with the wall could be attributed to the fact that the value of the volume fraction in this point is strongly dependent on molecular details of the models, as far as the monomers and the potential well are concerned. Table 3.3 summarizes the volume fractions at contact with the wall for four different concentrations.

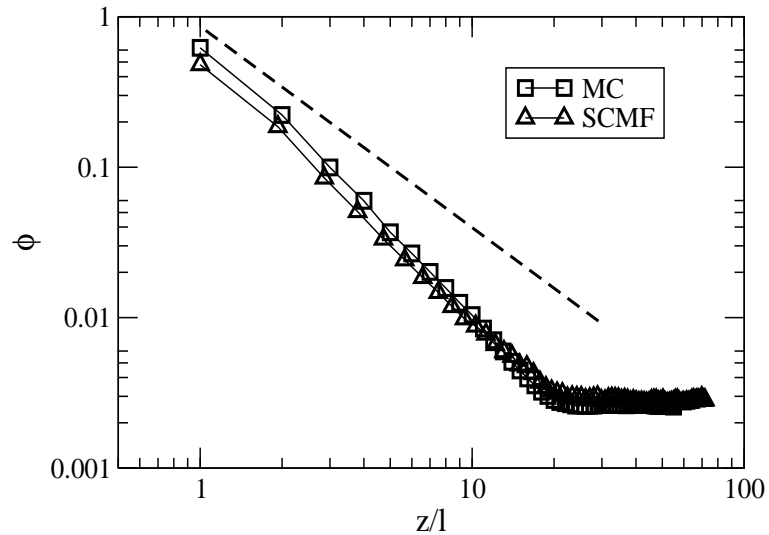


Figure 3.8: Comparison of the total monomer volume fraction profiles obtained from Single Chain Mean Field (SCMF) and Monte Carlo (MC) simulations. Conditions of the system are: $N = 200$, $\phi^0 = 0.0026$ and $\varepsilon = -1 kT$. The dashed line corresponds to a power law $-4/3$. SCMF: triangles and MC: squares

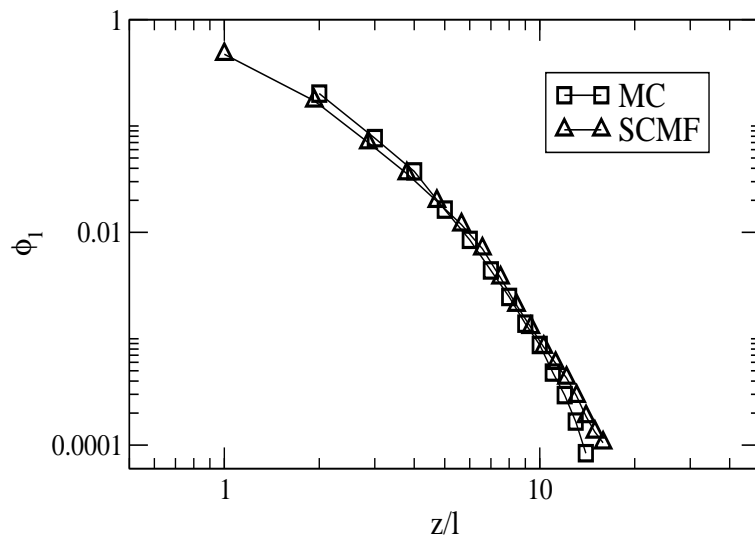


Figure 3.9: Comparison of the loop volume fraction profiles obtained from Single Chain Mean Field (SCMF) and Monte Carlo (MC) simulations. Conditions of the system are: $N = 200$, $\phi^0 = 0.0026$ and $\varepsilon = -1 kT$. SCMF: triangles and MC: squares

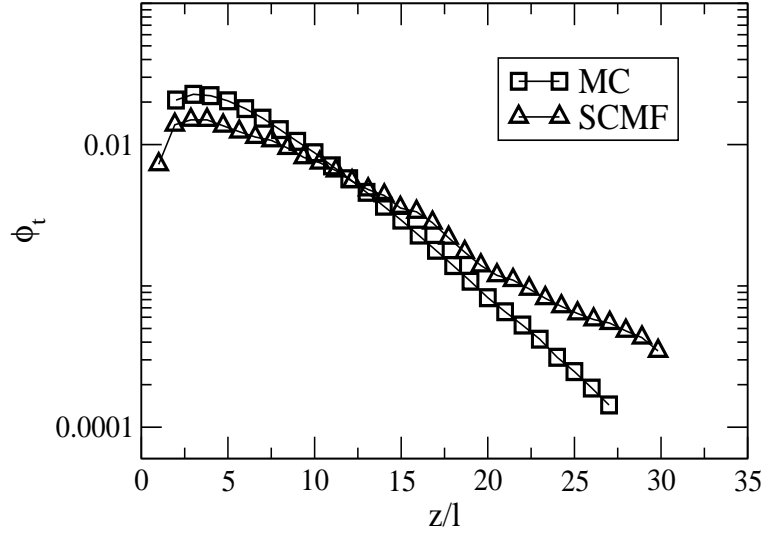


Figure 3.10: Comparison of the tail volume fraction profiles obtained from Single Chain Mean Field (SCMF) and Monte Carlo (MC) simulations. Conditions of the system are: $N = 200$, $\phi^0 = 0.0026$ and $\varepsilon = -1kT$. SCMF: triangles and MC: squares

ϕ^0	$\phi^{SCMF}; N = 100$	$\phi^{SCMF}; N = 200$	$\phi^{MC}; N = 200$
0.0026	0.47	0.48	0.62
0.022	0.50	0.50	0.63
0.11	0.56	0.56	0.67
0.81	0.91	0.91	0.92

Table 3.3: Volume fraction at contact with the wall for different bulk monomer volume fractions. The results correspond to an adsorption energy $\varepsilon = -1kT$, being obtained by means of Single Chain Mean Field (SCMF) for polymer lengths $N = 100$ and $N = 200$, as well as for Monte Carlo (MC) simulations for chains $N = 200$

Despite the numerical differences in the volume fraction at contact with the wall, MC and SCMF results are consistent. In the case of SCMF values for $N = 100$ and $N = 200$, they indicate that this magnitude is rather independent of the size of the chain and only depends on the bulk concentration, for fixed adsorption energy ε . Furthermore, it is interesting to observe that, with a smooth increase of the bulk concentration, both models show that the surface is saturated at high bulk monomer concentration. However, a detailed analysis of this effect lies beyond the scope of this work.

The straight dashed line plotted in Fig. 3.8 corresponds to a slope of $-4/3$ which is the scaling prediction for $N \rightarrow \infty$, according to eq. (1.36). It is not obvious the existence of a power-law regime (the exponent in the central region of the profiles would be near the -2 , and smaller near contact). With no doubt, the decay presented in both results is steeper than the scaling predictions for self-avoiding chains. Although this decay would seem close to that predicted by scaling arguments with ideal chains (the exponent is -2 for scaling laws with $\nu = 1/2$ and $d = 4$, given in eq. (1.38), c.f. section 1.2), one should not infer that the decay is correctly given by Markovian mean-field calculations. Effectively, the solution of the SCMF equations with Markovian overlapping chains shows an even steeper decay for this chain length. The same kind of behaviour is observed in the solution obtained with the Scheutjens-Fleer method [15]. This power-law regime, therefore, depends on bulk concentration for such moderately long chains, very far from the asymptotic limit where the scaling results would be valid. This effect has already been discussed in refs. [23, 24] and our data is in agreement with that fact.

In Fig. 3.9 we compare the SCMF and MC results for the loop monomer volume fraction profile in logarithmic scale. MC data suppresses the value at contact with the wall, attributed to trains. We observe that again, the agreement is very good, although the SCMF produces a slightly thicker layer. It is also noticeable that no power-law regime is identifiable in none of the data sets. Although scaling predicts a power-law decay of $-4/3$ for this quantity near the wall, the observed behaviour in the numerical data is in agreement with a faster initial decay, close to a power -3 .

Fig. 3.10 represents the volume fraction profiles of monomers belonging to tails in a semi-logarithmic scale. In this profile, the differences between the SCMF and MC results are more pronounced. The decay in the *distal* part of the layer is close to a single exponential decay in the MC data. SCMF data is affected by statistical inaccuracy at the low density part of the profile, but it is rather obvious that the data shows a much more slow decay. The exponential fit $\phi_t = A \exp(-\alpha z)$ to the distal region of the tail layer gives an exponent $\alpha = -0.244$ for the MC data, and -0.160 for the SCMF. This difference can be analyzed from another perspective, taking into account the fact that this exponent has to be inversely proportional to the characteristic size of the tails which can be defined as $l N_t^{3/5}$. Thus, we can write

$$\frac{\alpha(MC)}{\alpha(SCMF)} = \frac{0.244}{0.160} = 1.53 \simeq \left(\frac{N_t(SCMF)}{N_t(MC)} \right)^{3/5} \quad (3.9)$$

where the Flory exponent $3/5$ has been used since the bulk is very dilute and there is no screening of the excluded volume correlations. From this equation we can infer that $N_t(SCMF)/N_t(MC) \simeq 2.03$, which means that the size of the tails predicted is approximately twice that of the MC data. For consistency, we have verified, in addition, that our tail profile for $N = 100$ agrees very well with the tail profile obtained from MC data but with $N = 200$, confirming our estimation of the size of the tails. This discrepancy of a factor near 2 is surprising. Although the statistics that we have in our method in this part of the profile is rather poor, due to the fact that the differences between the tendencies exist all over the profile, we think that it cannot be attributed to the lack of statistics. Thus, assuming the correctness of the MC data, we attribute the discrepancy in the size of the tails, on the one hand, to the difference between the radius of gyration which is roughly of a factor of 1.53. On the other hand, MC data at contact with the wall is larger by a 20%, hence negatively contributing to the amount of material in the tail layer. In any case, the contribution of the tail layer to the profile is small except near the edge of the layer, where the overall density is small. Thus, this discrepancy is not relevant for the overall density profile, although has its importance as far as the description of the structure of the layer is concerned.

In table 3.4 the characteristic lengths of the layer for four different concentrations are shown

ϕ^0		z^*	λ	λ_l	λ_t	ξ	R_g
0.0026	<i>MC</i>	4.79	3.85	3.19	8.35	91.50	9.76
	<i>SCMF</i>	7.53	4.45	4.26	11.50	121.53	11.29
0.022	<i>MC</i>	4.71	5.36	3.58	9.91	18.44	9.76
	<i>SCMF</i>	7.60	6.91	4.41	14.88	24.49	11.29
0.11	<i>MC</i>	4.04	7.33	4.09	10.77	5.56	9.76
	<i>SCMF</i>	6.32	10.66	5.21	15.91	7.33	11.29
0.81	<i>MC</i>	3.44	7.93	4.62	9.56	1.25	9.76
	<i>SCMF</i>	5.38	13.52	6.23	16.19	1.65	11.29

Table 3.4: Characteristic dimensions of the adsorbed layer, in units of l , obtained from Single Chain Mean Field (SCMF) and Monte Carlo (MC) methods, for various bulk volume fractions.

The thickness of the layer has been calculated to be $\lambda = 4.45 l$ while for the tails its value rises up to $\lambda_t = 11.50 l$, which is close to the value of the radius of gyration of the chain, $11.29 l$. Notice also that the crossover length $z^* = 7.53 l$ is larger than the thickness of the layer, corresponding to a starved regime. Thus, the profile in the central and distal regions is dominated by one single length, namely λ [25] (or, equivalently, z^*). In the limit $N \rightarrow \infty$ the crossover length in the central regime is z^* while λ is important only near the cutoff of the layer in the distal region, since $z^* \ll \lambda$ [5, 6].

Figs. 3.11, 3.12 and 3.13 correspond to a higher volume fraction $\phi^0 = 0.11$, above the overlap concentration, considering the same chain length and adsorption energy as before. The general analysis comes along the same lines as in the previous case. The total monomer volume fraction of the adsorbed chains obtained from SCMF slightly deviates from the MC results in all the regime. This fact is rather obvious in the tail monomer profile, according to Fig. 3.13. This fact is reminiscent of non-screening of the excluded volume correlations in semidilute solution in our methodology, since the major part of the tail layer is embedded in the bulk fluid at this concentration. Effectively, the bulk correlation length has been calculated from eq. (3.2) obtaining $\xi = 7.33 l$, while the thickness of the layer is $\lambda = 10.66 l$ (see Table 3.4). The thickness of the tail profile is in turn $\lambda_t = 15.91 l$. Therefore, it seems rather clear that as the concentration increases, the lack of screening tends to slightly deviate the profiles from the MC simulation data, yielding thicker layers. Finally, the calculated value of the crossover length is $z^* = 6.32 l$. Notice that ξ is very close to z^* which indicates that this concentration is very close to $\phi_1 = v_p c_1$ at which the loop layer enters in contact with the bulk polymers.

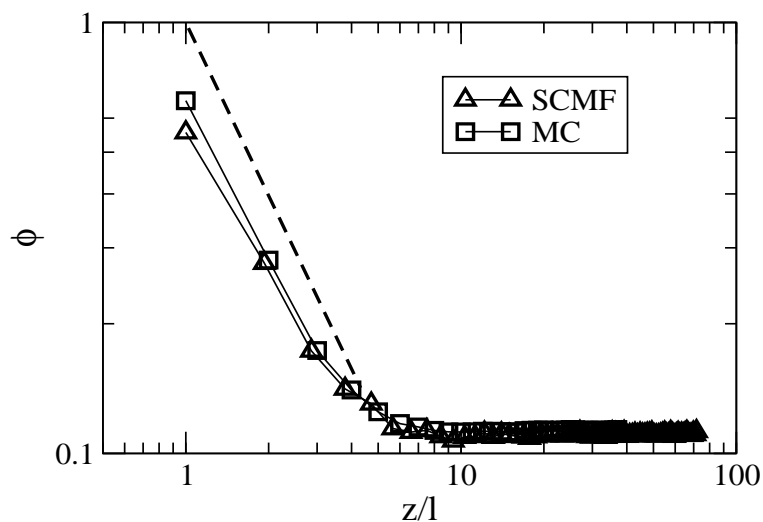


Figure 3.11: Monomer volume fraction profiles obtained from Single Chain Mean Field (SCMF) and Monte Carlo (MC) simulations. Conditions of the system are: $N = 200$, $\phi^0 = 0.11$ and $\varepsilon = -1 kT$. The dashed line corresponds to a power law $-4/3$. SCMF: triangles and MC: squares

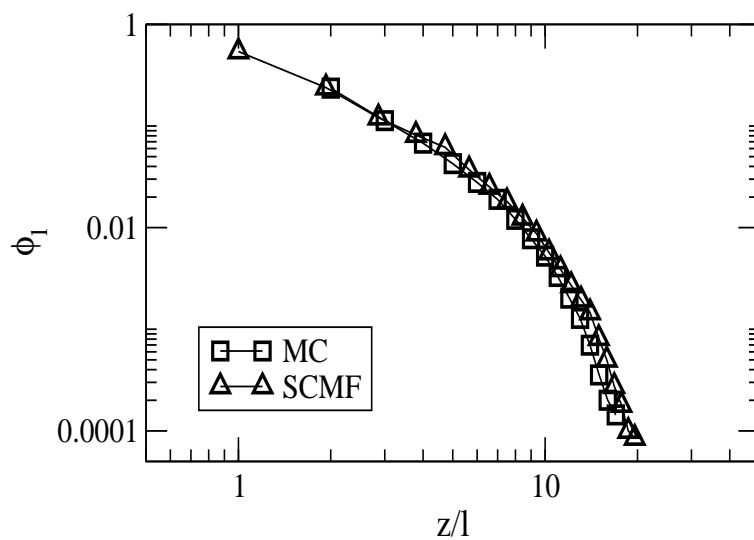


Figure 3.12: Loop volume fraction profiles obtained from Single Chain Mean Field (SCMF) and Monte Carlo (MC) simulations. Conditions of the system are: $N = 200$, $\phi^0 = 0.11$ and $\varepsilon = -1 kT$. SCMF: triangles and MC: squares

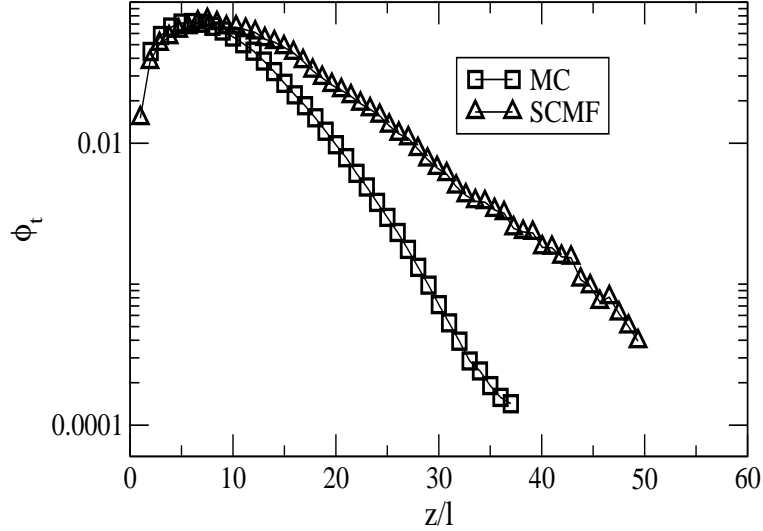


Figure 3.13: Tail volume fraction profiles obtained from Single Chain Mean Field (SCMF) and Monte Carlo (MC) simulations. Conditions of the system are: $N = 200$, $\phi^0 = 0.11$ and $\varepsilon = -1 kT$. SCMF: triangles and MC: squares

In general one can say that SCMF and MC results increasingly deviate as the concentration increases and the behaviour of MC chains tend to be more ideal as the concentration approaches the melt. To illustrate this point, in Figs. 3.14, 3.15 and 3.16 we present, respectively, the dependence of the total, loop and tail root mean square (*rms*) thickness of the adsorbed layer with the bulk volume fraction as obtained from SCMF and MC methods. The thickness of the loop layer is more insensitive to the variations of the bulk concentration, and shows a good agreement in all the studied regimes, as it is seen in Fig. 3.15 (Notice that the scale is finer than for the tail layer, for instance, and, in addition, there is a shift of about one l due to the different thickness of the adsorbing well in SCMF and MC calculations). The thickness of the tail layer, in turn, increases with concentration, essentially due to the progressive competition between chains to cover the same surface, which induces a decrease in the adsorption energy per chain. The increase of λ and λ_t with bulk concentration in our model is much more important than that found in MC calculations, especially beyond the overlap concentration, when the majority of the distal part of the layer is inside the homogeneous bulk. It is interesting to notice, however, the decrease of the thickness for concentrations above ϕ^* , due to the shrinking of the polymers as concentration increases (reduction of the blob size). Again, the non-screening of the excluded volume correlations do not produce such a decrease in the SCMF data, although the increase is slower and, in the case of the tails, even tends to a plateau.

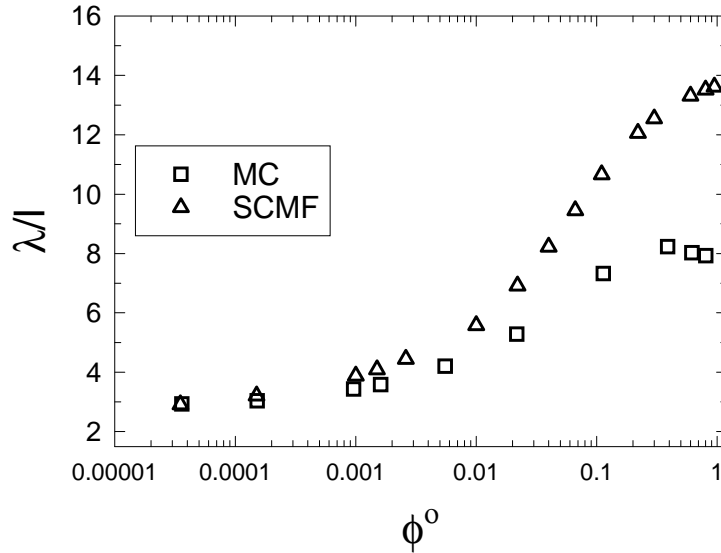


Figure 3.14: Variation of *rms* thickness as a function of bulk volume fraction. Conditions of the system: $N = 200$ and $\varepsilon = -1 kT$. Single Chain Mean Field results (SCMF) are represented by triangles and Monte Carlo results (MC) by squares.

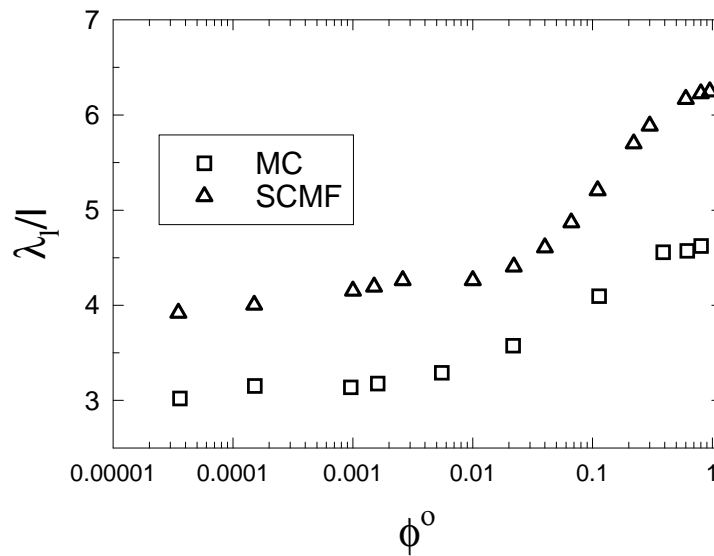


Figure 3.15: Variation of loop *rms* thickness as a function of bulk volume fraction. Conditions of the system: $N = 200$ and $\varepsilon = -1 kT$. Single Chain Mean Field results (SCMF) are represented by triangles and Monte Carlo results (MC) by squares.

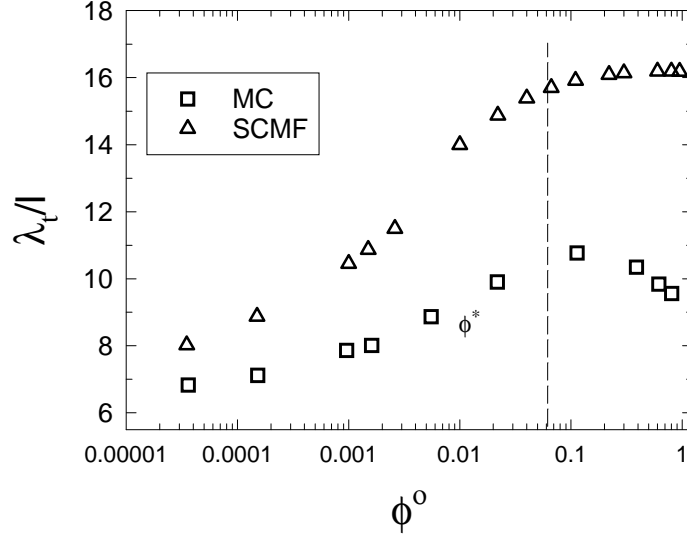


Figure 3.16: Variation of tail *rms* thickness as a function of bulk volume fraction. Conditions of the system: $N = 200$ and $\varepsilon = -1 kT$. Single Chain Mean Field results (SCMF) are represented by triangles and Monte Carlo results (MC) by squares. The value of ϕ^* , obtained from SCMF method, is equal to 0.061.

To end this section, we will present SCMF results of the adsorbance and we will compare them with simulation data available. The adsorbance has been defined as

$$\Gamma = \int_0^\infty c_a(z) dz \quad (3.10)$$

Thus, the defined adsorbance has dimensions of number of monomers per l^2 . The adsorbance of loop and tail monomers can be obtained from the same expression, replacing the corresponding adsorbed monomer concentration.

In Fig. 3.17 we present the adsorbance as a function of the concentration, for the conditions of chain length and adsorption energy previously used. We observe a good agreement between both series of data. The increase of the adsorbance starts near the crossover concentration, where the competition between the polymers to cover the surface causes them to prefer more elongated conformations, with larger loops and tails. This is the same effect that causes the thickness of the layer to increase, as has already been previously mentioned.

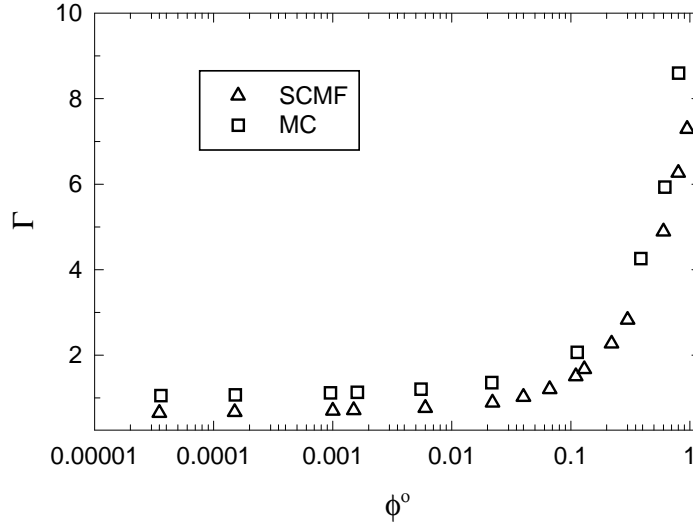


Figure 3.17: Variation of the adsorbance (number of monomers per l^2) in function of bulk volume fraction. Conditions of the system: $N = 200$ and $\varepsilon = -1kT$. Single Chain Mean Field results (SCMF) are represented by triangles and Monte Carlo results (MC) by squares

3.4 Comparison with SCF methods based on Markovian chains

In this section the effect of the use of Markovian (Gaussian) chains in the solution of the SCMF equations and its relationship with other self-consistent field methods, in particular with Scheutjens and Fleer [1], will be analyzed. In all cases we have used the same set of parameters as before, $N = 200$, $\varepsilon = -1kT$ and different bulk monomer volume fractions. For the SCF model, the data correspond to the same value l for the monomer length, identifying the parameter χ_s with the adsorption energy ε of our calculations [25, 26].

Figs. 3.18.a and 3.18.b show, respectively, loop and tail monomer volume fraction profiles from SCMF equations, using overlapping chains in the sampling, in comparison with the SCF data of Scheutjens and Fleer, at very dilute solution $\phi^0 = 0.0026$. In the case of tail monomer volume fraction profiles, we observe that the initial value differs from the SCMF calculations because the definition of the tails, in the first layer, is different but the rest of the layer agrees very well with the numerical SCF calculations in almost three decades. Notice also that we have plotted the previous SCMF results with self-avoiding

chains as well as the MC results, which follow a completely different trend. It is hopeless trying to identify a power-law regime in the figure, but it is obvious the faster decay shown by the markovian results (SCMF as well as SCF) with respect to the self-avoiding results, also pointed out by Bitsanis and collaborators [15, 23]. The tail layer profile is given in Fig. 3.18.b. In this case, the agreement between Markovian SCMF and SCF is restricted to one decade, due to the inaccuracy in our profile caused by the low value of the concentration in the distal part of the layer. In addition, the decay of the tail profile is faster for markovian chains than for self-avoiding. Effectively, an exponential fit of the form $\phi_t = A \exp(-\alpha z)$ gives $\alpha \simeq 0.279$ for the Markovian SCMF result and $\alpha = 0.313$ in the SCF case, which are very close.

For a semidilute solution with $\phi^0 = 0.11$, the agreement between the structure of the loop layer as resolved by Markovian SCMF and SCF is again very good in at least four decades, according to Fig. 3.19.a. As before, there is some deviation in the initial decay, probably due to the essential difference between the models and the lack of representative data in this proximal region. Again, the decay is much faster than for the self-avoiding case. The tail profile (Fig. 3.19.b) shows also deviations in the direction of a thicker layer. Since in this case excluded volume correlations along the chain are disregarded by both, the SCF model of Scheutjens and Flerer and our Markovian SCMF, the reason for the deviation has to be found in a lack of statistical meaning of the conformations chosen for the evaluation of the profiles. A more representative sampling should be used to obtain a better description of the outer part of the layer.

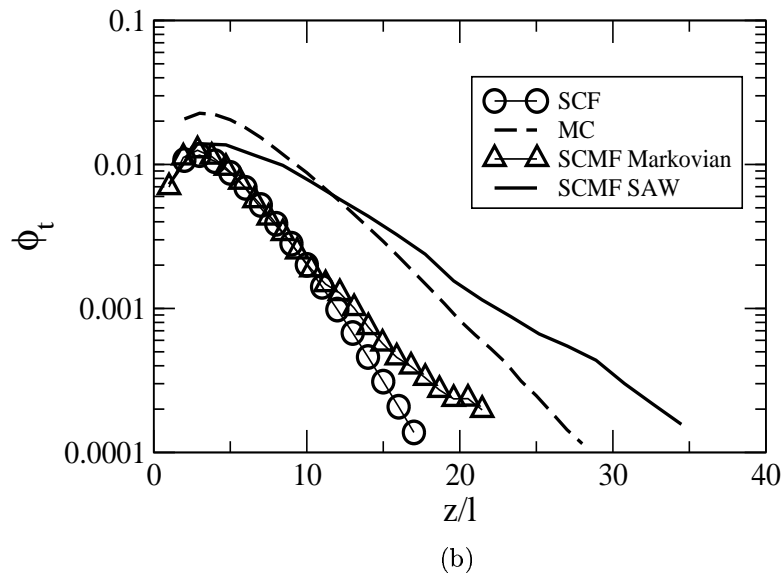
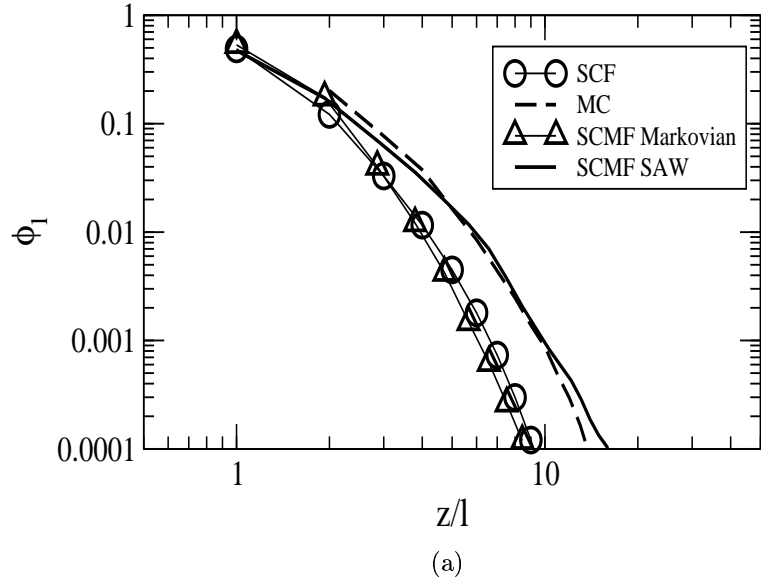


Figure 3.18: Loop (a) and tail (b) monomer volume fraction profiles corresponding to markovian and self-avoiding walk (SAW) chains. Conditions of the system: $N = 200$, $\phi^0 = 0.0026$, $\varepsilon = -1 kT$. Markovian results are obtained from Scheutjens-Fleer method (SCF) (circles) and Single Chain Mean Field (SCMF) method (triangles). In the case of self-avoiding walk results (SAW), they are obtained from Monte Carlo method (MC), dashed line, simulations and Single Chain Mean Field method (SCMF), full line.

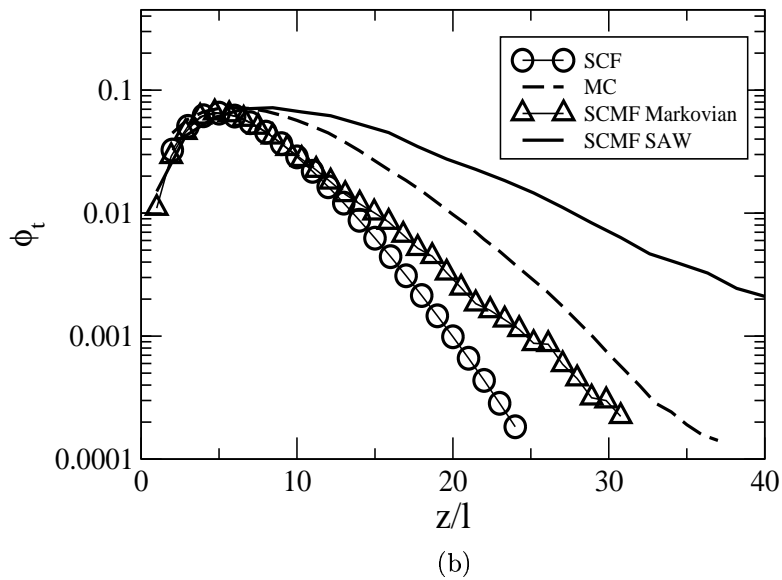
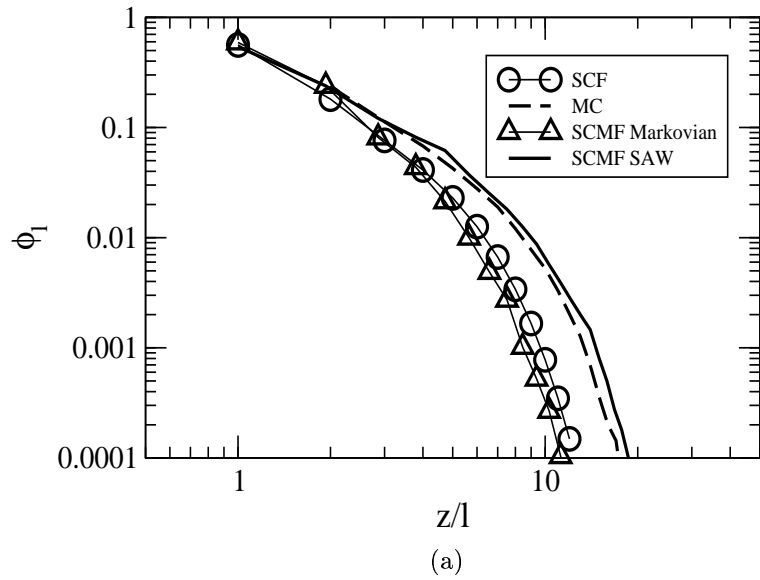


Figure 3.19: Loop (a) and tail (b) monomer volume fraction profiles corresponding to markovian and self-avoiding walk(SAW) chains. Conditions of the system: $N = 200$, $\phi^0 = 0.11$, $\varepsilon = -1 kT$. Markovian results are obtained from Scheutjens-Fleer method (SCF) (circles) and Single Chain Mean Field (SCMF) method (triangles). In the case of self-avoiding walk results (SAW), they are obtained from Monte Carlo (MC), dashed line, simulations and Single Chain Mean Field method (SCMF), full line.

3.5 Conclusions

The main purpose of this chapter has been to present and validate the results obtained from SCMF method for the case of the adsorption of polymers at flat surfaces. On the one hand we have been able to show the efficiency of the *importance sampling* method, introduced in chapter 2, applied in the framework of the known Single Chain Mean Field theory for the problem of polymer reversible adsorption. On the other hand, from our methodology, it has been possible to obtain results corresponding to self-avoiding and Markovian chains that have been compared, respectively, with other known methodologies as Monte Carlo simulations or the Markovian self-consistent field method of Scheutjens and Fleer. We will briefly discuss both points in what follows.

The advantage of the importance sampling is that all the samples of the one-chain configurational space contribute to the averages with the same weight, inducing to a reduction of the number of samples required for a problem such as polymer adsorption, characterized by a narrow well near a repulsive wall. Our results have been obtained with a reduced number of configurations (2×10^4), that can be handled by common PC's. To relax the probability distribution towards the desired bias, we have introduced a Metropolis rule, viewing the configurational file as a pseudo-system of independent chains in a biasing field. This procedure is clearly rather time-consuming although efficient enough. In addition, the procedure permits to arrive to the optimal sampling for each situation, something that has allowed us to a drastic reduction of the computer memory used in our calculations. However, other methodologies, such as the Rosenbluth chain regrowth algorithm [27] are actually being used in this context, with much less intensive use of CPU time [28]. It is worth mentioning again that the advantage of our SCMF field calculations with respect to true many-chains MC simulations is that the topology of the configurational space is much smoother in the former than in the latter and, furthermore, that the sampling file can be used in many different physical situations, not being necessary the reconstruction of the sampling in each case.

As far as the results are concerned, we have shown that the agreement between the SCMF results with self-avoiding chains and MC simulations is very good, despite the disparate nature of the models used in each case. We have obtained the same density dependence as found in MC simulations in dilute as well as semidilute solutions, in several magnitudes such as monomer density profile, loop density profile, adsorbance, etc. However, the major drawback of our method is the lack of screening of the excluded volume correlations along the chain. This fact leads to swollen chains under all situations, independently of the local monomer volume fraction. This effect is especially noticeable in homogeneous concentrated solutions, where the chain statistics is physically expected to be Gaussian (ideal), although SCMF results give self-avoiding statistics, typical of dilute solutions. Hence, tail monomer density profiles are generally thicker than found in MC simulations and, furthermore, the obtained thickness of the layer is larger than in MC,

especially for semidilute solutions. This fact has already been recognized in the literature [20, 22], and the explicit consideration of the chain excluded volume depending on the particular configuration of the chain is clearly a way to partially introduce the effect of the screening of the excluded volume correlations. This particular point will be analyzed in detail elsewhere. In general, the results of the SCMF theory give a quantitative description of the behaviour of inhomogeneous polymeric systems.

Last but not least, we have compared the results of our mean-field approach when overlapping chains are used. This procedure renders our approach conceptually equivalent to the Markovian SCF methodology, based on Edwards propagator, widely used in polymer chemical physics. Effectively, the profiles predicted by matching the parameters of the model, with no adjustable parameters, is excellent. Only the distal part of the adsorbed layer is affected in our case of a lack of representative statistics, and thus inducing to deviations in the tail profile in the last part. The formal relationship between the SCMF and the SCF methods based on ideal chain statistics has been shown [20, 22]. Here we have shown that the fundamental difference between the two methods is the explicit consideration of the correlations along the chain in the former. The SCF methods based on Edwards propagator [29] make explicit use of the Markovian character of the chain [30], the monomers interacting only with the self-consistent field. On the other hand, the SCMF technique with self-avoiding configurations takes into account the non-Markovian nature of the chain with excluded volume interactions. Of course, when this point is relaxed by allowing the generation of chains without internal excluded volume interactions, the Markovian character of these conformations is recovered and, therefore, Markovian SCMF and SCF results completely agree.

By our analysis, it is thus made clear the nature of the SCMF calculations and the importance of the one-chain excluded volume correlations in the problem of polymer adsorption, with relatively long chains. Thus, markovian SCF calculations correspond to our SCMF theory with overlapping chains. The behaviour predicted in this way quantitatively and qualitatively differs from that observed in the MC simulations. On the other hand, the agreement between our SCMF calculations with self-avoiding chains and the MC simulations indicate that the structure of the layer is mainly determined by the excluded volume correlations along one single chain, the many chain correlations being not so important. This behaviour has the roots in the local swelling of the chain, correctly accounted for by the SCMF equations. However, in the actual formulation of the theory, it is also clear that the screening of the excluded volume correlations by the local monomer density is not properly described.

Finally, despite the good agreement between SCMF with self-avoiding conformations and MC results for polymer adsorption, it is expected that the former leads to a classical behaviour in those properties that strongly depend on long wave-length correlations involving many chain behaviour, as in the vicinity of the critical points of phase separation. Obviously, this is due to the essential mean-field nature of the SCMF free energy.

3.6 Appendix A

3.6.1 Periodic boundary conditions

Monte Carlo simulations is the computational method of choice because it helps us to relate the equilibrium properties of polymeric systems (e.g. chains conformations, phase behaviour) to the atomic structure of these molecules. Therefore, simulations are a useful aid in the interpretation of experimental data and in addition to allow us to gain a better insight into the validity of theoretical models.

However, simulations have their limitations as, for example, computer speed and memory. Although computers are more and more capacity, in the most of simulations only a small sample of particles (only a few thousand of them) can be used, being this number many orders of magnitude smaller than the $\sim 10^{23}$ typically, found in experimental samples. Such restrictions lead to finite size effects, that is, spurious artifacts and systematic discrepancies compared to the bulk limit. Thus, in the case of simulating bulk phases, the main problem is the ratio of the particles at the surface compared with the size of the system. Therefore, in order to simulate bulk phases it is necessary to choose boundary conditions which mimic the presence of an infinite bulk surrounding our system [16].

In this method the primitive cell, containing N particles (in our case the particles are polymer chains), is considered as the primitive cell of an infinite periodic lattice of identical cells (Fig. 3.20), so that whether a particle or a polymer chain is moved in the primitive cell, its own periodic image move in the same way in the other cells, thus the density is kept constant in all the cells.

Application of this method leads to a high degree of correlation not present in a macroscopic bulk system, and this correlation can be much more important if the system is too small. Moreover, chain/chain interactions may occur between the chain and its images, which also introduces a high degree of correlation. Therefore, in practice are only considered short-range interactions. In that case all intermolecular interactions are truncated beyond a certain *cutoff distance* r_c , whose choice will depend on the model system under study [16].

It is also known the method of the *minimum image convention*. In this case, the interactions of a particle with its images are considered until the minimum distance between them.

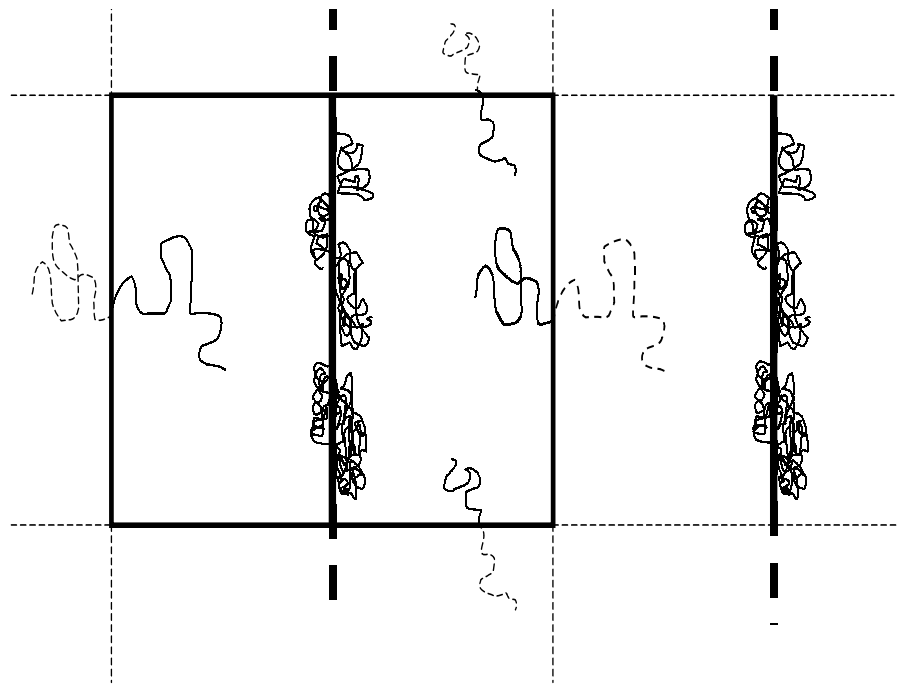


Figure 3.20: Illustration of periodic boundary conditions in the case of adsorption of polymers. The part of the conformation (dotted line) that passes the boundary plane is re-inserted in the opposite plane as a continuation of the original chain

Bibliography

- [1] G. J. Fleer, M.A. Cohen-Stuart, J. M. H. M. Scheutjens, T. Cosgrove and B. Vincent, *Polymers at Interfaces* (Chapman and Hall, London, 1993) and references there in.
- [2] I. Jones and P. Richmond *J. Chem. Soc. Faraday Trans.2* **73**, 1062 (1977).
- [3] S. F. Edwards *Proc. Phys. Soc. (London)* **85**, 613 (1965).
- [4] P. G. de Gennes *Macromolecules* **14**, 1637 (1981).
- [5] A. N. Semenov and J. F. Joanny *Europhys. Lett.* **29**, 279 (1995).
- [6] A. N. Semenov, J. Bonet Avalos, A. Johner and J. F. Joanny *Macromolecules* **29**, 2179 (1996).
- [7] A. Johner, J. Bonet i Avalos, C. C. van der Linden, A. N. Semenov and J. F. Joanny, *Macromolecules* **29**, 3629 (1996).
- [8] L. Auvray and J. P. Cotton, *Macromolecules* **20**, 202 (1987).
- [9] J. des Cloizeaux and G. Jannink, *Les polymres en solution: leur modlisation et leur structure* (Les editions de Physique, Les Ulis, 1988). The value of the exponent predicted by Renormalization Group calculations is $\nu = 0.588$. See chapter XII and refs. therein.
- [10] E. Eisenrigler, *Polymers near Interfaces*, (World Scientific Publishing, Singapore, 1993).
- [11] R. Zajac and A. Chakrabarti, *J. Chem. Phys.* **104**, 2418 (1996).
- [12] Jianwen Jiang, Honglai Liu and Ying Hu, *Macromol. Theory Simul.* **7**, 105 (1998).
- [13] P. -Y Lai, *J. Chem. Phys.* **103**, 5742 (1995).
- [14] Andrey Milchev and Kurt Binder, *Macromolecules* **29**, 343 (1996).

- [15] J. de Joannis, C. -W. Park, J. Thomatos and I. A. Bitsanis *Langmuir* **17**, 69 (2001). Notice that in this reference the acronym SCMF stands for *Self-Consistent Mean Field*, referred to the Scheutjens-Fleer theory described in ref. [1]. In our work we have used SCF for the Scheutjens-Fleer theory and SCMF to the Single Chain Mean Field theory of Szleifer and collaborators.
- [16] D. Frenkel and B. Smit, *Understanding Molecular Simulation* (Academic Press, San Diego, 1996).
- [17] P. G. de Gennes, *Scaling Concepts in Polymer Physics* (Cornell University Press, Ithaca, 1979)
- [18] C. M. Marques and J. F. Joanny, *J. Phys. (France) I* **49**, 1103 (1988).
- [19] P. F. Flory, *Principles of Polymer Chemistry*, (Cornell University Press: Ithaca, N. Y., 1953).
- [20] I. Szleifer and M. A. Carignano, in *Advances in Chemical Physics*, edited by I. Prigogine and S.A. Rice (John Wiley and Sons, New York, 1996).
- [21] A. D. Mackie, A. Z. Panagiotopoulos and I. Szleifer, *Langmuir* **13**, 5022 (1997).
- [22] M. A. Carignano and I. Szleifer, *J. Chem. Phys.* **98**, 5006 (1993).
- [23] J. de Joannis, *Equilibrium properties of polymer solutions at surfaces: Monte Carlo simulations*, PhD. thesis, University of Florida, (2000).
- [24] J. de Joannis, R. K. Ballamundi, C. -W. Park, J. Thomatos and I. A. Bitsanis, *Europhys. Lett.* **56**, 200 (2001).
- [25] G. J. Fleer, J. van Male and A. Johner, *Macromolecules* **32**, 825 (1999).
- [26] G. J. Fleer, J. van Male and A. Johner, *Macromolecules* **32**, 845 (1999).
- [27] M. N. Rosenbluth and A. W. Rosenbluth, *J. Chem. Phys.* **23**, 356 (1955)
- [28] Z. Al-Anber, J. Bonet Avalos and A. Mackie, (in preparation)
- [29] A. K. Dolan and S. F. Edwards, *Proc. R. Soc. London, Ser A.* **343**, 427 (1975).
- [30] M. Doi, *Introduction to polymer physics*, (Clarendon Press, Oxford 1996).

Chapter 4

Adsorption onto colloidal particles

Mixing colloids and polymers is a common process in the preparation of complex materials [1]. Many shear thinning fluids in paints and food industry are essentially such mixtures, at or out of equilibrium. Long polymers are also sometimes used to promote protein crystallisation from solution [2].

Adding polymers to a colloid solution is a versatile way of controlling the stability of the suspension, as has been shown by extensive fundamental experimental research. There are two main classes of systems depending on the sign of polymer/colloid interaction. In the case of repulsive polymer/colloid interaction the polymers induce an effective so-called depletion interaction between the colloids. Early studies describe large colloids as compared to the polymer size (or polymer correlation length in solution). In the fifties Osawa [3] presented a theory for the depletion interaction in mixtures of small and large colloids. Later, this was extended to colloid/polymer mixtures with proper account of the polymer structure by Joanny *et al.* [4]. Since then, the phase diagram of this system was considered more closely only by the liquid state theorists [5]. Many experimental data were also produced, among others, in the group of Poon and Pusey (Edinburgh) [6]. The equilibrium properties of repulsive systems with large colloids seem rather well understood.

The opposite limit of small colloids was first addressed in a seminal paper by de Gennes [7], who recognised that the interactions are weak, as it is easy to incorporate a small colloid in a polymer coil. Recently the colloid/polymer and colloid/colloid interactions were carefully analysed in a field theoretical approach by Eisenriegler and co-workers [8]. They stress that colloid/colloid interactions induced by the polymer are long ranged and saturate at contact. Moreover, they show that the variations of the colloid/colloid virial coefficient are non-monotonic with polymer concentration [9]. Recent work by Sear [10] and by Fuchs [11], the latter using integral equation methods, describe the phase diagram

of such mixtures in Mean-Field approach. Erukhimovich [12] is currently developing a field theoretical description together with A. Johner aiming at a widely accepted description.

Systematic experimental studies of the adsorbing case were undertaken twenty years ago by Cabane [13]. The understanding of polymer adsorption on flat surfaces was initiated earlier by Silberberg [14] and de Gennes [15]. An early model by Alexander [16] applies these ideas to the case of large spheres. A systematic description of curvature effects for adsorption on a single sphere is proposed by Birshtein and Borisov [17] for ideal chains and Marques and Joanny [18] for excluded volume chains, the latter also address surface fractality. Subsequently Aubouy *et al.* [19] stressed that a sphere of radius R , small enough to be covered by less than one chain of contour length N , will carry two long polymer tails, with a size of order N . Following this idea a small sphere satisfies $(R/l)^{d-1} < N$. As in earlier work the overall layer thickness (cut off length for tails) is essentially fixed by the bulk chemical potential. The small sphere criterion by Aubouy thus corresponds to a radius where loops start feeling curvature, in the picture of a layer decomposed into a loop and tail sublayers [20, 21].

Despite all the body of knowledge developed in recent years on polymer adsorption, little is known about the internal structure of the adsorbed layer, to the light of the recent developments, and how the curvature affects the structure. This is in fact an important analysis prior to the study of mixed systems colloid-polymer. The methodology developed in previous chapters is suitable to the analysis of the problem of polymer adsorption onto spherical (colloidal) particles of different sizes, from solutions of relatively short polymers, close to those found in many applications. A more theoretical analysis of the colloid-polymer mixture will be done in the next chapter.

Therefore, in this chapter we will apply the SCMF theory with the importance sampling method, the case of polymer adsorption onto isolated spherical particles of different radii. The very interesting problem of the bridging interaction between different colloidal particles will be addressed in a future work. The differences of the structure of the layer, adsorbance and other properties will be studied as functions of the relative size between the sphere and the polymer in the bulk as well as of the adsorption energy.

4.1 Numerical calculation details

To solve the SCMF problem, we have considered *off-lattice* polymers in a cubic box, adsorbing onto a spherical surface whose center is located at the center of the box. Two different polymer lengths will be considered, namely chains of $N = 100$ monomers in a box of size $L = 111.6l + 2R$, and $N = 200$ monomers in a system of $L = 223.2l + 2R$, where l is the monomer diameter and R is the radius of the sphere. Since periodic boundary conditions are considered, the size of the box has been chosen such that the chains can

never reach two images of the sphere at one time and adsorption on individual particles can be described. The adsorbing potential is here represented by a square well of width d and depth ε at the surface of the solid sphere. The internal energy term in the free energy of the SCMF problem shown in eq. (2.9), is thus given by the expression

$$U[\gamma, c_s(\mathbf{r}), c(\mathbf{r})] = U_{ext}[\gamma] = \varepsilon \int d\mathbf{r} \theta(d - |r - R|) \sum_{i=1}^N \delta(\mathbf{r} - \mathbf{r}_i[\gamma]) \quad (4.1)$$

where monomer-monomer, monomer-solvent as well as solvent-particle interactions are set to zero. This case represents an athermal solvent. In eq. (4.1), $r = |\mathbf{r}|$ is the distance to a given point from the center of the sphere, in which has been located the origin of coordinates. The thickness of the well is $d = 1.86l$ and different values of ε , $-0.35 kT$ and $-1 kT$, have been considered in this work to describe strong adsorption.

As before, the chains are modeled as pearl necklaces of non-overlapping beads of diameter l , whose centers are separated a fixed distance equal to its diameter. The excluded volume of the whole chain is taken as constant and equal to N -times the excluded volume per monomer. This excluded volume is again $v_p = 1.86l^3$ where the overlap of the exclusion of neighbouring monomers in the chain has been estimated. Due to the symmetry of the present problem, one can suppose that the mean-field constraint $\pi(\mathbf{r})$ depends only on the distance to the center of the sphere, r . The size of the box chosen is large enough so that π reaches the bulk value far before the boundaries of the box are met. Therefore, the space around the sphere has been divided from the surface into concentric layers of thickness $1.86l$, inside which π has been considered as constant. Although the volume of each layer is not constant, the smaller one, located at the surface of the colloidal particle, is sufficiently large to correctly satisfy the constraint equation, eq. (2.6).

The Monte Carlo evaluation of the configurational space integrals of eq. (2.17) has been done following the same lines as in the case of the plane wall, analyzed in the previous chapter. In this case, the configurational file contains the location of every monomer of non-overlapping chains that do not penetrate the spherical particle, stored together with its bias weight, $w[\gamma]$. The used number of chains is the same as before, 2×10^4 . In the same spirit as in the case of the plane wall, we have chosen to gather the chains of the sampling to the most relevant part of the phase space by choosing a bias field given by the Boltzmann weight

$$w[\gamma] \sim e^{-H_{mf}[\gamma]/kT} \quad (4.2)$$

for given suitable physical conditions of adsorption energy ε and bulk monomer fraction ϕ^0 . The Metropolis rule [22] is used to accept or reject a given change in the conformation of every chain, which are mutually independent in the mean field approach of this work.

The same global indicators, average energy and average number of adsorbed monomers, are used to know whether the system is equilibrated or not after many MC steps. An example of both magnitudes as a function of the number of MC steps is presented in Figs. 4.1 to 4.4, for two values of the sphere size ($R/l = 1.36$ and 55.3) with $N = 100$, $\varepsilon = -0.35 kT$ and $\phi^0 = 0.001$, in both cases. The fluctuations obtained in the case of the smallest sphere during the equilibration (Figs. 4.1 and 4.3) are larger than in the other sphere size (Figs. 4.2 and 4.4). This difference is due to the fact that the effective adsorption energy decreases if the available area is reduced. In the case of $R/l = 55.3$ once a polymer has been adsorbed it is more difficult to be desorbed from the spherical surface than in the case $R/l = 1.36$ during the MC process. Hence, more MC steps are necessary to get the system equilibrated because of the energy barriers to be overcome. In addition, the validity of a particular sampling for a given problem is here conditioned not only by the disparity between the bias and the physical conditions to be described, but also by the changes in the size of the sphere. Although it is possible to use the same bias with different sphere sizes, eliminating the conformations that would penetrate the sphere, it would be necessary to eliminate a vast majority of the chains, which would be located in a narrow region at the surface of the sphere, due to the bias process used. Consequently, the use of the same sampling in different sphere sizes makes the importance sampling methodology impractical.

4.2 Structure of the layer adsorbed onto a colloidal particle.

In comparison with polymer adsorption on flat surfaces, adsorption on spherical surfaces introduces a new length scale into the problem, that is, the radius of the sphere R . Therefore, the structure of the layer will depend on the relative values of this length, the overall size of the chain R_g , the bulk correlation length ξ (eq. (3.2)), and characteristic lengths of the adsorbed layer such as the crossover length z^* (eq. (3.5)) and the layer thickness λ (eq. (3.4)). We will pay special attention to polymer adsorption from a very dilute solution, which makes the penetration of the layer by free polymer to be irrelevant. Thus, finite size effects of the chains are more noticeable due to the fact that the outer tail layer is not embedded in the bulk solution [23, 24]. Therefore, the bulk correlation length, which is a length scale much larger than any length related to the polymeric layer, can be ignored in the analysis [24].

Polymer adsorption on spherical surfaces from dilute solutions presents different scenarios from those of adsorbed layers on infinite planar surfaces, described in the chapter 3. In spherical surfaces, the structure of the adsorbed layer, not only depends on the local curvature of the interface but also on the finiteness of the particle, which will eventually limit the number of chains that can be adsorbed. These scenarios are described below.

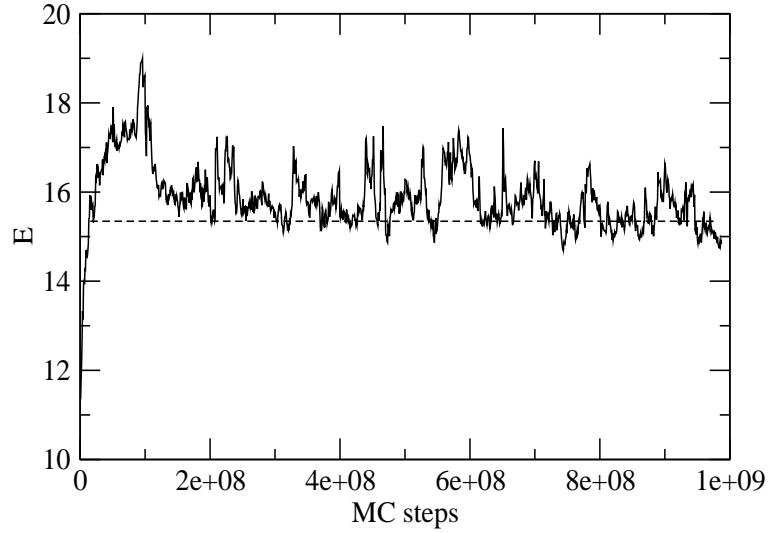


Figure 4.1: Variation of the energy of the configurational file, $E = -\sum_{\gamma} H_{mf}(\gamma)$, with Monte Carlo (MC) steps in the case of adsorption of polymers on a sphere of radius $R/l = 1.36$ with $N = 100$ and $\varepsilon = -0.35$.

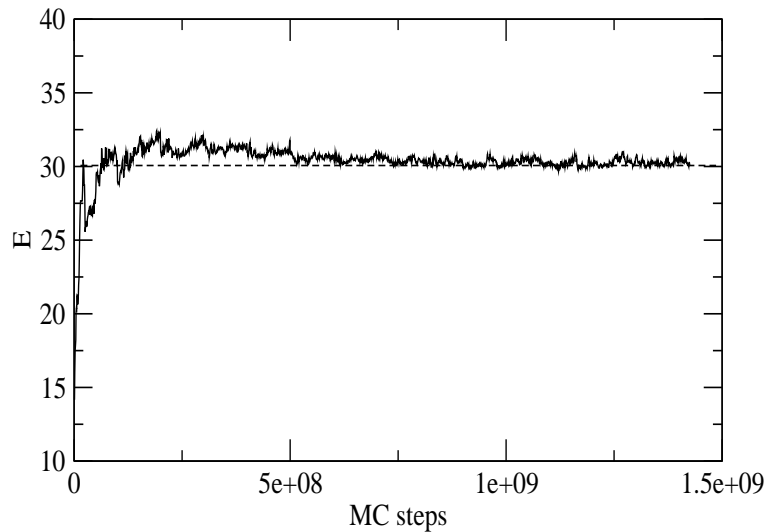


Figure 4.2: Variation of the energy of the configurational file, $E = -\sum_{\gamma} H_{mf}(\gamma)$, with Monte Carlo (MC) steps in the case of adsorption of polymers on a sphere of radius $R/l = 55.3$ with $N = 100$ and $\varepsilon = -0.35$.

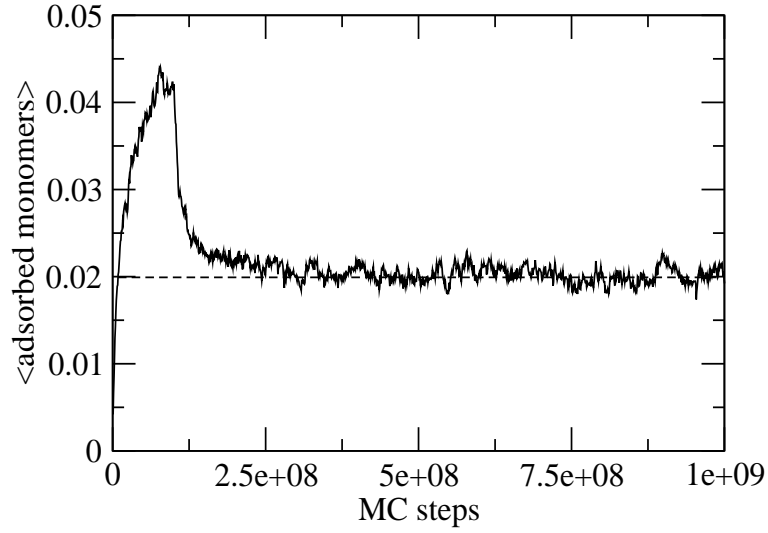


Figure 4.3: Variation of the average number of adsorbed monomers of the configurational file with Monte Carlo (MC) steps in the case of adsorption of polymers on a sphere of radius $R/l = 1.36$ with $N = 100$ and $\varepsilon = -0.35$.

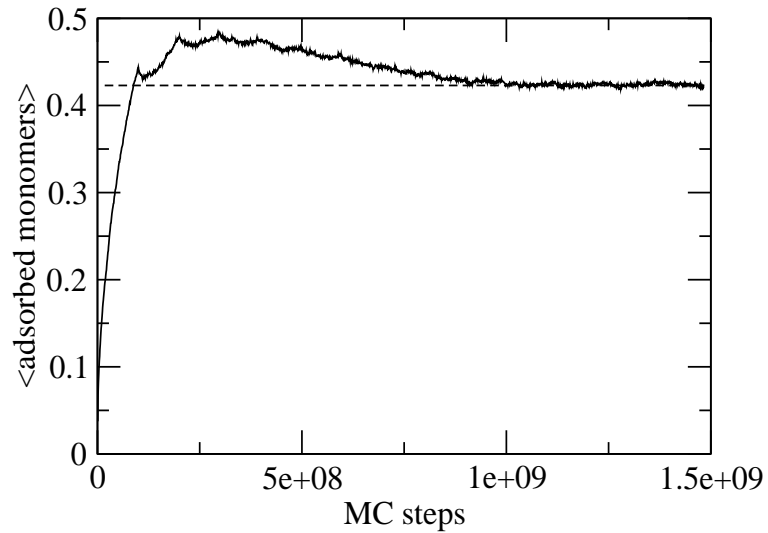


Figure 4.4: Variation of the average number of adsorbed monomers of the configurational file with Monte Carlo (MC) steps in the case of adsorption of polymers on a sphere of radius $R/l = 55.3$ with $N = 100$ and $\varepsilon = -0.35$.

First, if the size of the sphere is larger than the thickness of the layer, the adsorbed chains lie in a region of thickness $\lambda \ll R$ only slightly affected by the curvature of the interface, so that the same structure as in an infinite plane is expected from the scaling point of view [23]. In that case, we will observe a loop region crossing over an outer tail region at a distance z^* from the solid surface [23, 24]. The value of z^* in this region is very close to the value z_w^* , corresponding to a planar interface under the same physical conditions of adsorption energy and bulk density. One can then write

$$z^* \simeq z_w^* \sim lN^{1/(d-1)} \quad (4.3)$$

This length z_w^* will be further used to compare with the actual crossover distance z^* obtained for a curved interface. Moreover, since chains are not very long, we will always remain in the so-called starved regime [24], where z^* and λ are comparable. Hence, no power-law behaviour of the tail layer will be observed, but an exponential decay with the scale of λ . In an spherical geometry the adsorbance is given by

$$\Gamma = \frac{1}{R^2} \int_R^\infty dr r^2 c_a(r) \quad (4.4)$$

In this regime, Γ is dominated by the loop layer, if strong adsorption conditions are satisfied. Effectively, the assumption of a self-similar profile for $R < r \ll (R + z^*)$ yields a monomer density profile [25, 23] that scales as $l^{5/3}c(r) \sim 1/(r - R)^{4/3}$ that makes the integral in eq.(4.4) be dominated by the lower integration limit. Thus [26],

$$\Gamma \sim \frac{1}{l^{d-1}} \quad (4.5)$$

being d the dimensionality of space. In addition, many chains cover the spherical surface, since its extent is larger than the surface covered by a single chain. Second, if $z_w^* < R < \lambda$, the distal part of the adsorbed layer will be sensitive to the curvature. Since, by definition of z_w^* , this distal region is dominated by tails, the curvature effects are going to affect part of the tail layer. Effectively, only a few tails will go further than a distance R from the surface, adopting there a mushroom-like structure with little overlap and hence no self-similar profile beyond R . However, due to the fact that this part of the layer is subdominant, the overall structure remains unchanged. Effectively, assuming that a self-similar structure would exist up to the onset of curvature effects in the layer (the condition $z_w^* \ll R$ should in fact be required), one can estimate that one tail will leave the inner layer per R^2 of area, according to the scheme in Fig. 4.5, forming non-overlapping mushroom structures. According to this argument, there will be a number of long tails in the outer region of the order of 1. However, the adsorbance Γ is still dominated by the inner loop layer and is unaffected by the curvature, according to the argument given for

the previous case. Therefore, as far as scaling considerations are concerned, this second scenario is merely a crossover between a layer with properties of a planar surface and the next scenario.

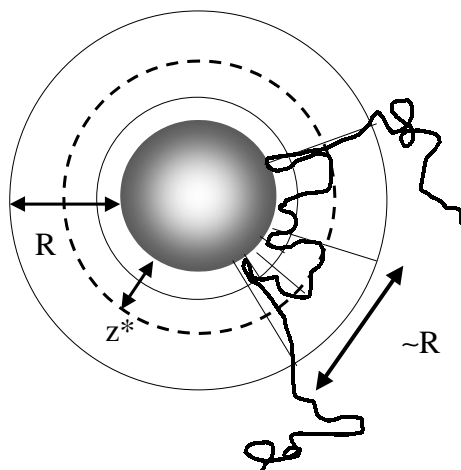


Figure 4.5: Representation of the adsorbed polymer layer on a particle whose radius R is $z_w^* < R < \lambda$, where z^* and z_w^* is the crossover distance corresponding to the adsorption on spherical and planar surfaces, respectively, and λ is the thickness of the layer of order the size of the polymer R_g .

Third, if $R < z_w^*$ the loop layer should merge into the space region $r > 2R$ where the curvature is relevant. However, large loops of g monomers with $lg^\nu \gg R$, ν being the Flory exponent $3/5$, are not likely to be found due to the finite size of the adsorbing surface. Effectively, the equilibrium loop and tail distribution is reached by the competition of two dynamic processes, namely a) two loops fuse in a larger one by the release of an adsorbed monomer (or train) from the surface, and b) a large loop breaks into two smaller by adsorption of at least one loop monomer. Similarly occurs when pairs loop-tail are involved. Thus, for small loops the surface is locally seen as flat and process a) and b) are comparable. However, for a couple of large loops, the finite size of the surface makes the process a) to be more likely than the process b). The repetition of the process and, hence, the growing of such large transient loop will end up in one chain end, becoming a long tail. Thus, in the outer part of the layer, mostly tails and a number of transient large loops of the order of 1 are expected. Therefore, the loop layer in this small sphere regime is confined to a region of thickness R , having to be the actual crossover distance as $z^* \sim R < z_w^*$ [27]. Thus, we expect that the tails will start growing larger as the radius decreases, and the number of adsorbed chains per particle will be close to 1.

Finally, for very small particles $R \ll z_w^*$, the adsorption energy per chain is so small that strong adsorption no longer takes place.

The third situation is the most interesting from a theoretical point of view since the large sphere case $R \gg \lambda \sim R_g$ reduces to the planar interface adsorption, largely studied in the literature [21, 24], and analyzed here in the previous chapter. The small sphere case, $R < z_w^*$, has an additional importance in applications such as flocculation, where long polymers can wrap several particles at one time, for instance [28, 29, 27, 30]. It is important to realize that the only two scaling regimes that can be described in strong adsorption are governed by the ratio between the particle radius and the crossover distance z_w^* which constitutes a critical radius corresponding to each chain size. Here, scaling arguments suggest that if $R \sim z_w^*$ the adsorbance due to loops in the inner layer is comparable to the amount of polymeric material found in the outer part of the layer, mostly beared by long tails,

$$\Gamma_l(R_c) = \Gamma_t(R_c) \quad (4.6)$$

To see this, consider a very small particle wrapped by one single polymer coil. The adsorbance due to the loop layer is thus dominated by the material due to small loops and trains very close to the surface and, thus, insensitive to the curvature. Hence, the adsorbance is given by the saturation of the surface

$$\Gamma_l \sim \frac{1}{l^{d-1}} \quad (4.7)$$

where d is here the dimensionality of space. For the tail outer layer, we can guess that will bear the rest of the material, due to the fact that there is only one single polymer wrapping the sphere (in fact, this scaling argument only requires that there are a few chains, of the order of 1, adsorbed onto the small particle). Hence,

$$\Gamma_t = \frac{N}{R^{d-1}} - \Gamma_l \sim \frac{N}{R^{d-1}} - \frac{1}{l^{d-1}} \quad (4.8)$$

Therefore, imposing the condition given in eq. (4.6), we arrive at the conclusion that

$$R_c \sim l N^{1/(d-1)} \quad (4.9)$$

This scaling relation is the same found for the crossover distance z_w^* in planar geometries [23], according to eq. (4.3). This fact reinforces the assumption that z_w^* is the only relevant length for strong adsorption from a dilute bulk, for both a planar interface as well as for curved surfaces. Other authors [19] have also described the three scenarios mentioned in this section. Their analysis is based on the consideration of an entropic contribution due to the loop distribution, $S(n)$, without making an explicit distinction between loops and tails. Thus, according to these authors, the crossover region $z_w^* < R < \lambda$ is described as

a region where long loops grow in the outer region, which differs from our point of view which states that the outer region, where the curvature is important, is always dominated by tails if the bulk is dilute. The SCMF calculations shown in this chapter are in support of this point of view.

4.3 SCMF results for adsorption onto spheres

We will focus our attention to the adsorption of chains of $N = 100$ monomers, modelled as self-avoiding chains, whose radius of gyration in a dilute bulk is found to be $R_g = 7.45l$ (see Table 3.1). We will mainly work in conditions of strong adsorption being the adsorption energy per monomer $\varepsilon = -0.35kT$. Taking into account that in a very dilute polymer solution the chain finite-size effects are more noticeable [23, 24], the value of the bulk monomer volume fraction considered is $\phi^0 = 0.001 \ll \phi^* \sim N^{-5/3}$ ($\phi^* \sim N^{-1}$, for Markovian mean-field). The overlap volume fraction is $\phi^* = 0.11$, as follows from eq. (3.3) and the fact that $\phi^* = v_p c^*$. Effectively, under these circumstances the bulk correlation length is much larger than the overall size of the polymer and will not be a relevant length until the overlap concentration is reached. Moreover, since the thickness of the layer scales as the radius of gyration of the chain, for fixed chain lengths we will be only concerned with the variation of the internal structure of the adsorbed layer and its properties as the sphere radius is changed.

The Fig. 4.6 shows the total monomer volume fraction profile for sphere radii ranging from $R = 1.36l$ to $R = 55.3l$, as a function of the distance to the center of the sphere. We have also included the profile obtained for the case of adsorption on plane surfaces, under the physical conditions mentioned above. The first aspect to be noted is the good agreement existing between the profile for plane surfaces and spheres of a radius much larger than the radius of gyration of the polymer in the bulk as, for example, in the case of a sphere of radius $R = 55.3l \gg R_g = 7.45l$. From a numerical point of view, we will consider that the curvature starts to affect the layer when the thickness of the tail layer (λ_t) is of the order of R . Note that $\lambda_t \simeq R_g \simeq 2\lambda_w$ (being λ_w the root mean square thickness of the corresponding adsorbed layer on flat surfaces), which makes this criterion to agree with the scaling description presented here as far as the different regimes are concerned.

The profiles look very similar already for $R \geq 18.1l$, and start to deviate from the plane surface results for $R \leq 8.8l \simeq R_g$, being this value $R = 8.8l$ similar to $\lambda_{w,t} = 8.17l$ obtained in the adsorption on flat surfaces in the same conditions (see Table 4.1). For a major clarity, we show in Fig. 4.7 the same profiles but in logarithmic scale and as functions of the distance to the surface. For radii $R \leq 8.8l$, we observe a progressive decrease of the volume fraction at contact. To give an interpretation of this result, in Fig.

4.8 we show the average energy per adsorbed chain $\langle H_{mf} \rangle_{adsorbed}$. We observe that in all cases studied, chains are strongly adsorbed, being $|\langle H_{mf} \rangle_{adsorbed}| > kT$. However, as the radius decreases, an increase of the average energy per chain is seen indicating, on the one hand, the onset of curvature effects on the layer when $R \sim R_g$ and, on the other, the competition between chains to cover the available surface at smaller sphere radius (finite size effects of the adsorbing surface).

Back to the analysis of the monomer volume fraction profiles, our results seem to indicate a straight section in the central part of the profile to which we can associate a power-law decay. The associated exponent ranges from -1.84 for the smaller sphere, to -2.27 to the largest one, which is close to the result for a plane wall (-2.15). However, the influence of the curvature is important even for the largest sphere, as can be deduced from the difference found in the volume fraction profiles between the largest sphere and the plane wall at large distances. In addition, it is more noticeable the lower value of the monomer volume fraction over all the profile as the radius decreases, something that can naturally be associated to a decrease in the average adsorption energy per chain. The extent of the profile, however, seems rather insensitive to the increase of the curvature, although one could intuitively expect a broadening of the profile as the average adsorption energy per chain is lowered. Hence, we may guess that the increase of the curvature of the adsorbing surface causes the outer part of the layer to have more room for the long tails and loops to accommodate to a mushroom structure, whose typical size would be then of the order of R_g , compensating in this way the loss of effective adsorption energy. From another point of view, as already observed in the case of the plane wall, the decay of the monomer volume fraction profile is faster than predicted by scaling arguments. This is due to the small size of the polymeric chains considered in this work, clearly far from the asymptotic limit $N \rightarrow \infty$, where the scaling is valid. This effect has already been discussed in the previous chapter. In the case of spherical particles, there is a slight dependence with the radius of the sphere, since the smaller ones show slower decay rates, which can be explained with the same arguments as for the width of the profile. For completeness, in Fig. 4.9 we have plotted the adsorbed end-monomer distribution for three of the radii studied. Besides the overall decrease in the number of chain ends as the radius decreases, there is not a substantial change in the qualitative behaviour for such short chains. Furthermore, the profiles do not indicate any power-law decay.

In table 4.2, the average number of adsorbed chain ends for different sphere sizes, in the ranges $r \geq R$ as well as $r \geq 2R$ (being r the distance from the center of the sphere), is presented. From these results, we can see the different scenarios, mentioned in the previous section. Effectively, if $R \leq 18.1l$ the average number of adsorbed chain ends at distances $r \geq 2R$ lies between 1 (when $R/l = 1.36 \ll R_g/l$) and 10, as scaling laws predicted [27]. However, for radii $R \geq 18.1l$ this number of adsorbed chain ends decreases due to the adsorbed chains lie in a region of thickness $\lambda \ll R$ whose structure is similar to the obtained one on flat surfaces [23, 24].

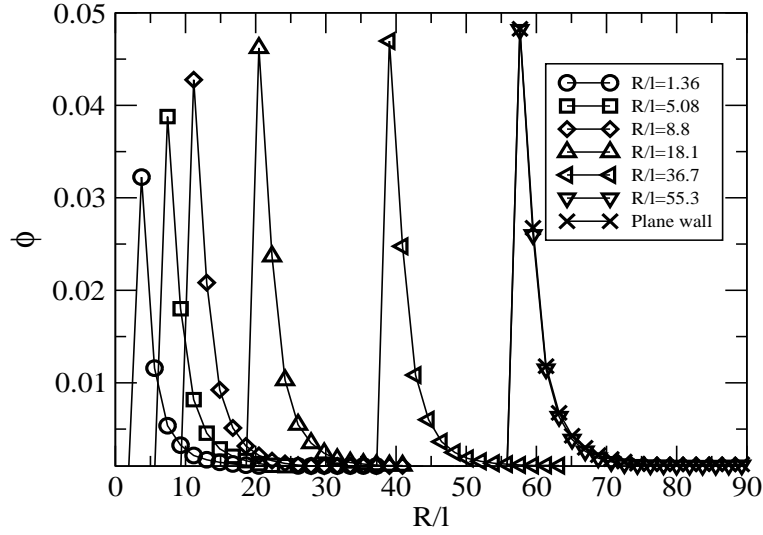


Figure 4.6: Total monomer volume fraction profiles for different sizes of sphere ($R/l = 1.36$ (circles), 5.08 (squares), 8.8 (diamonds), 18.1 (triangles), 36.7 (triangles left) and 55.3 (triangles down)) as a function to the center of the sphere. The total monomer volume fraction profile corresponding to the adsorption on flat surfaces (crosses) is also plotted.

R/l	1.36	5.08	8.8	18.1	55.3	<i>plane wall</i>
z^*/l	4.16	4.95	5.26	5.63	6.01	6.08
λ/l	8.23	6.64	6.04	5.41	4.97	4.90
λ_l/l	3.26	3.06	2.99	2.92	2.92	2.91
λ_t/l	9.69	8.82	8.59	8.29	8.03	8.17

Table 4.1: Characteristic lengths of the adsorbed layer obtained from Single Chain Mean Field method (SCMF) for sphere radii ranging from $R = 1.36l$ to $R = 55.3l$ and for plane wall case. System conditions: $N = 100$, $\phi^0 = 0.001$ and $\varepsilon = -0.35kT$.

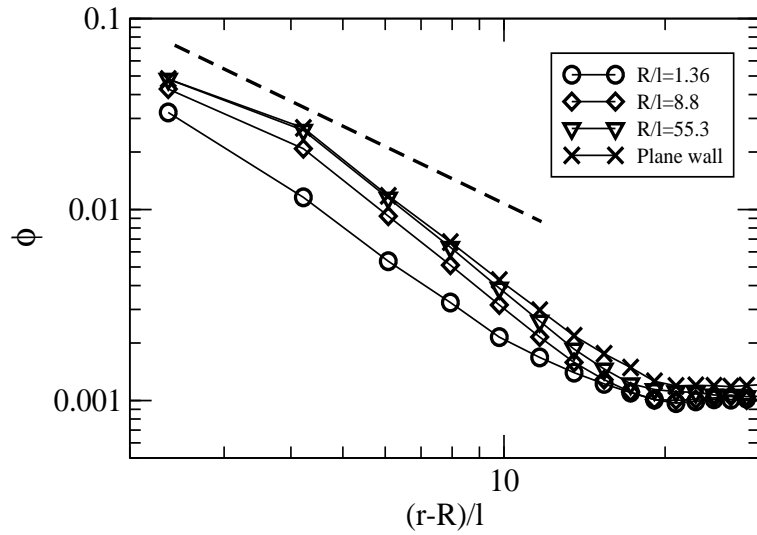


Figure 4.7: Total monomer volume fraction profiles for different sizes of sphere ($R/l = 1.36$ (circles), 8.8 (diamonds) and 55.3 (triangles down)) as well as for the adsorption on planar surfaces (crosses), as a function to the distance from the surface. Dashed line shows a power law of $-4/3$.

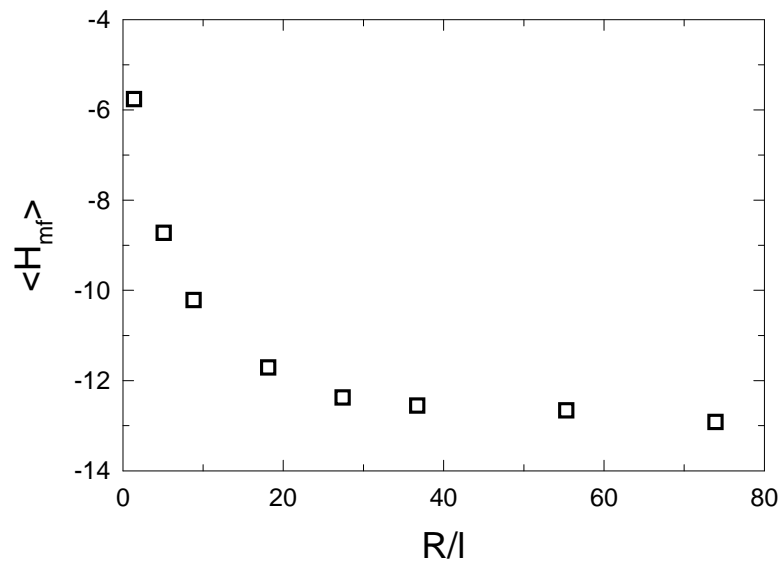


Figure 4.8: Variation of the average energy per adsorbed chain ($\langle H_{mf} \rangle$) with the sphere size.

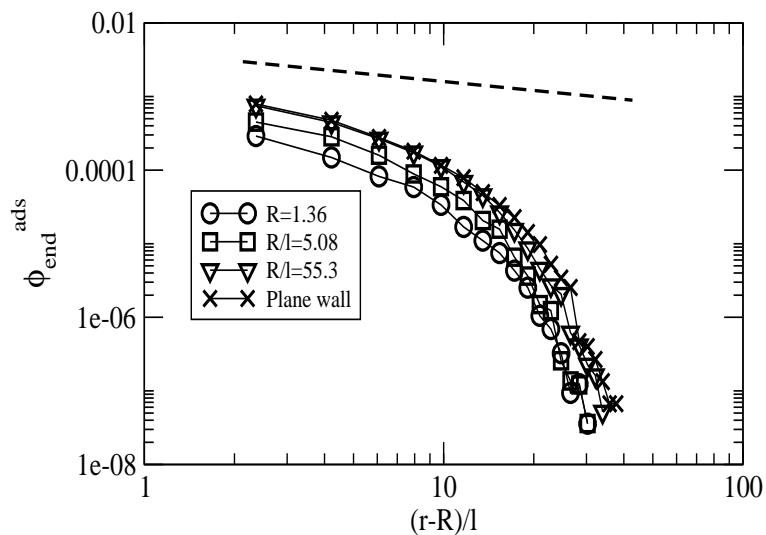


Figure 4.9: Variation of the adsorbed end-distribution for different sizes of sphere ($R/l = 1.36$ (circles), 5.08 (squares) and 55.3 (triangles down)) as well as for the adsorption on plane surfaces (crosses), with respect to the distance from the surface. Dashed line shows a power law of -0.532 .

R/l	1.36	5.08	8.8	18.1	36.7	55.3
$\langle n^{\circ} \text{end} \rangle \quad r \geq R$	2.6	8.56	19.09	65.23	243.69	532.86
$\langle n^{\circ} \text{end} \rangle \quad r \geq 2R$	2.6	4.11	2.83	0.38	0.0	0.0

Table 4.2: Average number of adsorbed chain ends at distances $r \geq R$ and $r \geq 2R$, being r the distance from the center of the colloidal particle. System conditions: $N = 100$, $\phi^0 = 0.001$ and $\varepsilon = -1 kT$.

As far as the distribution of tails and loops are concerned, Figs. 4.10 and 4.11 show in logarithmic scale the volume fraction profile of monomers belonging to loops and, respectively, to tails, as a function of the sphere radius for the physical conditions discussed in this work. In both cases, the profiles are not significantly different from those observed in adsorption onto planar surfaces. The most noticeable aspect to be commented is on the fact that the increase of the curvature results in lower values of the monomer volume fraction of each species, slightly more important for loops (Fig. 4.10) than for tails (Fig. 4.11). However, in both cases their extent is comparable, independently of the size of the sphere. The loop distribution does not show any tendency to a power-law decay. The tail profiles are close to an exponential decay ($\phi_t = A \exp(-\alpha r)$) at the wide outer part of the layer. The exponent corresponding to tail profiles ranges from $\alpha = -0.344$ in the case $R = 1.36l$, $\alpha = -0.346$ for $R = 8.8l$ to $\alpha = -0.327$ for $R = 55.3l$ being the latter very close to the adsorption on flat surfaces (the value obtained for the exponent in the case of plane surfaces, under these conditions, is $\alpha = -0.322$). These differences in the value of the exponent can be attributed to different average size of the tails.

It is also very interesting to numerically find the value of the crossover length z^* for each radius. In Fig. 4.12 we have plotted the variation of the crossover distance with the radius of the sphere. In this figure, the straight line corresponds to the value of the planar wall crossover length z_w^* . The decreasing value of z^* with the increase of the curvature indicates, effectively, that the relative importance of tails with respect to loops is larger for small spheres than for large spheres. However, our data are not conclusive enough as to prove that $z^* \sim R$ for $R \ll z_w^*$ according to the scaling arguments given above [27]. In addition, it is interesting to notice that z^* is sensitive to the curvature far before the critical radius $R = z_w^*$ is reached, and in fact for radii much larger than the overall size of the chain in the bulk, R_g . In this system of relatively short chains, where all the characteristic lengths are of the same order of magnitude, we cannot expect a sharp transition between the different regimes, but a broad crossover between the large sphere to the small sphere behaviours. Effectively, elongated conformations of the chain are sensitive to the curvature in the outer part of the layer, making that the studied properties differ from the plane wall results even for very large spheres such as $R = 55.3l \gg R_g$. In the Fig. 4.13 is also given the ratio z^*/z_w^* as a function of R/z_w^* for the adsorption of chains with length $N = 100$ and 200 , $\phi^0 = 0.001$ and $\varepsilon = -0.35 kT$. From this figure, it is suggested that z_w^* is indeed the relevant length for curved interfaces.

The different sizes of the loop and tail layers can be seen from the dependence of their root mean square (*rms*) thickness with the sphere size (Fig. 4.14). Although the average thickness of both species increases as R decreases, the effect the increasing curvature is more noticeable in the tail layer, due to the fact that tails dominate the outer part of the adsorbed layer. The values of the thickness deviate from the planar geometry values far before the critical radius is reached, again due to contribution of elongated conformations of the chain, which explore also regions far from the interface (Fig. 4.15).

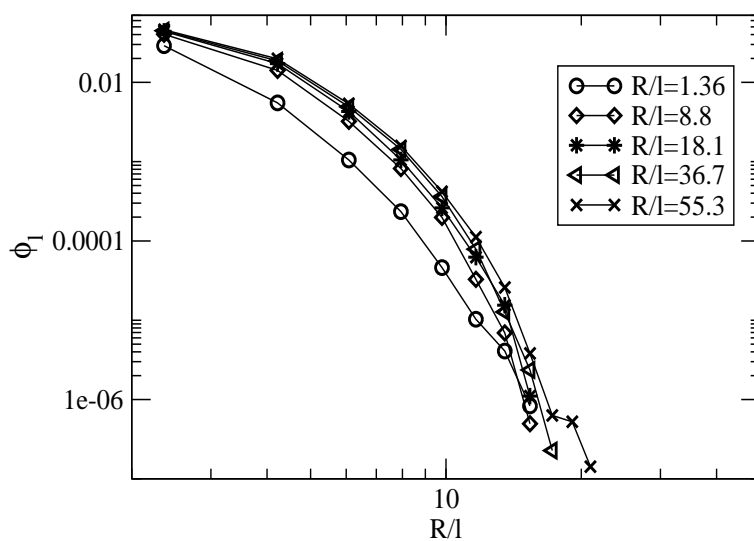


Figure 4.10: Loop volume fraction profiles as a function of sphere radius ($R/l = 1.36$ (circles), 8.8 (diamonds), 18.1 (stars), 36.7 (triangles left) and 55.3 (crosses)). System conditions: $N = 100$, $\varepsilon = -0.35 kT$ and $\phi^0 = 0.001$.

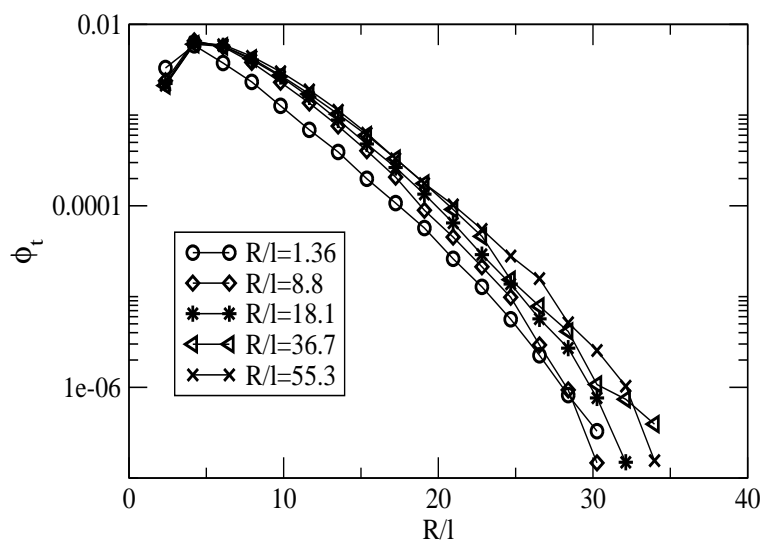


Figure 4.11: Tail volume fraction profiles as a function of sphere radius ($R/l = 1.36$ (circles), 8.8 (diamonds), 18.1 (stars), 36.7 (triangles left) and 55.3 (crosses)). System conditions: $N = 100$, $\varepsilon = -0.35 kT$ and $\phi^0 = 0.001$.

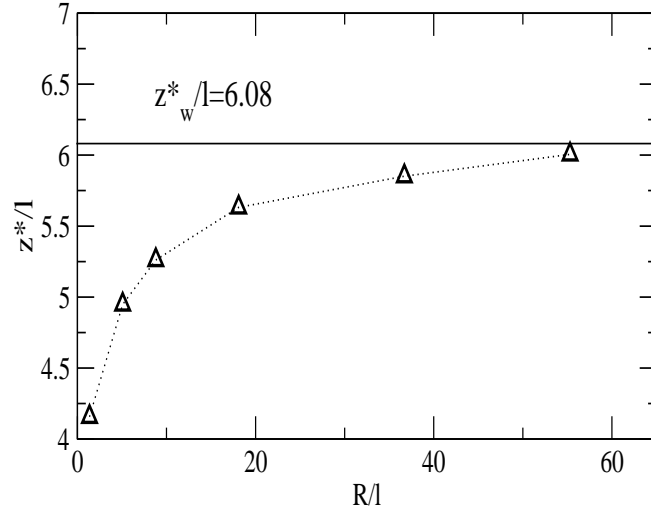


Figure 4.12: Variation of the crossover distance z^* with the sphere size. Full line shows the crossover distance (z_w^*) obtained in the adsorption on flat surfaces. System conditions: $N = 100$, $\varepsilon = -0.35 kT$ and $\phi^0 = 0.001$.

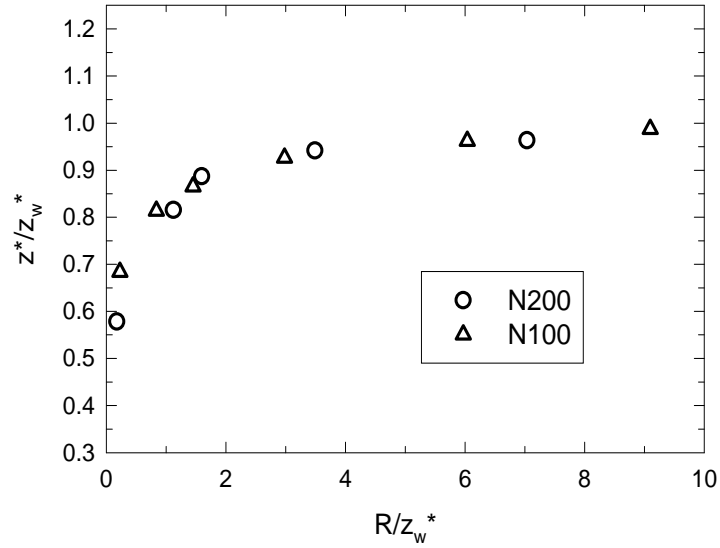


Figure 4.13: Variation of z^*/z_w^* as a function of the ratio R/z_w^* for two chain lengths ($N = 100$ (triangles) and 200 (circles)), $\phi^0 = 0.001$ and $\varepsilon = -0.35 kT$. The values of z_w^*/l are 6.08 and 7.86 for $N = 100$ and 200, respectively.

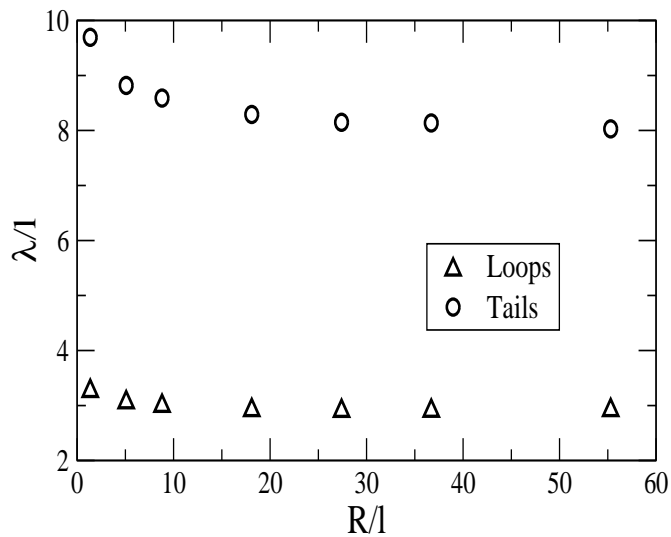


Figure 4.14: Variation of the loop (triangles) and tail (circles) *rms* thickness with the sphere radius. System conditions: $N = 100$, $\phi^0 = 0.001$ and $\varepsilon = -0.35 kT$.

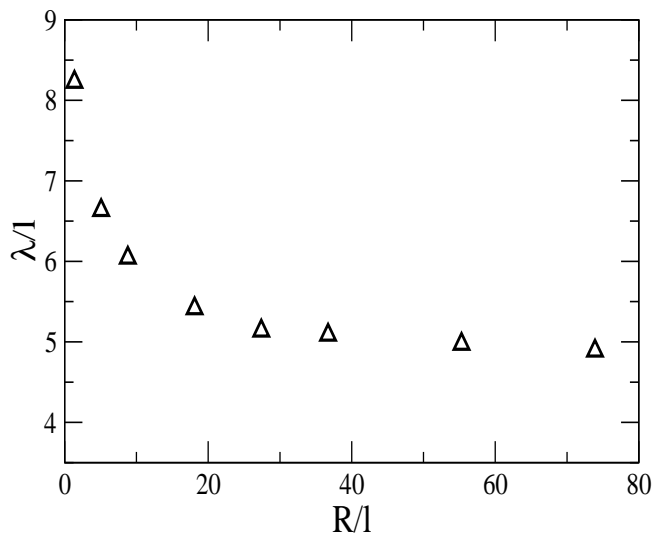


Figure 4.15: Variation of the *rms* thickness with the sphere radius. System conditions: $N = 100$, $\phi^0 = 0.001$ and $\varepsilon = -0.35 kT$.

Another indicator of the behaviour of polymer adsorption with the curvature of the surface is the adsorbance Γ as well as the adsorbances due to loops (Γ_l) and tails (Γ_t) defined from eq. (4.4). In Fig. 4.16, we indicate the behaviour of the adsorbance as a function of the sphere radius. Again, it is observed that the adsorbance increases as the radius R decreases, showing the same behaviour as other magnitudes as the *rms* thickness, with the same qualitative explanation. Taking into account this conclusion, we can mention the work presented by Wijmans *et al.* [28] using a markovian self-consistent field theory to study the adsorption of diblock copolymers (A_nB_m) onto small colloidal particles, so that in the limiting case of an adsorbing homopolymer (only A segments), both magnitudes (adsorbance and layer thickness) presented the same qualitative behaviour.

However, it is interesting to pay some attention to the relative behaviour of the loop and tail adsorbances shown in Fig. 4.17. Notice that the critical radius R_c , where $\Gamma_l(R_c) = \Gamma_t(R_c)$ (see eq. (4.6)), takes the value here $R_c \simeq 5.08l$. Notice that this value is very close to $z_w^*/l = 6.08$, as was suggested by the scaling argument. Therefore, the crossover distance z_w^* is indeed an intrinsic property of the polymeric chain and the dimensionality of the physical space, whose implications go beyond the crossover between loops and tails in adsorption onto flat surfaces and as such should be recognized. In the Fig. 4.18 is given the variation of the loop and tail adsorbance with the sphere size being the chain length $N = 200$, $\phi^0 = 0.001$ and $\varepsilon = -0.35 kT$. In this case, the value of critical radius takes the value $R_c \simeq 8.8l$, which is very close to $z_w^* = 7.86l$, obtaining the same behaviour as the adsorption of chain lengths $N = 100$.

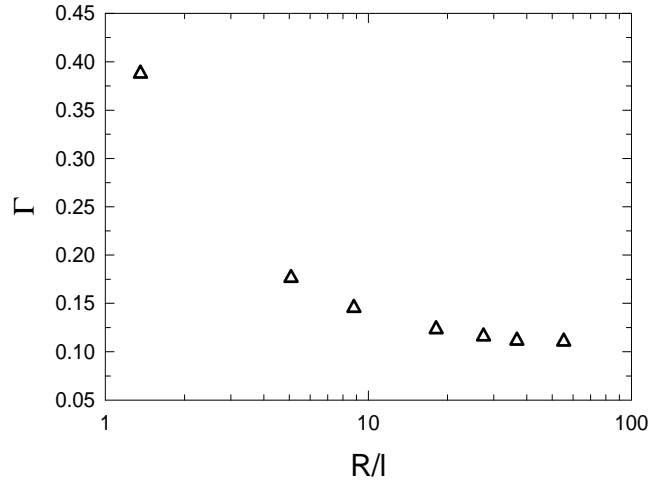


Figure 4.16: Variation of the adsorbance (number of monomers per l^2) with the sphere size. System conditions: $N = 100$, $\phi^0 = 0.001$ and $\varepsilon = -0.35 kT$.

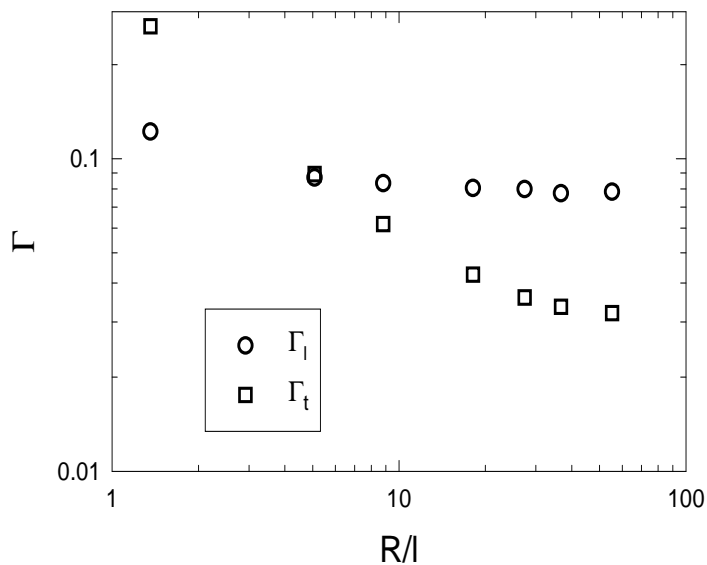


Figure 4.17: Variation of the loop (circles) and tail (squares) adsorbance (number of monomers per l^2) with the sphere size. System conditions: $N = 100$, $\phi^0 = 0.001$ and $\varepsilon = -0.35 kT$

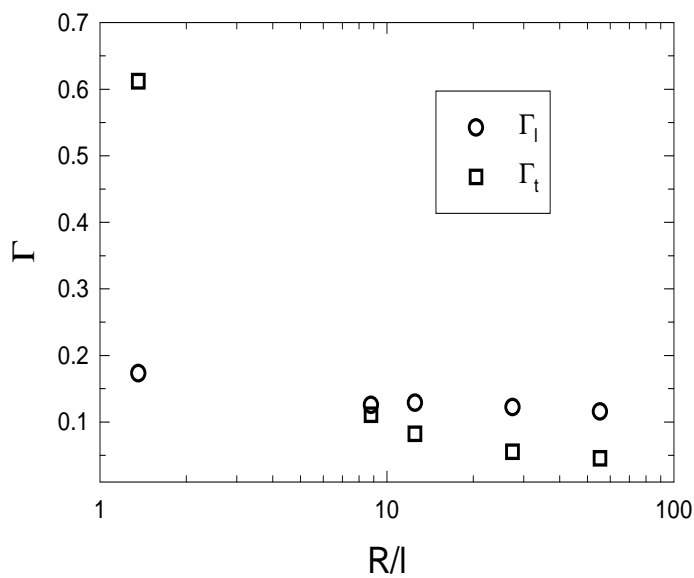


Figure 4.18: Variation of the loop (circles) and tail (squares) adsorbance (number of monomers per l^2) with the sphere size. System conditions: $N = 200$, $\phi^0 = 0.001$ and $\varepsilon = -0.35 kT$

Further insight into the layer structure can be obtained the histograms of loops and tails (Figs. 4.19 and 4.20), proportional to the probability of finding in the adsorbed layer a loop, respectively a tail, of n monomers in the rank $n \pm \Delta$, in other words $\mathcal{P}(n, \Delta)$. This quantity can be associated to the entropy of loops and tails in some theoretical treatments [19]. In our case we have computed these histograms to analyze the effect of the curvature in the distribution of sizes of the species of the adsorbed layer. Effectively, on one hand, the loop distribution is rather insensitive to the curvature of the surface. There is a slight shift of the distribution towards large loops at the smaller sphere considered here, but it seems that there is no significant change in the behaviour.

On the other hand, the tail length distribution is very sensitive to the curvature. Initially, for the large sphere case, the distribution is a single exponential. However, with the increase of the curvature the amount of small tails, very frequent in the large sphere case, decreases in favor of an increase of the long tails, the inversion taking place at a lengths between 30 and 75 monomers. Notice that for $R/l = 5.08 < z_w^*/l$ the decay is very slow, and even becomes bimodal at $R/l = 1.36$. The bimodal nature of the profile at the small sphere case, with maxima roughly at $n = 9$ and $n = 60$ can be interpreted as follows. For the small sphere there is on average of about one polymer covering the sphere. Admitting that on average the chain will cover the whole adsorbing surface, we can expect that the sum of length of the two tails be rather constant. Thus, a long tail should be accompanied by a short tail on average. Therefore, the presence of the two maxima indicates that the preferred conformation for the small sphere case is one long tail together with a small tail, that is, the sphere being located near one polymer end.

However, if we consider higher adsorption energies of ε the behaviour is different. In the Figs. 4.21 and 4.22, we represent, respectively, the loops and tails histograms taking into account two values of $\varepsilon = -0.35$ and $-1 kT$ (being $R/l = 1.36$). In the case of loop length distribution, the amount of small loops increases with the value of ε , as we can see in the Fig. 4.21. Hence, the probability of finding loops of large size decreases as the value of ε is more negative. For the case of the tails, the length distribution is very sensitive to ε . From these results, represented in the Fig. 4.22, we can see that an increase of the adsorption energy may produce a high probability of finding the colloidal particle close to the middle of the polymer chain, instead of being localized near the end.

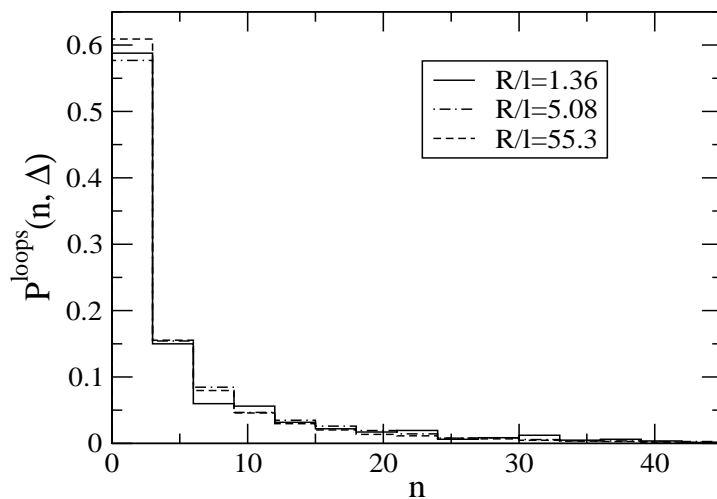


Figure 4.19: Histogram of loops for three sphere sizes ($R/l = 1.36$ (full line), 5.08 (dash dot line) and 55.3 (short dash line)). System conditions: $N = 100$, $\phi^0 = 0.001$ and $\varepsilon = -0.35 kT$.

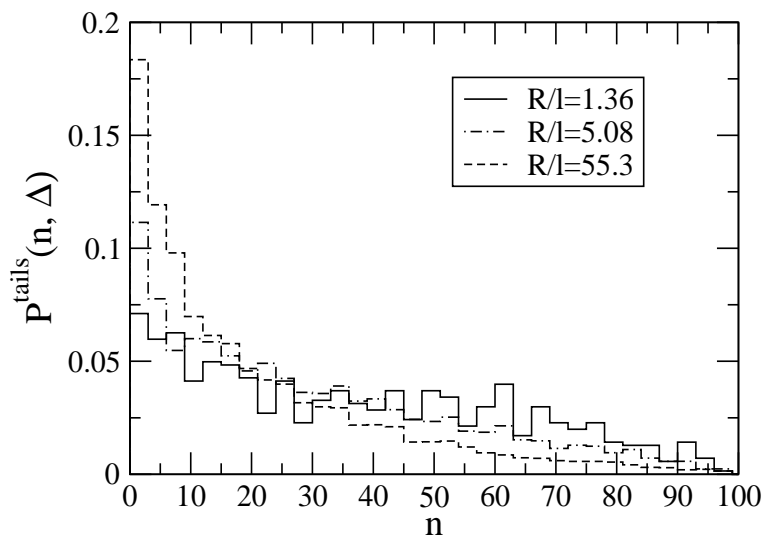


Figure 4.20: Histogram of tails for three sphere sizes ($R/l = 1.36$ (full line), 5.08 (dash dot line) and 55.3 (short dash line)). System conditions: $N = 100$, $\phi^0 = 0.001$ and $\varepsilon = -0.35 kT$.

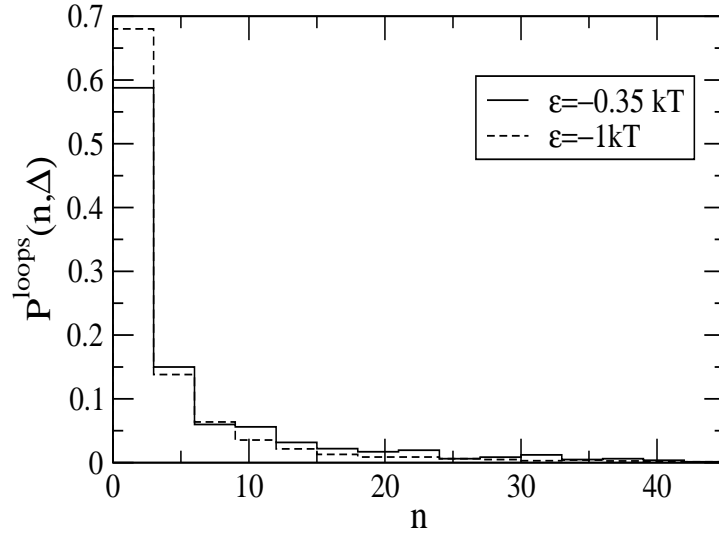


Figure 4.21: Histogram of loops for two values of ε ($-0.35 kT$ (full line) and $-1 kT$ (dashed line)) considering the sphere size $R/l = 1.36$, $N = 100$ and $\phi^0 = 0.001$.

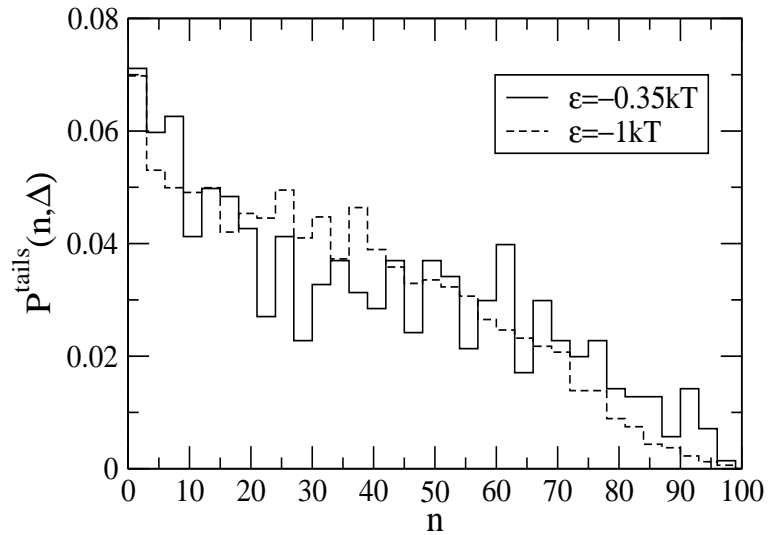


Figure 4.22: Histogram of tails for two values of ε ($-0.35 kT$ (full line) and $-1 kT$ (dashed line)) considering the sphere size $R/l = 1.36$, $N = 100$ and $\phi^0 = 0.001$.

This conclusion is also confirmed from the Figs. 4.23 and 4.24, in which are represented the probability that an adsorbed chain has a tail of size n_1 in the range $n_1 \pm \Delta$ and the other, of size n_2 in the range $n_2 \pm \Delta$. The sphere size is $R/l = 1.36$, the polymer length, $N = 100$, $\phi^0 = 0.001$ and two values of ε ($-0.35 kT$ (Fig. 4.23) and $-1 kT$ (Fig. 4.24)) have been considered. In the case of $\varepsilon = -0.35 kT$, we have an area of higher probability corresponding to tail sizes of m_1 between 10 and 20, while the tail size m_2 takes values between 60 and 80. Therefore, these results indicate that the colloidal particle is found near one polymer end, thus confirming the results plotted in Fig. 4.20. However, for the value of $\varepsilon = -1 kT$, the contour plot presents different maxima approximately in the line $m_1 + m_2 \cong 70$ indicating that it is equally probable to find the particle at any location along the chain, and that the loop and tail material is approximately the same for every conformation. It is interesting to point out that this conclusion has been also found by scaling analysis of polymer-colloid systems that we will describe in the next chapter.

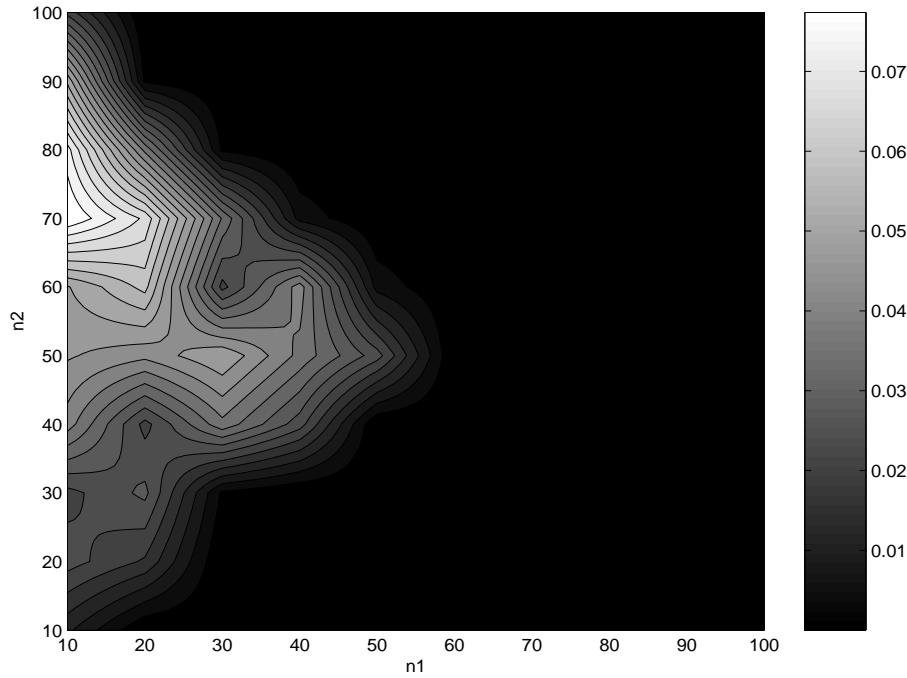


Figure 4.23: Contour plot of tails for the sphere size $R/l = 1.36$. System conditions: $N = 100$, $\phi^0 = 0.001$ and $\varepsilon = -0.35 kT$. We name the shortest tail as n_1 and the largest as n_2 .

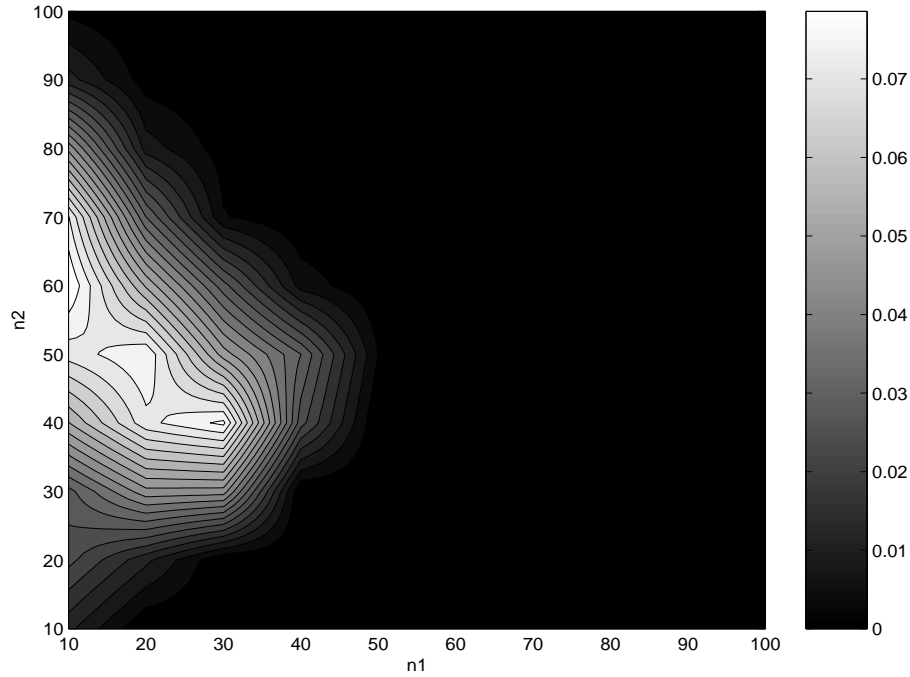


Figure 4.24: Contour plot of tails for the sphere size $R/l = 1.36$. System conditions: $N = 100$, $\phi^0 = 0.001$ and $\varepsilon = -1 kT$. We name the shortest tail as n_1 and the largest as n_2 .

4.4 Conclusions

In this chapter, the problem of polymer adsorption onto spherical surfaces has been addressed by means of the SCMF theory, based on an importance sampling of the one-chain conformational space described in chap. 2. Contrary to the case of planar interfaces, there is little work done on curved surfaces. We expect that the results presented in this chapter will contribute to shed some light on the interplay of the curvature with the different length scales describing polymer adsorption. We have centered our attention on adsorption from a dilute solution due to the fact that the finite size effects are more noticeable than in semidilute regimes. Effectively, because of the bulk correlation length does not play any role in the problem and free chain penetration can be completely ignored in the interpretation of the data. Our results show the variation of the adsorbed monomer profiles as well as those of monomers belonging to loops and tails, indicating that the overall effect is small and mostly due to the decrease of the effective adsorption energy per chain as well as the available adsorbing surface when the radius of the particle decreases. However, other magnitudes show a much more noticeable variation. Effectively, the adsorbance, as well as, the layer thickness increase when the curvature is increased, in

particular, when the loop layer start to be sensitive to the curvature for $R < R_c \sim z_w^*$. The internal structure of the layer, described along this work, entangles with the curvature effects in the sense that it seems rather clear that for small spheres the loop layer remains confined in a layer of thickness R , leaving a few very long tails outside. This structural information can be of relevance in applications, when functionalized ends come into the play [31]. We have also found the preferred conformations presented in the polymer adsorption on small particles, considering the different positions of the adsorbing sphere along the polymer chain. We have shown that for values of $\varepsilon = -0.35 kT$, the sphere seems to have preference to occupy positions near the edge of the chain, probably to favor the entropic gain of having many monomers belonging to a long tail. However, increasing the adsorption energy ($\varepsilon = -1 kT$) has been demonstrated that the particle not only may be located near one polymer end, but also may occupy other positions along the chain. This conclusion has been confirmed by a scaling analysis [27], described in the next chapter. Finally, we want to mention again the fact that the crossover length scale z_w^* seems to play a very important role in curved interfaces, beyond the already discussed in planar interfaces. On the one hand, the critical radius at which the adsorbances of loop and tail monomers are equal scales as z_w^* , which is, in addition, the length that characterize the onset of the important curvature effects on the structure of the layer discussed above. We think that in the starved regime, the relevant length is z_w^* instead of the thickness of the layer, as suggested in refs. [32].

Bibliography

- [1] D. H. Napper, *Polymeric Stabilization of Colloidal Dispersion*, (Academic Press, 1983); W. B. Russel, D. A. Saville and W. R. Schowalter, *Colloidal Dispersions*, (Cambridge University Press, Cambridge UK, 1989).
- [2] A. M. Kulkarni, A. P. Chatterjee, K. S. Schweizer and Zukoski *Phys. Rev. Lett.* **83**, 4554 (1999).
- [3] S. Asakura and F. J. Osawa, *J. Chem. Phys.* **22**, 1255 (1954).
- [4] J. F. Joanny, L. Leibler and P. G. de Gennes, *J. Polym. Sci. Polym. Phys.* **17**, 1073 (1979).
- [5] M. Fuchs and K. Schweizer, *Journal of Physics-Condensed Matter.* **14**, 239 (2002).
- [6] A. Moussaid, W. C. K. Poon, P. N. Pusey and M. F. Soliva, *Phys. Rev. Lett.* **82**, 225 (1999).
- [7] P. G. de Gennes *C. R. Acad. Sc. Paris B* **288**, 359 (1979).
- [8] A. Hanke, E. Eisenriegler and S. Dietrich, *Phys. Rev. E* **59**, 6853 (1999).
- [9] E. Eisenriegler, *J. Chem. Phys.* **113**, 5091 (2000).
- [10] R. Sear, *Phys. Rev. Lett.* **86**, 4696 (2001); preprint (2002).
- [11] M. Fuchs and K. Schweizer, *Europhysics Letters* **51**, 621 (2000); M. Fuchs and K. Schweizer, *Phys. Rev. E* **64** (2001).
- [12] I. Y. Erukhimovich *et al.* In preparation.
- [13] B. Cabane and R. Duplessix, *J. Phys. France* **48**, 651 (1987); F. Lafuma, K. Wong and B. Cabane, *J. Coll. Int. Sci* **143**, 9 (1991); K. Wong, P. Lixon, F. Lafuma, P. Lindner, O. Aguerre Charriol and B. Cabane, *J. Coll. Int. Sci* **153**, 55 (1992); K. Lindell and B. Cabane, *Langmuir* **14**, 6361 (1998).
- [14] A. Silberberg, *J. Phys. Chem.* **66**, 1872 (1962); **66**, 1884 (1962).

- [15] P. G. de Gennes, *Macromolecules* **14**, 1637 (1981); **15**, 492 (1982).
- [16] S. Alexander, *Journal de Physique* **38**, 977 (1977).
- [17] T. M. Birshtein and O. V. Borisov, *Polymer* **32**, 916 (1991).
- [18] C. Marques and J. F. Joanny, *J. Phys. France* **94**, 1103 (1988).
- [19] M. Aubouy and E. Raphaël, *Macromolecules* **31**, 4357 (1998).
- [20] A. N. Semenov, J. F. Joanny and A. Johner, *Theoretical and Mathematical Models in Polymer Research*, (Ed. A. Grosberg, Academic Press, Boston, 1998).
- [21] G. J. Fleer, M. A. Cohen Stuart, J. M. H. M. Scheutjens, T. Cosgrove and B. Vincent, *Polymers at Interfaces*, (Chapman and Hall; London, 1993) and references there in.
- [22] D. Frenkel and B. Smit, *Understanding Molecular Simulation* (Academic Press, San Diego, 1996).
- [23] A. N. Semenov and J.F. Joanny, *Europhys. Lett.* **29**, 279 (1995).
- [24] A. N. Semenov, J. Bonet i Avalos, A. Johner and J. F. Joanny, *Macromolecules* **29**, 2179 (1996).
- [25] P. G. de Gennes, *Scaling Concepts in Polymer Physics* (Cornell University Press, Ithaca, 1979).
- [26] A. Johner, J. F. Joanny and M. Rubinstein, *Europhys. Lett.* **22**, 591 (1993).
- [27] A. Johner, J. F. Joanny, S. Díez Orrite and J. Bonet Avalos, *Europhys. Lett.* **56** (4), 549 (2001).
- [28] C. M. Wijmans, F. A. M. Leermarkers and G. J. Fleer, *Langmuir* **10**, 1331 (1994).
- [29] T. Cosgrove, P. C. Griffiths and P. M. Lloyd, *Langmuir* **11**, 1457 (1995).
- [30] L. V. Zherenkova, D. A. Mologin, P. G. Khalatur and A. R. Khokhlov, *Colloid Polym. Sci.* **276**, 753 (1998).
- [31] Victoria S. Stenkamp and John C. Berg, *Langmuir* **13**, 3827 (1997).
- [32] G. J. Fleer, J. van Male and A. Johner, *Macromolecules* **32**, 825 (1999).

Chapter 5

Scaling analysis of polymer-colloid systems

Having analyzed the problem of polymer adsorption onto isolated spherical particles, in this latter chapter we will develop a preliminary theoretical analysis on the problem of colloid-polymer mixtures. To have some idea about the different scenarios that can be found, we have undertaken here an scaling analysis based on the work of Semenov, Joanny and collaborators [1], in which the tails were explicitly taken into account. Furthermore, we have centered our attention on the case of small adsorbing colloids [2] $R \ll z_w^*$, in which one chain adsorbed on one colloid has two long tails with a size fixed by the overall contour length N . In the presence of many chains a small colloid may nonetheless carry two or more chains giving rise to a star-shaped complex. We calculate the abundance of such complexes in dilute solution. In semi-dilute solution similar polymer stars form on a colloid, which act as effective crosslinks that percolate on a gelation line.

5.1 Formation of colloid/polymer complexes

5.1.1 Adsorption on a flat wall

As already mentioned in previous chapters, the standard model for the adsorption of a long neutral chain onto a flat wall was proposed twenty years ago by de Gennes. It starts from the remark that the local polymer/polymer correlations in the adsorption layer should be the same as in a homogeneous solution at the local concentration $c(z)$, with z the distance from the wall. The local correlation length [3] in the layer is then given by $\xi = c^{-\nu/(\nu d-1)}$ with ν the swelling (Flory) exponent and d the dimension of space. Inside the adsorption

layer of thickness λ the only characteristic lengthscale is the distance to the wall, the local correlation length $\xi(z)$ is thus proportional to z . Hence the celebrated power law profile is equal to

$$c(z) \sim z^{-\frac{(\nu d - 1)}{\nu}} \quad (5.1)$$

where the exponent is approximately $-4/3$. The fast decay of this profile indicates that the adsorbance Γ is dominated in the strong adsorption limit by the small loops although this approach does not need to discuss the detailed structure of the layer in terms of loops and tails, as done by the Dutch group [4]. It is nonetheless possible to deduce the loop distribution under the assumption that loop-monomers dominate over tail-monomers near the wall. If a self-similar profile is assumed, each loop of size larger than n feels up a correlation volume of radius z at heights up to n^ν . The loop-size distribution $D(n)$ can thus be rewritten in terms of the correlation disk-density at height z :

$$\int_{z^{1/\nu}}^{\infty} D(n') dn' = \frac{1}{z^{d-1}} \quad (5.2)$$

This equation is essentially the statement of the existence of a self-similar profile. The loop-size distribution is obtained by differentiation: $D(n) = n^{-\nu(d-1)-1}$. The loop-size distribution is used as a measure of the loop partition function Z_l . The tail partition Z_t function is linked to the loop partition by considering that a loop of size n can be built by connecting two tails of size $n/2$ initially within reach of each other [5]:

$$Z_l = Z_t^2 n^{1-\gamma} \frac{n^{\nu(d-1)}}{n^{\nu d}} \quad (5.3)$$

The second factor stands for loosing two free chain ends, the last one is a geometric factor specifying that the tails are within reached (here we make no difference between n and $n/2$ as the prefactor remains unknown). This relation is rather general and does not imply loop-monomer dominance. Assuming loop-monomer dominance, (Z_l is known), Z_t can be deduced [5] :

$$Z_t = n^{\frac{-\nu(d-2)+\gamma}{2}-1} \quad (5.4)$$

This partition function in turn determines the chain end distribution: $c_{end}(z) \sim z^{-\beta/\nu}$ (c.f. eq. 3.8) where β is the order parameter exponent linked to the previous critical exponents by the general relation: $2\beta = \nu d - \gamma$. The relation $n^\nu \sim z$ is used to transform the contour length n into distance z .

The tail-monomer concentration can in turn be calculated from the tail partition function; due to the slow decay of the tail partition function integral is actually dominated by the upper bound. About $2\Gamma/N$ ends are located beyond any distance z from the wall, any of this tails fills a correlation volume at any distance, hence the tail monomer concentration $c_t(z)$ is given by :

$$c_t(z) = \frac{\Gamma}{2N} z^{\frac{1}{\nu}-1} \quad (5.5)$$

Comparing the tail-monomer profile to the loop-monomer profile show that the loop-monomer dominance assumption fails for $z = z_w^* \sim N^{\frac{1}{d-1}}$ (as we described in the section 1.2.2 of the chapter 1.).

At larger distances, tail-monomers dominate over loop-monomers and build up de Gennes' power law profile. Each correlation volume is then filled by one tail starting further from the wall, this sets the end point concentration to $c_{end}(z) = z^{-d}$. Reverting the arguments in the loop-monomer dominance regime it is now possible to get the tail partition function, loop partition function and loop-monomer profile.

$$Z_t = N^{\frac{\gamma+\nu d}{2\nu(d-1)}} n^{-1-\nu(d-1)} \quad Z_l = N^{\frac{\gamma+\nu d}{\nu(d-1)}} n^{-1-\gamma-\nu(2d-1)} \quad c_l(z) = N^{\frac{\gamma+\nu d}{\nu(d-1)}} z^{\frac{-2\nu d+1-\gamma}{\nu}} \quad (5.6)$$

Note the strong power law decrease of the loop-monomer concentration beyond z_w^* , with an exponent close to -6 for $3D$ excluded volume statistics.

5.1.2 Adsorption onto colloidal particles: Adsorption Regimes

As we have shown in the previous chapter, the polymer adsorption onto colloidal particles is influenced by the ratio between the size of the polymer and the sphere. If the colloidal particle is much larger than the polymer radius of gyration (see Fig. 5.1.a), the particle is coated by a thin adsorbed layer whose structure is similar to the layer described in the polymer adsorption on flat surfaces. However, as the radius of the sphere decreases ($R < z_w^*$) the number of adsorbed polymer is also reduced until it is close to 1 and the loop layer is confined in a region of size of the order of the sphere radius, while the tails do not play any influence in the adsorbed layer. The Fig. 5.1.b represents this situation in which we can see a very long polymer chain wrapping the sphere and forming a layer with two long free arms containing most of the monomers [2]. A similar picture has been already described in the previous chapter from the results obtained by the SCMF methodology. Thus, considering polymer chains of length $N = 100$ adsorbed on small spheres (of size $R/l = 1.36 < z_w^*/l$), the average number of tails obtained is of the order of 2 (see table

4.2). However, an increase of the radius of the sphere, produce a change in the structure of the adsorbed layer in order to the number of tails that go in beyond R is reduced until the adsorbed chains lie in a region of thickness less than R (for $R/l = 55.3 \gg R_g/l$, the average number of tails obtained, to distances beyond R , is zero).

In this way, there is the possibility that two or more different chains are adsorbed on the same colloidal particle forming structures with four or more long free arms escaping from the sphere. Therefore, in the description of colloidal particles in polymer solution, the prediction of the types of structures formed as the result of interaction of macromolecules with the particles, may be an interesting problem. We can mention theoretical works based on RISM integral equation technique [6], in which the theory is used to understand the interaction between colloidal particles and macromolecules in the regimes of weak and strong adsorption, and experimental studies carried out by Cabane and Duplessix [7, 8] using small-angle neutron scattering in a semidilute aqueous solution of PEO containing spherical micelles of SDS molecules. The origin of the physical association produced by the interaction polymer-colloidal particle, will be described in the following sections.

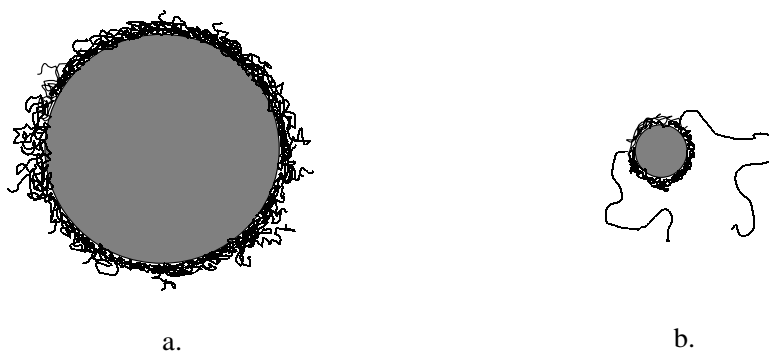


Figure 5.1: Adsorption of polymers onto colloidal particles: large sphere (case a) and small sphere (case b).

5.1.3 Polymer/colloid star-shaped complexes

Depending on the stoichiometry of the polymer/colloid mixture, different complexes are expected. If colloids are in excess, one chain wraps several colloids building a necklace. Though the single chain state is the preferred one if polymer is in excess, some colloids will accommodate a small number of chains, building star-shaped complexes. In the following we will mainly comment on star-shaped complexes.

The abundance of those complexes is fixed by a balance between extra interactions of

the branches and some entropy gain. At large scale a star-shaped complex has the properties of a star-polymer with polydispersed arms. Duplantier [9] gave a general expression for the partition function of a polymer (with N monomers) of any topology. This expression generalises the one for linear chains

$$Z_G = N^{\gamma_G} \quad (5.7)$$

The new susceptibility exponent γ_G for an arbitrary connected graph G is constructed from vertex exponents, entering the star description, and depends on the number of independent closed loops. For symmetric star-polymers with all p arms identical, the expression reduces to $Z = N^{\gamma_p}$. The exponent γ_p is the same for $p = 1$ and $p = 2$ (these both values of p describe a linear chain), it goes through a (formal) maximum between $p = 1$ and $p = 2$ and decreases as a power-law at high p in accordance with the Daoud and Cotton [10] blob model $\gamma_p \sim -p^{d/(d-1)}$ where d is the dimension of space. The exponents γ_p are exactly known in $2D$ [9]. In $3D$ only a low order ε -expansion is known.

For a star with polydisperse arms all of different size ranging from the smallest N_1 to the largest N_p the partition function can be constructed step by step: Let first all p arms have the smallest size N_1 , the partition Z is $N_1^{\gamma_p}$, let now grow all chains but one to the next size N_2 , Z becomes $N_1^{\gamma_p} N_2^{\gamma_{p-1}} / N_1^{\gamma_{p-1}}$, in the next step, all outer chains but one grow to the next size N_3 and so on. As a result,

$$Z_p = N_1^{\gamma_p - \gamma_{p-1}} N_2^{\gamma_{p-1} - \gamma_{p-2}} \dots N_{p-1}^0 N_p^{\gamma_1 - 1} \quad (5.8)$$

Let us first consider the simpler case where only one chain wraps the colloid. Only $n_a = 4\pi\Gamma R^2$ monomers go into small loops covering the surface of the colloid. The energy gain upon adsorption of the small loops is $F_a \sim 4\pi R^2$ in thermal energy units, in case of strong adsorption. These small loops are almost of monomeric size and the small-loop layer resembles a $2D$ melt, the partition function of the small loop strand is described by $n_a^{\gamma_a}$ with γ_a as the susceptibility exponent corresponding to adsorbed chain whose value is assumed to have the same value as in a two-dimensional melt. For chains such that the two tails are only of length $n_t = R^{1/\nu}$ the partition function of the two uncorrelated tails is the same as on a flat surface, of order $n_t^{\gamma_t - \nu - 2}$. All together, the partition function reads in this case $Z_a = R^2 n_a^{\gamma_a - 1} n_t^{\gamma_t - \nu - 2} \exp F_a = Z_{a,0} \exp F_a$ where R^2 stands for the choice of the starting point of one tail on the colloid. On the other hand for a very long chain wrapping the colloid, the partition function of the complex scales with the chain size as for a free chain $Z_0 = N^{\gamma - 1}$, being $\gamma = 1.16$ the susceptibility exponent for a polymer chain in a good solvent [5]. Imposing a smooth crossover between the two limits at $N = n_t$, we get the partition function of the one chain complex ;

$$Z_1 = Z_{a,0} n_t (N/n_t)^\gamma \exp F_a \quad (5.9)$$

When q chains wrap around the small colloid, a $2q$ -star shaped complex is obtained. Let us characterise each chain by the smallest of its two arms (the largest is essentially its complement to N) and let again N_1 be the smallest of these $p = 2q$ arms (all by definition smaller than $N/2$). The partition function of the complex can be obtained in a way similar to Z_1 , as a result $Z_q = n_a^{q-1} Z_{a,0}^q \exp F_a I_t(q)$ where the small loop contribution is explicit and the first factor stands for the ways to choose the lengths of the q adsorbed loop sequences (throughout q is assumed not to be a large number). The last factor stands for the configuration integral of the large tails :

$$I_t(q) = \int_{n_t}^{N/2} \left(\frac{N_q}{n_t}\right)^{\gamma_{q+1}-\gamma_q} \left(\frac{N-N_q}{n_t}\right)^{\gamma_q-\gamma_{q-1}} dN_q \dots \int_{n_t}^{N_2} \left(\frac{N_1}{n_t}\right)^{\gamma_{2q}-\gamma_{2q-1}} \left(\frac{N-N_1}{n_t}\right)^{\gamma_1-1} dN_1 \quad (5.10)$$

The value of $I_t(q)$ strongly depends on whether the integrals are dominated by the lower boundary or not. After the general shape of the $\gamma_p(p)$ plot, the slope $\gamma'_p(p)$ becomes very negative at high p , there is a value p^* of p where $\gamma_{p-1} - \gamma_p$ becomes smaller than -1 .

Let us first suppose that there are not many chains so that $2q < p^*$ in that case the lower boundary can be shifted to zero in all integrals and :

$$I_t(q) \sim N^q \left(\frac{N}{n_t}\right)^{\gamma_{2q}-1} \quad (2q < p^*) \quad (5.11)$$

The chains in the star-shaped aggregate adopt mainly symmetric configurations.

In the very opposite case $q > p^*$, where there are many chains in one aggregate, all integrals are dominated by the lower boundary and:

$$I_t(q) \sim n_t^q \left(\frac{N}{n_t}\right)^{\gamma_q-1} \quad (q > p^*) \quad (5.12)$$

The chains adopt dissymmetric configurations with only one long tail per chain (this would be expected from Daoud and Cotton blob model [10]).

In the intermediate regime $q < p^* < 2q$

$$I_t(q) \sim n_t^q \left(\frac{N}{n_t}\right)^{\gamma_{p^*-1} + p^* - q} \quad (q < p^* < 2q) \quad (5.13)$$

There are essentially p^* long tails. Note that the intermediate regime crosses over smoothly with the previous ones.

In the following we focus on small p -values corresponding to symmetric aggregates which are more abundant.

5.1.4 Star-shaped complexes at equilibrium in dilute solution

If the density ρ of colloidal particles is very small and if the polymer is in a dilute solution, each chain complexes at most one particle. We call ρ_q the density of spheres bound q chains. Considering the complex formation as a chemical reaction, the density ρ_q is given by the mass action law,

$$\rho_q/\rho_0 = \frac{Z_q}{Z_0^q} \left(\frac{c}{N} \right)^q \quad (5.14)$$

where c is the monomer concentration. When F_a is large there are almost no free colloids and most particles are bound to a single chain $\rho \sim \rho_1$. High- q aggregates are rare and the only important aggregates are those with two chains; their density is

$$\rho_2 = \rho c n_a Z_{a,0} n_t^{\gamma-\gamma_a} N^{\gamma_4-2\gamma+1} \quad (5.15)$$

It decreases with N and increases with the radius of the colloidal particle as a power law. Inserting approximate values of the critical exponents we get $\rho_2 = \rho c R^{2.7} N^{-0.6}$.

At higher colloid densities one chain carries many colloids and forms a necklace aggregate, necklaces in turn form a small fraction of decorated star-shape complexes; these will not be discussed in this work.

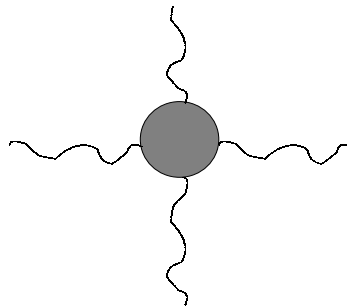


Figure 5.2: Star-shaped complex ($q=2$, $p=4$)

5.1.5 Gelation in semidilute solution

Above the overlap concentration $l^d c^* = N^{1-d\nu}$ of polymer coils, the polymer form a temporary network of mesh size ξ , the correlation length of polymer concentration fluctuations or blob size. Properties of such solutions of long, strongly overlapping chains are essentially insensitive to the chain length,. This is in particular true for the density of colloids linked to two blobs. To ensure a smooth crossover at c^* the density ρ_2 in the semi-dilute should be of the form $\rho_2 = \rho n_a Z_{a,0} n_t^{\gamma-\gamma_a} c^\alpha$ with $\alpha = 1 + \frac{2\gamma-\gamma_a-1}{3\nu-1}$, in which less than one colloid per correlation volume is assumed.

Each particle bound to two different chains acts as a physical cross-link between chains. If the density of cross-links is large enough, all the chains are connected and the solution can be considered as a physical gel. The gelation transtition occurs if there are of order of two or slightly less cross-links per chain, i.e if the density of cross-links is $\rho_2 \sim c/N$ [3]. This gives the gelation line of the solution at

$$\rho_{gel} \sim \frac{n_t^{\gamma_a-\gamma}}{N n_a Z_{a,0}} c^{-\left(\frac{2\gamma-\gamma_a-1}{3\nu-1}\right)} \quad (5.16)$$

As we ignore prefactors throughout, our rough criterion for gelation is sufficient. Inserting critical exponents we obtain: $\rho_g = c^{-0.8} R^{-2.7} N^{-1}$. The concentration of colloidal particles at the gelation threshold decreases both with the monomer concentration and with the sphere radius. It vanishes when N tens to infinity at fixed polymer concentration; when the molecular weight is large, there is indeed less than one colloid per polymer mesh for strongly overlapping polymer solutions.

5.2 Conclusions

In this chapter we present scaling results for mixtures of polymers and small adsorbing spheres. Special attention is payed to star-shaped complexes that form by adsorption of several (typically two) chains on the same colloid in dilute polymer solution with polymer in large excess. It is shown that partition function of complexes comprising only a few adsorbed chains are dominated by configurations where chains have symmetric long tails. These configurations have been already confirmed from the numerical results obtained by SCMF methodology, in which an increase of the adsorption energy demonstrated that the particle may occupy positions along to the chain close to the middle of it (see Fig. 4.23 and 4.24), obtaining, thus, tails of similar sizes or, at least, not preferring a very asymmetric conformation. In contrast, if many long chains are forced on a colloid, the partition function is dominated by dissymmetric configuration where each chain only

contributes one long tail in accordance with results of the Daoud and Coton star-model. The crossover between different regimes can be expressed in term of the vertex exponents introduced by Duplantier [9]. The abundance of complexes is calculated as a function of colloid radius, chain length and concentrations.

Semidilute solutions are described as a transient network of entangled chains by the standard concentration-blob model. Here again one colloid has some probability to link to different chains. The abundance of colloids bearing polymer crosses does not depend on chain length in the strongly overlapping regime and is obtained here from a simple cross over argument (a different argument is used in ref. [2]). Beyond a critical average number of crosslinks per chain, the solution undergoes a percolation transition and forms, in that sense, a gel. The transition is located at vanishing colloid density for very long, strongly overlapping, chains. This validates *a posteriori* our assumption that there is less than one colloid per polymer mesh. This assumption is relaxed in ref. [2].

Our theory is restricted to scaling arguments. It seems difficult to describe the subtle correlations between star-arms at low (finite) number of arms in more details. Also are more detailed Markovian Mean-Field theories not well suited here, they are space-dimension independent and obscure the new physics introduced by curvature (for example the criteria $\Gamma R^2 = N$ and $R = z_w^* \sim N^{1/3}$ are not equivalent and a spurious regime opens). Therefore, the numerical tools developed in this work seem suitable for an analysis of the problem of suspensions of colloidal particles and long polymeric chains, especially due to the fact that the SCMF method keeps track of the excluded volume correlations, as it is the case of the scaling approach discussed in this chapter. Therefore, this fact opens a line for much future work.

From a practical point of view the assumption of flexible chains may not always hold at the level of the colloid radius. The description of a single stiff macromolecule wrapping a colloid is available [11](also in the charged case [12]). A description of complexes involving several chains should be possible even in the case of semi-flexible chains at least at the scaling level. In addition to the latex particles, silica colloids, or micelles used in previous experiments it should be possible to use fullerenes or modified fullerenes as model colloids [13, 14]. Again, the incorporation of stiffness in the framework of SCMF theory is not a complex matter that can be carried out in the near future.

Bibliography

- [1] A. N. Semenov, J. F. Joanny and A. Johner, *Theoretical and Mathematical Models in Polymer Research*, (Ed. A. Grosberg, Academic Press, Boston, 1998).
- [2] A. Johner, J. F. Joanny, S. Díez Orrite and J. Bonet Avalos, *Europhys. Lett.* **56** (4), 549 (2001).
- [3] P. G. de Gennes, *Scaling Concepts in Polymer Physics*, (Ed. Cornell University Press, Ithaca, NY, 1979).
- [4] G. J. Fleer, M. A. Cohen Stuart, J. M. H. M. Scheutjens, T. Cosgrove and B. Vincent, *Polymers at Interfaces*, (Chapman and Hall; London, 1993)
- [5] A. N. Semenov and J. F. Joanny, *Europhysics Letters* **29**, 279 (1995).
- [6] P. G. Khalatur, L. V. Zherenkova and A. R. Khokhlov *J. Phys. II France* **7**, 543 (1997).
- [7] B. Cabane and R. Duplessix, *J. Phys. France* **48**, 651 (1987).
- [8] B. Cabane and R. Duplessix, *Colloids. Surf.* **13**, 19 (1985).
- [9] B. Duplantier, *J. Stat. Phys.* **54**, 581 (1989).
- [10] M. Daoud and J. P. Cotton, *J. Physique* **43**, 531 (1982).
- [11] H. Schiessel, R. F. Bruinsma and W. M. Gelbart, *Journal of Chemical Physics* **115**, 7245 (2001).
- [12] K. K. Kunze and R. R. Netz, *Phys. Rev. Lett.* **85**, 4389 (2000).
- [13] Y. Ederle and C. Mathis, *Macromolecules* **30**, 2546 (1997).
- [14] Larissa S. Litvinova, Veniamin G. Ivanov, Maxim V. Mokeev and Vladimir N. Zgonnik *Mendeleev Commun.* **193**, (2001).

Chapter 6

Perspectives

In this work, we have modified the methodology known as Single Chain Mean Field (SCMF) aiming at its application to polymer adsorption problems. The structure of the polymeric layer has been examined in equilibrium with a bulk solution for different adsorption energies and molecular weights, considering both flat and spherical (colloidal particle) surface geometries. In this way, it has been possible to calculate numerically properties, which can be also experimentally measured, such as monomer volume fraction profiles, adsorbance or the thickness of the adsorbed layer.

Thus, our main interest has been the study of solutions of linear, flexible and neutral chains, in the presence of an attractive solid interface, where the chains can reversibly adsorb. However, an interesting subject of study may be found in the influence of the architecture of chains that we consider in the structure of the adsorbed polymer layer.

As we have seen during this work, the structure of the adsorbed polymer layer can be described in terms of loops, trains and tails. However, this picture is only applied to the case of homopolymer chains on surfaces. Different architectures can be distinguished depending on the structure of the polymer and the nature of the groups involved. Thus, we can mention the case of chains with star shaped, whose conformation on the surface may be composed by a number of tails originate from around a central block, chains containing groups with a preferential affinity to the surface or even chains with different degrees of flexibility.

It is clear, from this point of view, that for a full description of the structure of the adsorbed layer it is necessary to know the amount of polymer that is adsorbed, the type of groups that are in contact with the surface, as well as their proportion, the thickness of the adsorbed polymer layer or the distribution of polymer segments from the surface. In that way, many theoretical and numerical studies have been concentrated on the effects of molecular structure on the adsorbed polymer layer, owing to its several

applications in science and technology. Thus we can mention simulation calculations reported by Striolo and Prausnitz [1] in the area of branched polymers. As well in the area of semiflexible chains whose first works were developed 50 years ago by Krarty and Porod [2] and, however, this kind of chains are still considered as a nontrivial polymer problem [3, 4, 5] or even the Monte Carlo simulations of adsorbed random copolymers [6].

In this work, the numerical results, obtained from Single Chain Mean Field approach, have shown the different scenarios that describe the dependence of the adsorbed polymer layer with the curvature of the colloidal particle. In all these cases, the homopolymer chains have been considered as flexible and linear. Therefore, as we have mentioned above, the adsorption behavior may be changed depending on the architecture of the polymer chain considered. In this way, taking into account the adsorption onto colloidal particles, it would be interesting to study the variation of the structure of adsorbed layer depending on the nature of the polymer chain in a wide range of sphere sizes. Furthermore, the SCMF methodology developed here seems a suitable tool to complement the present theoretical interest in the resolution of the conformation of the polymer chains adsorbed on a surface.

Flocculation of colloidal particles through a polymer solution

The addition of polymer into colloidal suspensions has a crucial effect on the aggregation and kinetic stability of colloidal particles. Therefore, these physical phenomena have been studied in several experimental [7] and theoretical [8] works.

In the case of adsorption of polymer on colloidal particles, this mechanism produces a considerable effect in these systems. At strong adsorption, each particle is covered with a dense polymer layer and a small amount of high molecular weight polymer may induce to link of colloidal particles by bridging fragments of chains. This mechanism causes the appearance of macroscopic regions rich in colloidal particles, i.e. the *flocculation* of the system.

The presence of small spherical particles (colloidal particles) in a non-adsorbing polymer solution also induce the aggregation mechanism [7]. In this case the influence from the polymer causes the attraction between two colloidal particles. This behavior is due to polymer chains are outsed from the gap between both particles thus, the gradient in polymer concentration, near the particles, leads to a positive surface energy that induces this attractive interaction.

The thickness of the depletion zone is of the order of R_g corresponding to the polymer chain in dilute conditions and of the order to the correlation length ξ in semidilute solutions. Between the analytical theories, we can mention the work developed by T. Odijk [9], based on the self-consistent approximation and more recently, the work presented by Tuinier and Lekkerkerker[10] in which the polymer segment concentration profiles ob-

tained for arbitrary polymer-sphere size ratio are shown. In this way, it is possible to compare these results with those obtained from SCMF results, considering non-adsorbing polymer chains, for a wide range of colloidal particles' sizes and chain lengths.

As we have commented above, the flocculation of colloidal suspensions can be produced by two different mechanisms, depending on the interaction between the polymer chains and the colloidal particles. During this work, we have shown the variation presented by the structure of adsorbed polymer layer depending on the size of the sphere (colloidal particle) considered. Therefore, taking into account these results, the flocculation of colloidal particles through bridges formed from the adsorbed polymer layers, may present different ways of aggregation in order to the size of the colloidal particle is varied. Thus, from this information, it would be interesting to study, using the SCMF methodology described in this work, how the structure of the adsorbed polymer layer affects the colloidal flocculation.

Therefore, these subjects, just reviewed, are part of the possibilities of research that may be open by the development of mean-field methods which can take into account correctly both the excluded volume correlations along the chain as well as the screening of such correlations when semidilute polymer solutions are under study.

Bibliography

- [1] Alberto Striolo and John M. Prausnitz, *J. of Chem. Phys.* **114**, 8565 (2001).
- [2] O. Krarty and G. Porod, *Recl. Trav. chim. Pay-Bas* **68**, 1106 (1949).
- [3] A. N. Semenov, in preparation.
- [4] T. Sintes, K. Sumithra and E. Straube, *Macromolecules* **34**, 1352 (2001).
- [5] E. Yu. Kramarenko, R. G. Winkler, P. G. Khalatur, A. R. Khokhlov and P. Reineker, *J. Chem. Phys.* **104**, 4806 (1996).
- [6] T. Cosgrove, N. A. Finch and J. R. P. Webster, *Macromolecules* **23** 3353 (1990).
- [7] A. P. Gast, C. K. Hall and W. B. Russel, *J. Colloid Interface Sci.* **96**, 251 (1983).
- [8] V. Chaplain, M. L. Janex, F. Lafuma, C. Graillat and R. Audebert, *Colloid Poly. Sci.* **273**, 984 (1995).
- [9] Theo Odijk, *Macromolecules* **29**, 1842 (1996).
- [10] R. Tuinier and H. N. W. Lekkerkerker, *Macromolecules* **35**, 3312 (2002).

Currículum Vitae

PERSONAL DATA:

Name: Silvia Díez Orrite

Birth: 13/08/72 **Place of birth:** Madrid (Spain) **Sex:** Female

Address:

Departament d'Enginyeria Química, Universitat Rovira i Virgili, Tarragona, 43003, Spain.
Tel: +34 977 55 97 11.

C/ Mallorca, nº 15, Tarragona Tel: +34 606 081339 (Permanent)

e-mail: sdiez@etse.urv.es

EDUCATION:

B.Sc. (Hons) in Chemistry

Universidad Complutense de Madrid, 1995

EXPERIENCE:

01/10/97-31/6/02

Teaching Assistant, Universitat Rovira i Virgili. Tarragona (Spain)

- Undergraduate course *Laboratory of Chemical Engineering*, Dr. Jordi Grifoll
- Undergraduate course *Transport Fenomena*, Dr. F. Giralt

December 1996

Researcher Assistant, Universidad Complutense de Madrid (U.C.M)

01/1/97-01/09/97

Researcher Assistant, Consejo Superior de Investigaciones Científicas (C.S.I.C.)

COMPUTER:

Experience FORTRAN programmer (writing and debugging of programs)

SKILLS:

Familiar with UNIX and DOS operating systems, administrating LINUX RedHat and COMPAQ Tru64 UNIX.

LANGUAGES:

English (4^o level of the Escola Oficial d'idiomes) and Catalan.

INTERESTS:

Travel, Cinema

PUBLICATIONS

- A. Johner, J. F. Joanny, S. Díez Orrite and J. Bonet Avalos, *Gelation and phase separation in colloid-polymer mixtures*, Europhys. Lett. **56**(4), 549 (2001).
- S. Díez Orrite, J. Bonet Avalos, A. Johner and J. F. Joanny, *Adsorption of flexible polymers on small colloids: Complexes and Gels*, Macromolecula Symposia (in press).
- S. Díez Orrite, A. Mackie and J. Bonet i Avalos, *Novel Single Chain Mean Field methodology. Application to the polymer adsorption on flat surfaces I* (submitted to Macromolecules).
- S. Díez Orrite, A. Mackie and J. Bonet i Avalos, *Comparison of Single Chain Mean Field with other methodologies. Application to the polymer adsorption on flat surfaces II* (submitted to Macromolecules).
- S. Díez Orrite, A. Johner and J. Bonet i Avalos *Polymer adsorption onto colloidal particles*(in preparation)

CONTRIBUTIONS TO CONFERENCES

- S. Díez and J. Bonet i Avalos, *Novel single chain mean field methodology. Application to the adsorption of long polymer onto planar surfaces and colloidal particles*, Surfactants in Solution Symposium, Barcelona (Spain), June 2002.
- S. Díez and J. Bonet i Avalos, *Novel single chain mean field methodology. Application to the adsorption of long polymer onto planar surfaces and colloidal particles*, FISES2002, Tarragona (Spain), May 2002.
- S. Díez, A. Mackie, J. Bonet i Avalos, *Polymer adsorption onto colloidal particles. A theoretical and simulation study*, Oud Poelgeest (the Netherlands), March 2002.
- S. Díez, J. Bonet i Avalos, A. Johner and J. F. Joanny, *Adsorption onto colloidal particles: Structure of layer and phase diagram*, Chains @ Interfaces, Evora (Portugal), Enero 2001.
- S. Díez, J. Bonet i avalos, A. Johner, J. F. Joanny, *Adsorption onto colloidal particles: Structure of layer and phase diagram*, FISES2000, Santiago de Compostela (Spain), Septiembre 2000.
- Silvia Díez Orrite, Josep Bonet i Avalos, *Structure of Polymer Layers Adsorbed onto Colloidal Grains*, oral presentation, FISES99, Santander (Spain), May 1999.
- S. Díez, M. Álvarez, E. Lomba y F. J. Bermejo, *High Frequency dynamics in some liquid binary alloys*, Liquid and Amorphous Metals, Dortmund (Alemania), 1998.

COURSES AND VISITS

- Visit to Dr. A. Johner's research group, in the Institute Charles Sadron (CNRS), Strasbourg (France), 18/6/2002-18/7/2002.
- Methods in Molecular Simulation, UMIST, Manchester (UK), 2001.
- Visit to Dr. Igal Szleifer's research group, Department of Chemistry, University of Purdue, Indiana (United States), November-December 2000.
- Visit to Drs. J. F. Joanny and A. Johner, in the Institute Charles Sadron (CNRS), Strasbourg (France), thanks to *Program Beques fora de Catalunya*, Generalitat de Catalunya, 01/01/2000-01/03/2000.
- Research work *Tensión superficial cerca de un punto crítico. Modificación de una técnica experimental* in the Universidad Complutense de Madrid, obtaining the maximum score. Supervisor: Dra. Aurora Compostizo Saudo, December 1996.

- Methods in Molecular Simulation, University of Bristol, Bristol (UK), April 1996.
- Introducció a la física de polimers (Dr. Igal Szleifer), Universitat Rovira i Virgili, Tarragona (Spain), 1999.
- Introducció a la ciència macromolecular (Dr. Yohan Cohen), Universitat Rovira i Virgili, Tarragona (Spain), 1998.